CAPITAL UNIVERSITY OF SCIENCE AND TECHNOLOGY, ISLAMABAD

Organic Semiconductor and Nano-materials based Physical Sensors

by

Shahid Shafique

A dissertation submitted in partial fulfillment for the degree of Doctor of Philosophy

in the

Faculty of Engineering
Department of Electrical Engineering

2023

Organic Semiconductor and Nano-materials based Physical Sensors

By

Shahid Shafique

(DEE-151005)

Dr. Karim Sallauddin Karim, Professor

University of Waterloo, Canada

(Foreign Evaluator 1)

Dr. Yecheng Zhou, Associate Professor

Sun Yat-Sen University, China

(Foreign Evaluator 2)

Dr. Muhammad Mansoor Ahmed

(Dissertation Supervisor)

Dr. Khasan S. Karimov

(Dissertation Co-Supervisor)

Dr. Noor Muhammad Khan

(Head, Department of Electrical Engineering)

Dr. Imtiaz Ahmad Taj

(Dean, Faculty of Engineering)

DEPARTMENT OF ELECTRICAL ENGINEERING

CAPITAL UNIVERSITY OF SCIENCE AND TECHNOLOGY

ISLAMABAD

2023

Dedicated to

My Parents, Sister & her family,

Brother Dr. Umar Shafique & his family,

Wife Dr. Rizwana Shahid and Kids Salman & Ayesha for their endless love, sacrifices, support and prayers.

CAPITAL UNIVERSITY OF SCIENCE & TECHNOLOGY
ISLAMABAD

Expressway, Kahuta Road, Zone-V, Islamabad
Phone:+92-51-111-555-666 Fax: +92-51-4486705
Email: info@cust.edu.pk Website: https://www.cust.edu.pk

CERTIFICATE OF APPROVAL

This is to certify that the research work presented in the dissertation, entitled "**Organic Semiconductor and Nano-materials based Physical Sensors**" was conducted under the supervision of **Dr. Muhammad Mansoor Ahmed**. No part of this dissertation has been submitted anywhere else for any other degree. This dissertation is submitted to the **Department of Electrical Engineering, Capital University of Science and Technology** in partial fulfillment of the requirements for the degree of Doctor in Philosophy in the field of **Electrical Engineering.** The open defence of the dissertation was conducted on **August 09, 2023**.

Student Name : Shahid Shafique (DEE151005)

The Examination Committee unanimously agrees to award PhD degree in the mentioned field.

Examination Committee :

(a) External Examiner 1: Dr. Arshad Saleem Bhatti
Professor
Virtual University, Islamabad

(b) External Examiner 2: Dr. Ibrahim Qazi
Professor
IST, Islamabad

(c) Internal Examiner : Dr. Muhammad Riaz
Associate Professor
CUST, Islamabad

Supervisor Name : Dr. Muhammad Mansoor Ahmed
Professor
CUST, Islamabad

Name of HoD : Dr. Noor Muhammad Khan
Professor
CUST, Islamabad

Name of Dean : Dr. Imtiaz Ahmad Taj
Professor
CUST, Islamabad

AUTHOR'S DECLARATION

I, **Shahid Shafique (Registration No. DEE151005)**, hereby state that my dissertation titled, "**Organic Semiconductor and Nano-materials based Physical Sensors**" is my own work and has not been submitted previously by me for taking any degree from Capital University of Science and Technology, Islamabad or anywhere else in the country/ world.

At any time, if my statement is found to be incorrect even after my graduation, the University has the right to withdraw my PhD Degree.

(**Shahid Shafique**)

Dated: 9 - August, 2023

Registration No : DEE151005

PLAGIARISM UNDERTAKING

I solemnly declare that research work presented in the dissertation titled "**Organic Semiconductor and Nano-materials based Physical Sensors**" is solely my research work with no significant contribution from any other person. Small contribution/ help wherever taken has been duly acknowledged and that complete dissertation has been written by me.

I understand the zero-tolerance policy of the HEC and Capital University of Science and Technology towards plagiarism. Therefore, I as an author of the above titled dissertation declare that no portion of my dissertation has been plagiarized and any material used as reference is properly referred/ cited.

I undertake that if I am found guilty of any formal plagiarism in the above titled dissertation even after award of PhD Degree, the University reserves the right to withdraw/ revoke my PhD degree and that HEC and the University have the right to publish my name on the HEC/ University Website on which names of students are placed who submitted plagiarized dissertation.

(**Shahid Shafique**)

Dated: ٩ - August, 2023

Registration No : DEE151005

List of Publications

It is certified that following publication(s) have been made out of the research work that has been carried out for this dissertation:-

1. **Shahid Shafique**, Khasan S. Karimov, Muhammad Abid, Muhammad Mansoor Ahmed, Khakim M. Akhmedov, Aziz-ur-Rehman, "Carbon nanotubes, orange dye, and graphene powder based multifunctional temperature, pressure, and displacement sensors," *Journal of Materials Science: Materials in Electronics,*, vol. 31, Number 11, pp. 8893-8899, 2020.

2. Kh. S. Karimov, M. M. Ahmed, M. Saleem, **S. Shafique**, M. Akmal, "Orange dye based field effect transistor as humidity sensor," *Optoelectronics and Advanced Materials - Rapid Communications,*, vol. 14, Number 9-10 , pp. 416-420, 2020.

3. Kh. S. Karimov, M. Saleem, Kh. M. Akhmedov, M. M. Ahmed, A. Hassan, **S. Shafique**, "Orange dye based temperature sensor," *Proceedings of the Romanian Academy Series A-Mathematics Physics Technical Sciences Information Science,* Series A, vol. 22, Number 2/2021, pp. 173–178.

4. **S. Shafique**, U. Munir, M. M. Ahmed, Kh. S. Karimov, "Fabrication and characterization of orange dye, graphene and silicone adhesive composite based flexible humidity sensors," *Journal of Materials Science: Materials in Electronics,* vol. 34, Number 7, pp. 622, 2023.

(Shahid Shafique)
Registration No: DEE-151005

Acknowledgement

All praise to **Almighty ALLAH**, the Most Gracious, and the Most Merciful for His blessing given to me during my study and in completing my dissertation.

I would like to express my heartiest gratitude to my supervisor **Prof. Dr. Muhammad Mansoor Ahmed**, Vice Chancellor, Capital University of Science and Technology (CUST), and co-supervisor **Prof. Dr. Khasan Sanginovich Karimov**, Ghulam Ishaq Khan Institute of Science and Technology (GIKI), Swabi, It was a wonderful experience and learning opportunity to work with them as a PhD student. They supported me in every step of my studies in topic selection, experimental work, paper publications and dissertation writing. They also provided positive encouragement, knowledge and a warm spirit to complete my research objectives.

I am thankful to the administration of CUST for providing me with an excellent environment perfect for conducting my research. I would like to thank the Dean, Faculty of Engineering, **Prof. Dr. Imtiaz Ahmad Taj**, and Head of Electrical Engineering Department, **Prof. Dr. Noor M. Khan** for their continuous encouragement and support during the entire span of my studies at CUST.

Furthermore, I would also like to express my sincere gratitude to all the members of **Microelectronics and RF Engineering** research group, especially **Mr. Usama Munir** and **Mr. Suleman Khan** for their kind support.

Finally, I would like to express my feelings of gratitude to my parents, family and friends for their exceptional love and encouragement throughout of my life and eventually to achieve my goals that would not have been possible without their sincere co-operation and love.

(Shahid Shafique)

Abstract

Organic semiconductor processing is relatively less technology-demanding compared to its in-organic counterparts. The characteristics of an organic semiconductor can comfortably be altered by involving simple techniques, such as, mixing an organic semiconductor powder with another appropriate substance. Taking these facts into consideration, organic semiconductor based various sensors have been developed in this dissertation for their potential use in the industry.

In the first part of the research, Organic Field Effect Transistors (OFETs) based sensors were developed which can measure both ambient humidity as well as temperature. The channel of the OFET was defined by drop casting orange dye, OD (8 wt.%) and sugar (8 wt.%). Finished devices were then tested in a humidity chamber. It was observed that water molecules in OD-sugar film changes the channel conductivity. Accordingly, this translates the variation in ambient humidity into an electrical signal. The response and recovery times of these sensors were 11 s and 32 s when relative humidity (RH) changes from 50% to 90%, respectively. Additionally, the properties of OFETs were also investigated as a temperature sensor. It was shown that the channel impedance of OD-sugar based OFET sensor increases with increasing values of temperature provided the device is exposed to air. On the other hand, the same variable decreases by increasing temperature, if the device under investigation is encapsulated.

In the second part of the research, flexible and low in cost humidity sensors were developed. The first category of sensors had 300 nm thick silver (Ag) metal as bottom electrodes with an inter electrode spacing of 16 μm, deposited on top of a flat rubber substrate. A $9 - 11$ μm thick film comprising of orange dye (20 wt.%), graphene (30 wt.%) and silicone adhesive (50 wt.%), was deposited on Ag electrodes to define the channel. In the second category, a $5 - 6$ μm thick gate layer consisting of graphene (50 wt.%) and silicone adhesive (50 wt.%) was additionally deposited on top of the channel layer to achieve organic field effect transistor (OFET) based sensors. The impedance variation of the fabricated sensors was investigated by varying RH at various frequencies. It has been observed

that the output impedance of these sensors decreases with the increase in RH. It was observed that both type of sensors offered stable response for temperature range 22 °C – 75 °C and for a time interval of 240 hours.

The third part of the research, presents design, fabrication and investigation of carbon nanotubes CNTs, orange dye (OD) and graphene based multifunctional sensors. The output of the multifunctional sensors is observed as change in resistance and impedance values as a function of temperature, pressure and compressive displacement. An increase in both resistance and impedance of the sensors is observed with increase in temperature. The temperature coefficients of the sensors having resistances $\sim 470\ \Omega$ and $\sim 890\ \Omega$ were $1.0\%C^{-1}$ and $1.9\%C^{-1}$, respectively, when evaluated for temperatures ranging from 30 to 65 °C. For applied pressure 0 kgf/cm^2 to 0.1 kgf/cm^2 and displacement 0 to 110 μm, the resistance of the multifunctional sensor exhibited a decrease 1.3 to 12.7 times and 3.18 to 7.53 times, respectively. The proposed multifunctional sensor could be a good candidate to measure temperature, pressure and displacement of an industrial unit.

The fourth part of the research presented design, fabrication and characterization of strain sensors fabricated using a composite of MWCNTs (45 wt.%) and silicon adhesive (55 wt.%). The finished devices were characterized at a frequency of 100 Hz and 1 KHz. These sensors exhibited strain sensitivity of 32.1 (at 100 Hz) and 28.8 (at 1 kHz) under tension whilst, under compression, the observed sensitivity was 18.5 and 14.2 at 100 Hz and 1 kHz, respectively.

Contents

List of Figures

List of Tables

Abbreviations

ADC	Analog-to-digital converter
AFM	Atomic force microscope
AgNPs	Silver nanoparticles
AlPcCl	Aluminum phthalocyanine chloride
Al_2O_3	Aluminum Oxide
AMIS	Area-asymmetric organic metal–insulator
$BaTiO_3$	Barium titanate
CAS	Chemical abstracts service
CH_4	Methane
$C_{17}H_{17}N_5O_2$	Orange dye molecule
CNF/CB	Cellulose nanofiber/carbon black
CNT	Carbon nanotubes
CO_2	Carbon dioxide
COFs	Covalent organic frameworks
CPNTs	Carboxylated polypyrrole nanotubes
CPU	Central processing unit
$CuMn_2O_4$	Spinel copper manganese oxide
CuPc	Copper phthalocyanine
DCLD	Dual conducting layer dome
DNA	Deoxyribonucleic acid
EA	Activation energy
ECG	Electrocardiogram
EM	Electromagnetic

$F_{16}CuPc$	Fluorinated copper phthalocyanine
FESEM	Field emission scanning electron microscopy
FET	Field effect transistor
FGSs	Functionalized graphene sheets
GNP	Graphene nanoplatelets
GNS	Graphene nano-sheets
h-BTNCs	Hexagonal barium titanate nanocrystals
H_2O	Water
HOMO	Highest occupied molecular orbital
I	Current
IDC	Interdigitated capacitors
IoT	Internet of things
ITO	Indium tin oxide
LiCl-KIT-6	Lithium chloride (LiCl)-loaded 3D cubic mesoporous silica KIT-6
LTDOFET	Low trap-state density OFET
LUMO	Lowest unoccupied molecular orbital
$MAPbI_3$	Methylammonium lead iodide
MAPTAC	[3(methacrylamino)propyl] tri-methyl-ammonium-chloride
MFS	Multifunctional sensors
MIS	Metal insulator semiconductor
MG	Methyl green
MMA	Methylmethacrylate
MWCNT	Multi walled carbon nanotube
N_2	Nitrogen
NiPc	Nickel phthalocynanine
NMOECT	Nanomesh organic electrochemical transistor
NO_2	Nitrogen oxide
NOI	Nothing on insulator
OD	Orange dye
OFET	Organic field effect transistor
OLED	Organic light emitting diode

OP-TFTs	Organic polymer TFTs
OSC	Optical stimulated current
OTFT	Organic thin-film transistor
PABA	Para-aminobenzoic acid
PABA-NCS	Para-aminobenzoic acid-core shell nanoparticles
PANI	Polyaniline
PCB	Printed circuit board
PDMS	Poly(dimethyl siloxane)
PEDOT:PSS	Poly(3,4-ethylenedioxythiophene):Poly(styrene sulfonate)
PEMC	Porous ecoflex-multiwalled carbon nanotube composite
PEN	Poly(ethylene naphthalate)
pH	Potential of hydrogen
PLA	Polylactide
PMAPTAC	[3-(methacrylamino) propyl] tri-methyl ammonium chloride
PMMA	Poly(methyl methacrylate)
PNIPAM	Poly(N-isopropylacrylamide)
POC	Point of contact
PPy	Polypyrrole
PTC	Positive temperature coefficient
PU	Polyurethane
PV	Photovoltaic
PVDF	Polyvinylidene fluoride with different polypeptides
PVF_2	Polyvinylidene fluoride
RF-CPU	Register file – Central processing unit
RFID	Radio frequency identification
rGO	Reduced graphene oxide
RH	Relative humidity
SAW	Surface acoustic wave
SCLC	Space charge limited current
SDBS	Sodium dodecyl-benzenesulfonate
SGS	Small-gap semiconducting

SSWCNT	Suspended single walled carbon nanotube
SWCNT	Single walled carbon nanotube
tascPLA	Three-arm stereo complex polylactide
TCNQ	Tetracyanoquinodimethane
TFT	Thin-film transistor
THz	Terahertz
TiO_2NPs	Titanium dioxide nanoparticles
ToF	Time of flight
TrFE	Trifluoroethylene
TSC	Thermal stimulated current
TSCL	Transverse space-charge limited
TSL	Thermal stimulated luminescence
UV	Ultraviolet
UV Vis.	Ultraviolet visible
V	Voltage
VO_2(3-fl)	Vanadium oxide
VT	Threshold voltage
XRD	X-ray diffraction

Symbols

α	Temperature coefficients of impedance
β	Adjustment factor
Δ	Rate of Change
ϵ	Longitudinal strain
θ	Trap factor
μ	Carrier mobility
π	Pi
ρ	Resistivity
σ	Conductivity
Ω	Ohm
χ	Experimental error
b_0	Width at foot of beam
P	Maximum load
h	Thickness of the beam
E_l	Modulus of elasticity
q	Electronic charge
J	Current density
k	Boltzmann's constant
I_{ds}	Drain to source current
V_{ds}	Drain-source voltage
V_{gs}	Gate-source voltage
R_{ini}	Initial resistance
R_{fin}	Final resistance

RH_{ini}	Initial relative humidity
RH_{fin}	Final relative humidity
S_R	Resistive sensitivity
S_I	Current sensitivity
H^+	Positive hydrogen ion
W	Conduction channel width
L	Conduction channel length
C	Gate capacitance
$I_{ds(sat)}$	Saturated drain to source current
V_t	Threshold voltage
$I_{ds(lin)}$	Linear drain to source current
g_m	Transconductance
Z	Impedance
T	Temperature
d	Thickness of the OD powder
A	Crossectional area of the sample
n	Concentration of charges
e	Electron charge
τ	Mean free time
m	Mass of electron
s	Second

Chapter 1

Introduction

1.1 Organic vs Inorganic Semiconductors

Semiconductors are materials whose electrical properties lies between those of insulators and metals. The conductivity of these materials can be modified by making changes in their material composition. Based on their composition, semiconductor materials are further classified into two broad categories; inorganic and organic semiconductor materials. Inorganic semiconductors, which are normally employed in single-crystalline forms, are non-carbon based material such as silicon, germanium or gallium arsenide; whereas, organic semiconductors are carbon based materials. Another difference between them is in their charge transport mechanism. In inorganic semiconductors (crystalline), electrons move in wide bands as delocalized plane waves and subjected to a very limited scattering, and hence, show relatively high mobility (e.g. 1.5×10^3 $cm^2V^{-1}s^{-1}$). Whereas, in case of organic semiconductors, the charge transport is based on carriers hopping between localized states associated with organic molecules. In this process, electrons undergo significant scattering which results in relatively low electron mobility (1-3 cm^2 $V^{-1}s^{-1}$).

In the last five decades, inorganic semiconductor technology has been dominating the large area of electronics industry. Materials like silicon, germanium and gallium arsenide are mostly used as inorganic semiconductors. These inorganic semiconductors are deposited at high temperature and employed complex deposition techniques. These complex fabrication techniques increase the manufacturing cost and also require expensive technology. Compared to inorganic materials, organic semiconductor materials offer attractive advantages as they require simple and inexpensive fabrication processes [1–3]. Most of the organic semiconductor based devices are fabricated at low temperature (around room temperature) by utilizing inexpensive deposition/manufacturing equipment. Low temperature fabrication of these devices allow the use of low cost flexible substrate such as plastic. Common techniques used by the industry to process organic semiconductor materials are vacuum thermal evaporation, spin coating, and slot die coating. Photovoltaic (PV), organic light emitting diodes (OLEDs), and organic field effect transistors (OFETs) are some commercially available examples of organic semiconductors [4–7].

Organic semiconductor thin films have low charge carrier mobility compared to amorphous silicon [8, 9]. However, these crystalline inorganic materials are expensive to use for large area electronics application. Electronic devices utilizing organic semiconductors offer a huge advantage in inexpensive applications. For instance, OLED displays are abundantly utilized as a part of consumer electronic products [10]. Similarly, organic thin film transistors (OTFT) are considered as a substitute for applications like radio frequency identification (RFID) tags and E-paper.

The key benefit associated with organic semiconductors is the ease of deposition such as drop casting, spin coating, and centrifugal deposition, etc. These methods are frequently employed to deposit organic semiconductors thin layers on a substrate. Organic semiconductor deposition techniques are inexpensive, and do not require high temperature processing; thus, requires small investment to industrialize.

Organic semiconductors are amassed from π-conjugate bonds in which electrons move through π-electron cloud either by tunneling or hopping mechanism [11]. Organic semiconductors are doped to modify their conductivity just like inorganic semiconductors. However, doping in organic semiconductors is done by placing an electron to its conduction band, which increases its electron conductivity or by creating a vacancy in the valence band to increase hole conductivity.

Amorphous inorganic semiconductors are also getting good space in the industry these days. This is due to ease in their synthesis as that of organic semiconductors, because both can be synthesized at relatively lower temperatures than what is usually required in the crystalline form of inorganic semiconductors. Additionally, amorphous semiconductors based devices normally do not require sintering/annealing after their fabrication; hence, provide ease of fabrication on one hand and on the other hand, this also reduces the fabrication cost. There are many potential advantages which are associated with amorphous inorganic semiconductors; such as, the availability of finite density of states at the edges of valence and conduction bands which allow localized movement of carriers with relatively small amounts of energy, making them suitable for low power devices. Amorphous inorganic semiconductors also have delocalized density of states just as inorganic semiconductors. By virtue of this, their electrical characteristics also involve discrete valence-conduction band properties as that of inorganic semiconductors. In the nut shell, amorphous inorganic semiconductors characteristics are explained involving both hoping as well as drift based electrical conductions. This made amorphous inorganic semiconductors more versatile for many industrial applications such as solar cell, photoelectrocatalysis and photocatalysis. [12]

Although, amorphous inorganic semiconductors offer both localized and delocalized conductions which enable them for a wider range of applications in the semiconductor industry. Yet, they are not suitable for flexible electronics which are getting popularity in many industrial applications especially, in sensors and in those gadgets which are used in medical applications. Many wearable sensors are fabricated on plastic substrates using organic semiconductors which provide a conformity of the device with the human body for accurate data acquisition [13].

1.2 Organic Semiconductor Materials

Organic materials exhibiting semiconductor properties are known as organic semiconductor materials. These materials consist mainly of carbon and hydrogen atoms. A conjugated organic semiconductor materials, on the basis of their molecular weight can broadly be classified as:

(a) **Single molecule based semiconductor:** Single molecule organic semiconductors are defined by relatively small molecules typically, with a non-repeating structure called *monomers*.

(b) **Short chain based semiconductor:** Short chain organic semiconductors are also known as *oligomers*, which comprised of limited number of monomer units.

(c) **Long chain based semiconductor:** A long chain organic semiconductors are also known as *polymer*. A polymer molecule consists of linked chain of monomers, which are typically connected by a covalent bond.

These carbon based materials have conductivity similar to metals or semiconductors. They differ in their processing and deposition techniques for example oligomers are usually processed and deposited in vacuum; whereas, the polymers are mostly prepared in solutions and deposited with techniques like spin coating or inkjet printing. Examples of both oligomers and polymers are shown in Figs. 1.1(a) and 1.1(b), respectively.

Polymers are soluble and can be dissolved in an organic solvent. Polymer thin films can be processed using solution-processing techniques such as spin coating or printing. The structural properties of polymer thin films depend on the deposition techniques and the choice of solvent.

Oligomers on the other hand, are mostly insoluble and thus needed a sophisticated deposition techniques such as vacuum thermal evaporation. Thin films of small-molecules, when deposited, have more order in their structure than polymer thin films do.

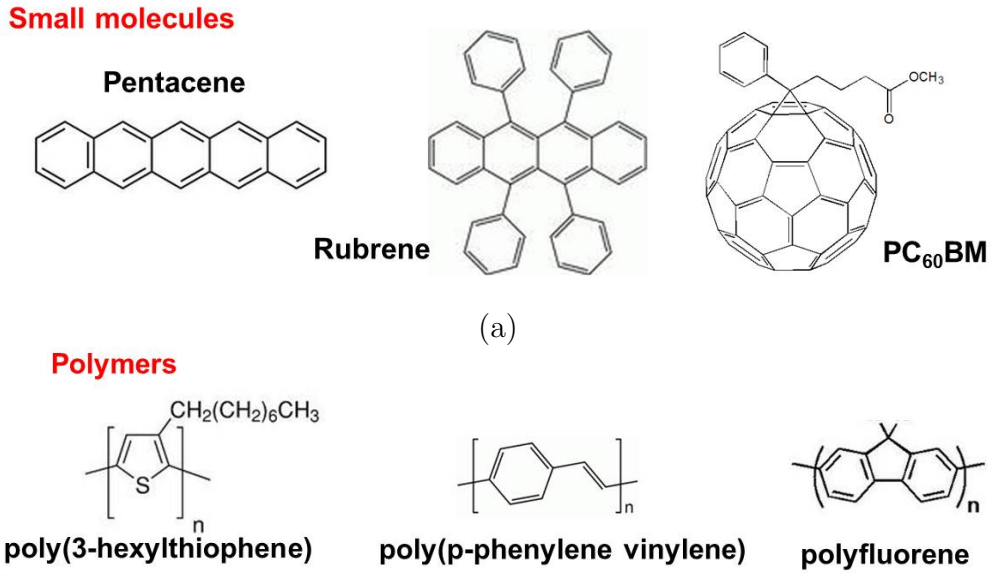

FIGURE 1.1: (a) Examples of small chain based organic materials (oligomers). (b) Examples of long chain based organic materials (polymers).

It has been shown that small-molecule devices show superior performance compared to devices based on polymers. However, many highly efficient polymers have recently been engineered and show equivalent or even better efficiency when used to fabricate devices.

Research efforts have been carried out in academia and industry to develop suitable materials that can be utilized in displays, smart cards/RFID, bio medicine and sensors etc. These efforts resulted in advance processing and material synthesis techniques. By controlled variation in assembly and ordering of different oligomers, polymers, and nanocrystals, have resulted in improved mobility of these materials.

Yan *et al.* in [14] presented the progress in the organic semiconductor-based circuits made in the recent years. Fig. 1.2 shows the evolution in term of mobility for organic and hybrid semiconductors. This figure speaks that with the passage of time, the mobility of these materials has improved however, a saturating trend in the value of mobility is observed (Fig. 1.2) once the mobility of organic material has passed amorphous silicon mobility value. This could be associated with the conducting properties of a given organic

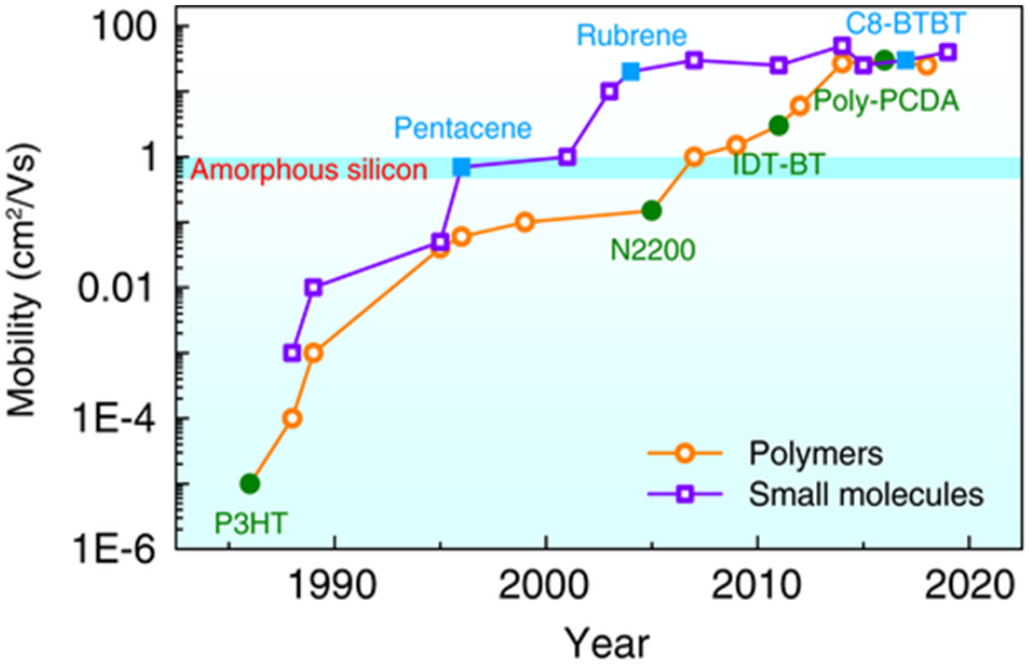

FIGURE 1.2: Evolution in term of mobility for Organic materials.

semiconductor which is technically similar to that of an amorphous semiconductor. An improvement in hole mobility beyond 50 cm^2Vs^{-1} will be trending towards the hole mobility of inorganic semiconductor and thus, difficult to achieve and may require designing of new organic semiconductors.

1.3 Advantages of Organic Semiconductors

Organic semiconductors have several advantages, which are listed below:

(a) Deposition of organic thin films at low temperature.

(b) Based on the selection of organic material, the moisture resistance of an organic semiconductor device can be controlled.

(c) They have low melting and boiling points compared to inorganic counterparts.

(d) Organic semiconductors are relatively more sensitive to external agents; thus, ideal for use as active material for making sensors.

(e) They require less cost for large scale fabrication.

(f) They are abundantly available in nature, as all living organisms have organisms are organic and can exist in amorphous, polycrystalline and crystalline morphologies.

(g) Flexible devices can be fabricated by employing organic semiconductors.

1.4 Properties of Organic Semiconductors

An organic semiconductor possesses weaker bonding compared to inorganic semiconductors, which are covalently bounded e.g. silicon (Si). Because of this weak bonding among neighbouring molecules, there exists a weak de-localization of electronic wave functions that affects the charge carrier transport behaviour and optical properties.

1.4.1 Optical Properties

Organic semiconductors have weak electronic de-localization, which offers two important peculiarities [15].

(a) First, the presence of spin states (singlet and triplet) as in isolated molecules.

(b) Second, the optical excitations (excitons) are mostly localized on one molecule and hence possess considerably low binding energy of typically $0.5 - 1$ eV, with results in independent positive and negative charge carriers pair. For charge transport, this binding energy needs to be overcome.

1.4.2 Charge Transport

In organic semiconductor materials, band or hopping transport is the prime transport mechanism [15]. Band transport mechanism is observed mostly for pure

organic molecules at low temperature as electronic delocalization in organic semiconductors is weak resulting in small bandwidth compared to inorganic semiconductors. Thus, molecular crystals mobilities (at room temperature) ranges from 1 to 10 $cm^2(Vs)^{-1}$ [16]. The characteristic feature of band transport is that temperature dependence follows a power law behaviour.

$$\mu \propto T^{-n} \quad \text{with} \quad n = 1, 2, \cdots \tag{1.1}$$

At low temperature, deviation from such behavior is because of the presence of large number of traps [17].

In amorphous organic solids, hopping transport mechanism is observed, which results in smaller values of mobility, which is defined by Eq. 1.2

$$\mu(F,T) \propto \exp\left(-\frac{\Delta E}{kT}\right) \times \exp\left(\frac{\beta\sqrt{F}}{kT}\right) \tag{1.2}$$

where, ΔE is the difference between energy levels, k is Boltzmann's constant, F represents electric field, β is an adjustment factor, and T is absolute temperature.

In organic semiconductors, charge mobility depends on the space-charge, trapping-effects, and the charge carrier injection mechanism [18–22].

Two methods are being used for measuring charge carrier mobility in organic semiconductor materials: time of flight (TOF) method and $I - V$ response of single-carrier device in the region of space charge limited current (SCLC).

Conventionally, charge mobility and distribution of traps energy level was determined by TOF method, which results in extremely low carrier densities. Whereas, devices operate at higher densities of injected charges; they result in partial trap filling by carriers and space charge effects. At present, efforts are made to characterize organic semiconductors by experimentation, whose results are near to device operational conditions [15].

In TOF technique, organic material is exposed to light pulse and transient current response is measured under the effect of bias voltage. The time shift in the peak of transient current shows TOF of the carriers. One can interpret mobility under defined bias conditions from this TOF. However, the interpretation is not so accurate as real charge carriers motion is not so simple. Transient current response is effected by carrier mobility dispersion and diffusion of the carrier after being injected. In addition, double injection of carriers offer difficulty in estimating the transient current. Therefore, the transient current cannot guarantee the prediction of actual carrier motion [15].

1.5 Organic Semiconductor Devices

Organic semiconductor materials offer numerous advantages such as low fabrication cost, wide area application, and new functions (for example bio-sensing, etc.) compared to conventional silicon (or amorphous silicon) semiconductors. OLEDs are fabricated with a multi-junction between multiple organic semiconductor layers of different materials as shown in Fig. 1.3. Charge injection takes place from electrodes (cathode and anode) in the presence of applied electric field to the corresponding transport layers (electron or hole layer). Electrons and holes recombination causes generation of light. OLEDs have external quantum efficiency >10% and luminous efficiency is higher than 200 Lumens/Watt. These properties made OLEDs a suitable candidate for less expensive and energy efficient lighting solution based on organic semiconductor materials [23, 24].

OTFTs are yet another important application of organic semiconductors. OTFTs have shown a tremendous potential for large area sensor and display applications. Carrier mobility in OTFTs is greater than 1 $cm^2(Vs)^{-1}$ both for p and $n-$channel devices. This is sufficient for applications using low frequency spectrum.

Fig. 1.4 shows a crosssectional view of an OTFT. In this figure, it is shown that a thin film of organic semiconductor material is separated from gate electrode by using an insulating material. In OTFTs, the channel is formed by the charge

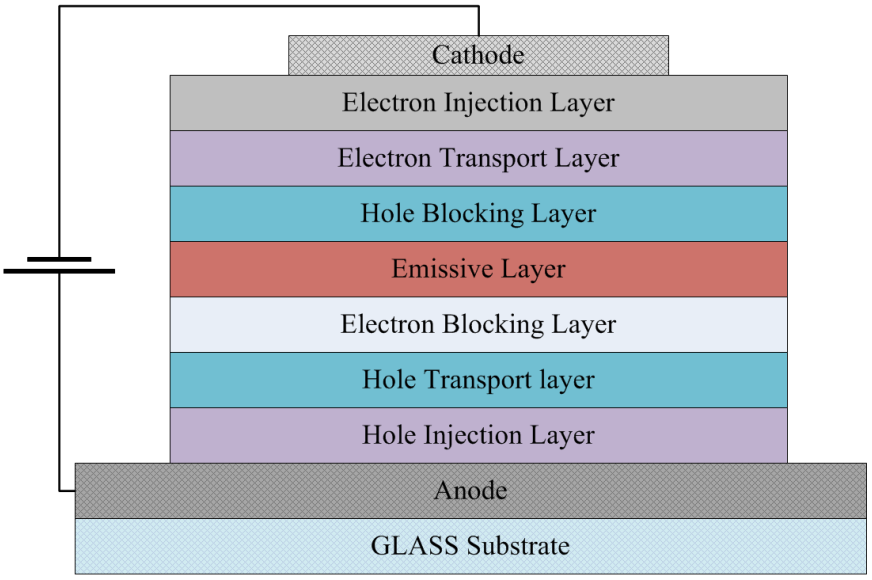

FIGURE 1.3: Schematic diagram of multilayer structure of an OLED.

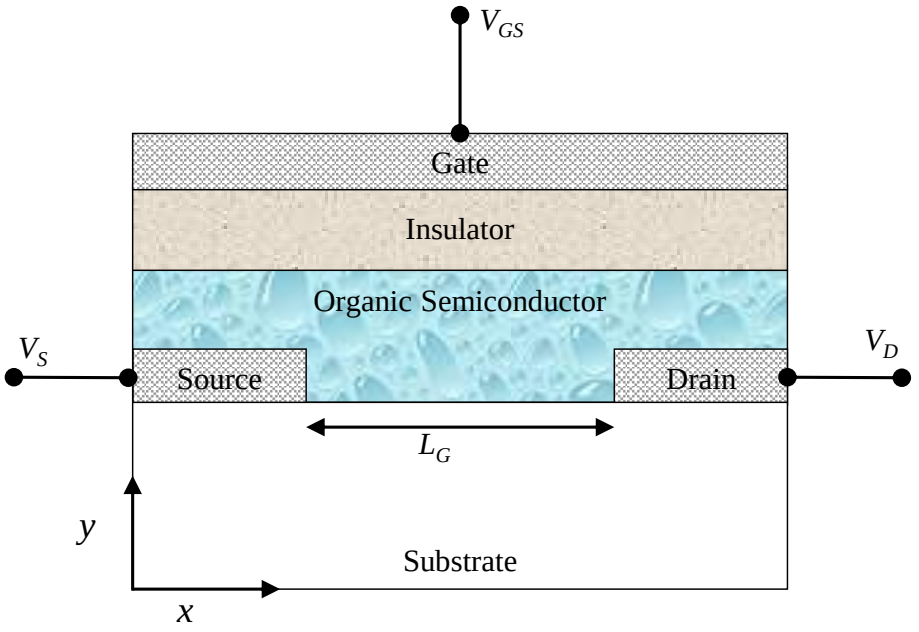

FIGURE 1.4: Cross-sectional view of organic thin film transistor (OTFT).

accumulation due to a field generated by V_{GS}. Furthermore, the substrate of the OTFT is generally an insulating material, which is normally chosen for flexible and low cost fabrication. The source and drain electrodes are fabricated using a metal, which makes direct contact with the organic semiconductor, thus, allowing the flow of carriers under the applied voltage V_{DS}.

OTFT comprises of source, drain, and gate. Both drain and source are physically

attached to semiconductor material where as insulator isolates the gate from the semiconductor. The gate voltage modulates the source-drain current flow under bias voltage, V_{DS} [15].

1.6 Charge Transport Mechanism

Charge transport mechanism in organic semiconductor materials involves the injection, transportation and recombination of charges. The external electric field influence the charge transport from one electrode to another. The detail of charge transport mechanism is explained below.

1.6.1 Charge Injection

Organic semiconductor electronic and optoelectronic devices performance normaly rely on the charge injection phenomena that exists between metal and semiconductor interface. Charge transport mechanism in organic semiconductors varies from inorganic semiconductors because of weak bonding (Van der Waals bond). Organic semiconductors have highly localized electronic states, and charge transport is primarily associated with charge hopping mechanism between these discrete energy states. Organic semiconductors do not have free carriers. The electrode and semiconductor interface off-set mostly defines the Fermi level and charge injection barriers. Charge injection process rely on average barrier height w.r.t metal Fermi level, energetic disorder, image potential, and applied electric field as shown in Fig. 1.5 [20, 25].

1.6.2 Charge Transport

Various charge transport models have been reported in the literature, however, trapping model with transverse space-charge limited (TSCL) and field dependent

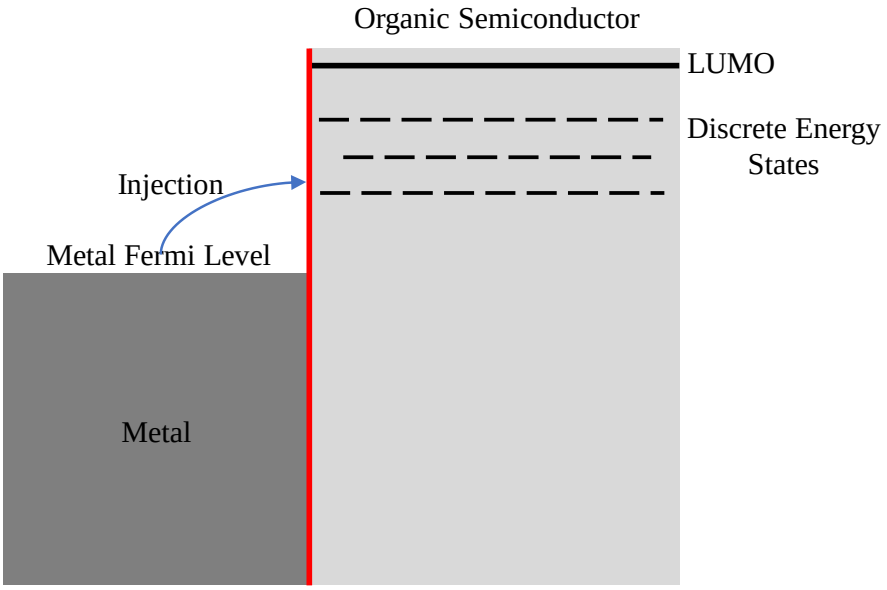

FIGURE 1.5: Under unbiased condition energy band diagram of metal-organic semiconductor is shown. Once the junction is biased, the electrons are injected from metal (cathode) to localized state. [20, 25].

mobility model have been used frequently and adapted by research community for the explanation of $I - V$ response in organic devices [26].

The TSCL model assumes that there exists certain traps distribution in energy space (localized states) between highest occupied molecular orbital's (HOMO) and lowest unoccupied molecular orbital's (LUMO). In an organic semiconductor, the terms HOMO and LUMO are employed such that HOMO is the highest filled valence band when compared with an inorganic semiconductor and LUMO is analogous to its conduction band. The gap between HOMO and LUMO defines the bandgap of a specific organic semiconductor and there are usually traps inside the bandgap of an organic semiconductor, defined by distinct energy states and free charge carriers get trapped in these energy states. Trapped charges can be released after obtaining energy from various sources; such as temperature, photo absorption, or other form of excitation; resulting into a current generation referred to as electrical response of an organic semiconductor device. It is a well established fact that traps are exponentially distributed inside an energy band and play an important role in determining the characteristics of a device.

The second model, which is field dependent mobility model takes into account the exponential dependence of hole mobility (μ_p) on square root of electric field over a wide range and can be expressed as [27]:

$$\mu_p = \mu_0 \exp\left[\sqrt{\frac{F}{F_0}}\right] \tag{1.3}$$

where μ_0 is the reference mobility, and F_0 denoted as a pre-factor and its value is sample dependent.

Mark and Helfrich [28] were the first to report exponential trap distribution model with constant mobility. Exponential trap distribution model takes into the account the concentration of free carriers, p_0 and it is significantly smaller compared to concentration of trapped carrier, p_t. Therefore, the trap distribution, h_t can be presented as a function of energy, E and is given by the following Eq. 1.4:

$$h_t(E) = \frac{N_t}{E_c} \exp\left(-\frac{E_n}{E_c}\right) \tag{1.4}$$

where N_t represents trap density, E_c denotes characteristic energy constant of the distribution and E_n represents the difference between trap and target energy state. The characteristic energy constant is proportional to characteristics temperature, T_c given as $E_c = kT_c$ (Here k is the Boltzmann's constant).

Traps in organic semiconductor amorphous materials are originated due to disorders, dangling bonds, and impurities, etc. Very often, free charge carriers get capture in these traps and thus, impacting the conduction process of an organic semiconductor [29].

Traps are divided into electron or hole traps as per their energy levels. The localized states close and below the LUMO and HOMO levels are called electron trap and hole trap states, respectively [30]. Impurities, deformities (structural) and self trapping phenomena's, etc. are some of the contributors of trap states [15]. Process parameters such as deposition rate and substrate temperature, etc. are also reported to create some traps [31].

1.7 Space Charge Limited Current (SCLC)

Region where charge concentration (electrons, holes or ions) is accumulated is known as space charge. The charges can be localized or mobile, resulting in a non-uniform localized electric field space. When directed by the non-uniform electric field, charges are transported and generate space charge limited current (SCLC). Most organic and polymer semiconducting materials exhibit SCLC characteristics as shown in Fig. 1.6 [32, 33]. Three well defined regions are derived from the Fig. 1.6, which are listed below:

(a) Region-I

(b) Region-II

(c) Region-III

1.7.1 Region-I

Region-I is the ohmic charge region, shown in Fig. 1.6, where applied voltage is increased slowly. The injected charges from electrodes are consumed to fill the trap states. A very small current is observed as some charges may succeed to reach the opposite electrode. Thus, the current in this region changes linearly with the increase in voltage. The current density (J) in this region can be written as [32, 33]:

$$\begin{cases} J = q\mu_p p_0 (V/L) \\ J = q\mu_p p_0 E \end{cases} \tag{1.5}$$

where q is the electronic charge, L is channel length and p_0 is the hole density.

1.7.2 Region-II

With the increase in voltage, device enters in Region-II called trapped space charge region, as shown in Fig. 1.6. For high voltage levels, excess charge carriers are injected from electrodes to organic semiconductor. This charge transport in organic

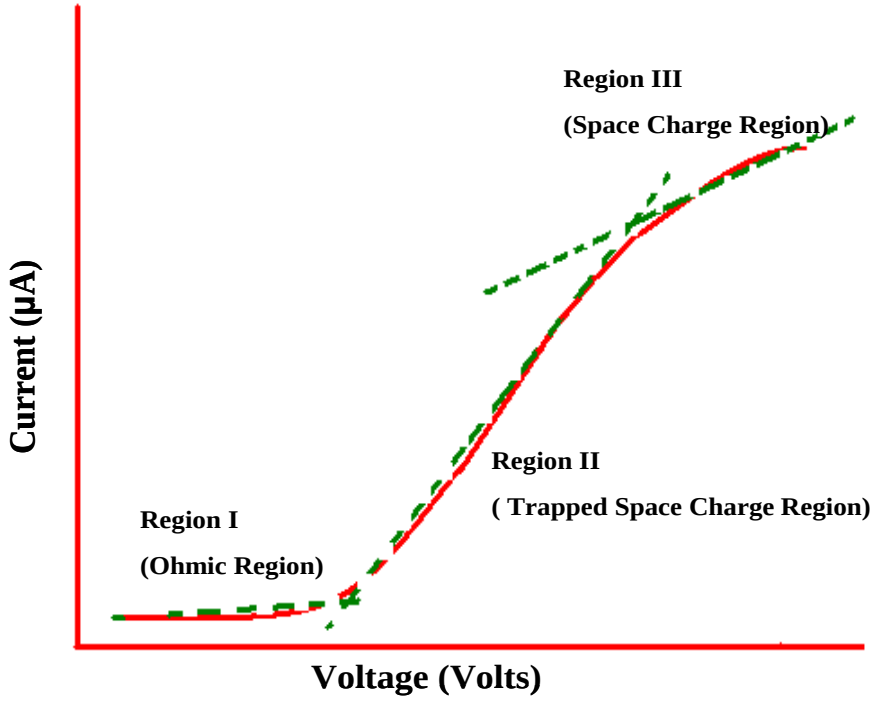

FIGURE 1.6: $I-V$ characteristics of a typical organic semiconductor diode [32, 33].

semiconductor is influenced by traps density. The excess charge in this region is controlled by the geometrical capacitance, C of the organic layer and defined as:

$$Q = CV \tag{1.6}$$

where

$$C = \frac{\varepsilon}{d} \tag{1.7}$$

where, $\varepsilon = \varepsilon_0 \varepsilon_m$; such as ε_0 represents permittivity of the free space and ε_m is dielectric constant of the material and d is the separation between two plates of the capacitor. Furthermore, trapped space charge limited current density can be expressed as [32, 33]:

$$J = \frac{9}{8}\varepsilon\theta\mu_p\frac{V^2}{d^3} \tag{1.8}$$

where θ is the trap factor, which differentiates Region-II from Region-III.

1.7.3 Region-III

With the increase in voltage, the device reaches a state where there are no traps left to be filled and device behaves as free of trap thin organic semiconductor film. The space charge limited current in this region can be expressed as:

$$J = \frac{9}{8}\varepsilon\mu_p\frac{V^2}{d^3} \tag{1.9}$$

Eq. 1.9 is known as Mott-Gurney law and it is the solid-state analogy of child law of SCLC in a vacuum [32, 33].

1.8 Organic Semiconductor Sensors

Devices that senses the physical, biological, chemical and environmental parameters and generates an output are known as sensors. External agents such as humidity, temperature, etc. are responsible for the variation in electrical properties of an organic semiconductor. Thus, by employing this property of organic semiconductors, one can use organic thin films for sensing applications [34]. Organic semiconductor based sensors offer following advantages:

(a) simple deposition process of thin films;

(b) sensitivity to environmental agents;

(c) cost effectiveness for large-scale production;

(d) high electronic tunability;

(e) high absorption coefficient and

(f) flexibility.

1.8.1 Impedance Sensing

Impedance sensors show the output as change in capacitance and/or resistance for an input. For example, organic semiconductor CuPc thin film sensor output

impedance changes with respect to gas absorption, e.g. NO_2 gas [35]. Also, CNTs based sensors show change in their impedance value by changing ambient humidity.

1.8.2 Semiconductor Device Dependent Sensing

These sensors are of complex nature because the sensing mechanism can alter the device (sensor) characteristics, e.g. shift in diode characteristics, and change in OFET threshold voltage, etc. Hamilton *et al.* [36] reported the variation in drain current of organic polymer TFTs (OP-TFTs) when exposed to white light. Similarly, Bartic *et al.* [37] reported organic semiconductor poly (3-hexylthiophene) based OFETs as sensing devices for charge detection in an aqueous medium.

1.8.3 Resonant Dependent Sensing

In resonant based sensors, variation in the resonance frequency is measured for an applied input. This change in frequency is due to variation in sensing material properties such as changes in mass or wave propagation. Semiconducting organic polymers (Polyacetylenes) are reported to be extensively employed in humidity sensors as base materials for resonance dependent sensing [38].

1.8.4 Electrochemical Dependent Sensing

These type of sensors are mostly used as chemical dependent sensors. In such sensors, variations in cell current, cell resistance and electrode potential are observed with respect to different analyte [39].

1.8.5 Image Sensing

Image sensors are composed of an array of photodiode coupled with backplane in a 2D space where each pixel consists of a light sensing diode and switch. The data

collected from the 2D array of photodiode mapped in color or gray scale, which represents a image. High performance organic photodiodes are of great interest as image sensors. Yu *et al.* [40] reported image sensing arrays fabricated in full-color with greater dimensional area. For efficient readout, these sensors require high photosensitivity with greater dynamic range, fast response time, and low dark current.

1.8.6 Charged Particle Dependent Organic Semiconductor Sensing

In these sensors, variation in electrical properties of organic semiconductor is measured with the interaction of high energy particles, which is similar to inorganic semiconductor materials. Beckerle *et al.* [41] reported a mechanism to detect 5 MeV α-particle efficiently using organic polymer semiconductor polyacetylene as base material for its thin film sensor.

1.9 Dissertation Outline

This dissertation reports the fabrication and characterization of organic semiconductor and nanomaterials based devices/FETs. These fabricated devices have shown sensitivity towards different physical parameters like temperature, humidity, strain , pressure , displacement. Based on the device sensitivity towards physical parameters, these fabricated devices are termed as humidity, temperature, pressure and strain sensors. The sensors fabrication and characterization have been organized as follows:

Chapter 1 presented fundamental concepts pertaining to organic semiconductor materials their classifications, advantages of using them in electronics devices, fundamental properties of organic semiconductor based materials and different sensing mechanism has been discussed. A brief introduction to charge transport mechanism in organic semiconductor materials has also been discussed.

Chapter 2 focuses on previously reported studies related to historical evolution of organic semiconductor based electronic devices. A detailed review has been presented with special focus on organic semiconductor based temperature, humidity, strain, pressure, displacement and multifunctional sensors. A comparative analysis of various designs is presented and based on the reported data research gaps for future study are developed.

Chapter 3 discusses OFETs based sensors which can measure both ambient humidity as well as temperature. These sensors are designed, fabricated, and tested for their potential use by the relevant industry. The channel of the OFET was defined by an organic material comprising of OD (8 wt.%) and sugar (8 wt.%). The properties of OFETs were investigated as ambient humidity and temperature. It has been shown that fabricated OFETs are highly sensitive to both the variables and can potentially be employed by the industry as thermistor and as a posistor.

Chapter 4 discusses a novel and low-cost composite humidity sensor technology, developed to accommodate the needs of flexible electronics for various monitoring applications. Flexible humidity sensors are realized using a composite active layer. Finished devices are then tested in a chamber. Impedance and capacitance variations as a function of humidity and frequency have been evaluated. The designed sensors, in general, can be employed in any industrial process where humidity and temperature ought to be controlled including biomedical instrumentation.

Chapter 5 discusses multifunctional sensors (MFS) which can measure temperature, pressure and displacement. They are fabricated using OD sandwiched by CNTs and graphene materials. The developed sensor, as a single device, can be installed to assess temperature, pressure and displacement in an industrial application.

Chapter 6 discusses fabrication and characterization of strain sensors, realized using a composite of MWCNTs and silicon adhesive. The finished devices, after the fabrication, are characterized at various frequencies. The developed sensors are light weight and smaller in size and therefore, can potentially be used in wearable electronics and biomedical equipment.

Chapter 7 discusses the outcomes achieved from this research and proposes possible extension which can be carried out as a future work.

Chapter 2

Literature Review

This chapter presents a brief introduction and historical evolution of organic semiconductor devices and their potential use in the development of different sensors. The sensors discussed here are being used to measure some of the most important and common parameters which one encounters in many industrial and daily life applications. A brief description and introduction to the material system used in the fabrication of these sensors are also presented.

2.1 Organic Semiconductor Electronic

Organic materials were known to be electrically insulators till the observation of photoconductivity in anthracene. Anthracene was known to be the first photoconductive organic material [42]. In 1960's, basic phenomena of charge carrier transport and optical excitation was observed in organic molecular crystal [43]. From that point onward, researchers and scientists actively started to synthesize polymers and doped organic materials.

In the 20^{th} century, enhancement in organic materials conductivity has attracted researchers to investigate the potential use of organic semiconductor materials for devices to supplement conventional inorganic materials [44, 45]. During this period, many organic semiconductors were studied, and based on their electrical

properties [46] and field effect phenomena, they were employed in electroluminescence applications [47]. Experiments were also conducted to control the electrical conductivity of different organic materials. One such example is that of polyacetylene which forms a unique group of conducting polymers of which electrical conductivity can be controlled by adopting different dopants [48]. With an improvement in polyacetylene, insulator and its interface, the metal insulator semiconductor (MIS) diode and FET showed advancements in electronic devices, such as TFT and MIS-type solar cells [49]. Similar efforts in photovoltaic development have been reported in the early 1980's [50]. By the end of 1990, carbon-based semiconductor devices entered into commercialization phase and, then, OLEDs (organic light emitting diodes) were available for commercial use [51].

Naturally available organic polymers are mostly insulators. The first polymer synthesized with significant conductivity was polyacetylene (polyethyne). Its electrical conductivity was discovered by a group of scientists who received the Nobel Prize of physics in 2000 for this contribution [52]. Immediately after the discovery of improved conductivity, scientists shifted their focus from synthesis of organic materials to fabrication technologies. A CPU on a plastic film substrate was fabricated with operational frequency of more than 10 MHz [53, 54]. Similar efforts in the direction of high performance RF-CPU and 8-bit microprocessor fabrication took place by employing glass and flexible substrates, respectively [55, 56]. Processor fabrication was greatly influenced by the development and advancements in large-area printing techniques. They made possible the production of circuits in large volumes on extremely thin and flexible substrates [57]. The factors that are directly related to the printing process are: variation in threshold voltage, trapped charges, contact resistance and capacitance [58]. Thus, a new concept of device physics for printed TFTs was introduced, defining the relationship, and its mechanism between the electrical characteristics of printed devices and the rheology of inks. Keeping these parameters in view, Fakuda *et al.* in 2015, have successfully fabricated printed OTFT that possess uniform and excellent electrical characteristics [59].

Investigation in synthetic polymer and organic small molecules had gained importance due to their use in cost effective, thin and flexible products [60]. Flexible sensors can be employed conformably to soft and irregularly surfaces such as human skin and fabrics. The effects of material development on current state of printable and flexible sensor technologies have been discussed in [61, 62]. These studies claimed that these sensors are getting more space in biomedical industry because of their improved performance and ease in fabrication.

The milestone of next decade is the transistor's footprint reduction to nanometers. In [63, 64], a miniaturized *p*-channel transistor was fabricated using CNTs, which occupies less than half the space compared to leading silicon technologies. Wearable sensors for health monitoring are heavily relying on organic semiconductor technology and methods for improving such sensors are discussed in Ref. [65]. Efforts in the area of organic semiconductor photo-detectors had been reviewed along with their performance, working mechanism, recent advances and future expectations in [66]. Similarly, researchers have fabricated an organic transistor that works fairly well both under low and high current conditions [67]. Recent progress in the fabrication of organic semiconductors FETs and associated challenges are discussed in Ref. [62]. They highlighted that OFETs morphological and structural features play an important role in determining their electrical properties. Similar efforts for the detection of electro-physiological signals such as electrocardiogram (ECG) were discussed by Wang *et al.* in [68]. They reported a nanomesh organic electrochemical transistor (NMOECT) which is a unique structure designed for biomedical organic devices. This structure comprises of nanomesh structure on polyurethane nanofibers which can potentially be employed to detect biomedical signals.

Another milestone in OFETs technology was the development of low trap-state density OFET (LTDOFET). In 2020, Huang *et al.* reviewed LTDOFET technology and its applications towards sensor development. Low voltage OFETs were possible because of this innovation, which, in-turn, reduces the sub-gap trap-state

density at the channel interface [69]. This LTDOFET technology along with different material systems and solution processes had been used to develop different sensors like bio-chemical, gas, pressure, electro-physiological and photosensor.

The use of organic semiconductors/ nanomaterials based sensors is greatly increased in biomedical applications. Park *et al.* in 2020, [70] proposed an efficient biosensor for the detection of important brain hormone known as dopamine (DA). This sensor was a FET with liquid-ion interdigitated microelectrodes (IMEs) gate, fabricated using carboxylated polypyrrole nanotubes (CPNTs) and dopamine-specific aptamers. The performance of these FET sensors was at par with the standard DA aptasensors.

Progress in 2D covalent organic frameworks (COFs) has been an important area of interest among scientific community. These COFs respond to external stimuli, for instance, gas molecules, pH values, temperature, electricity, light, etc. Moreover, COFs, their working mechanisms and various design strategies are related to chemical sensors and photoelectronic devices [71]. Potential of organic semiconductors sensors in biomedical applications have been discussed very recently in Ref [72], where it has been observed that organic semiconductors have a bright future in medical industry because of the versatility and conformability which inherently carried by organic semiconductor devices. Historical development on organic semiconductor technology is outlined in Table 2.1.

TABLE 2.1: A summarized history of organic semiconductor electronics and its various developmental stages.

Author's	Year	Developments	Ref.
Györgyi	1946	Organic semiconductors electronics.	[44]
Dörgyi	1948	Weak electric conductance in dyes.	[45]
Akamatu *et al.*	1950	Introduction of organic semiconductors.	[46]
Bernanose	1955	Electroluminescence in organic solids.	[47]
Chiang *et al.*	1977	Metallic conductivity in polyacetylene.	[48]
Ebisawa *et al.*	1983	Polyacetylene based OFET.	[49]
Chamberlain	1983	Photovoltaic effect in organic materials.	[50]

Author's	Year	Developments	Ref.
Koezuka *et al.*	1987	Polythiophene based OTFT.	[51]
Frängsmyr	2000	Conductive polymers synthesis.	[52]
Takayama *et al.*	2004	CPU fabrication on plastic film substrate.	[53]
Karaki *et al.*	2005	8-Bits Flexible microprocessor.	[54]
Dembo *et al.*	2005	RF-CPUs on flexible substrates.	[55]
Jacques *et al.*	2006	Differential amplifiers using polysilicon TFTs.	[56]
Myny *et al.*	2014	CPU with inkjet printed memory.	[57]
Noh *et al.*	2015	Printed flexible TFT based RF sensors.	[58]
Fukuda *et al.*	2015	Printed OFETs abased amplifiers.	[59]
Dey *et al.*	2015	Organic semiconductors in nano devices.	[60]
Rim *et al.*	2016	Organic materials for flexible sensors.	[61]
Moy *et al.*	2017	Development of biomedical organic devices.	[62]
Cao *et al.*	2017	CNT based nano transistor.	[63]
Burgt *et al.*	2018	Organic neuromorphic computing.	[64]
Iee *et al.*	2018	Wearable sensors for health monitoring.	[65]
Wang *et al.*	2020	Nanomesh organic electrochemical transistor.	[68]
Huang *et al.*	2020	Low trap-state density OFET technology.	[69]
Park *et al.*	2020	Bio sesnor with liquid-ion gate FET.	[70]
She *et al.*	2021	Recent progress of 2D COFs.	[71]
Kim *et al.*	2022	Organic vs inorganic semiconductors in biomedical applications.	[72]

2.2 Temperature Sensors

Temperature sensors are widely used in industrial automation, control systems and medical technology. There has been significant advancement in modern technologies like Internet of Things (IOT), wearable electronics, smart packaging and

biomedical healthcare systems. Temperature assessment for high-tech applications requires sensors to be flexible, smaller, thinner and lighter for enabling their instalment on small area and, more importantly, making them cost effective.

OFETs based temperature sensors offer many advantages, for e.g., low production cost, multi-stimuli detectability, flexibility, integrability with peer devices, low cross sensitivity. Therefore, they are best suited for many real world applications.

Monitoring human vitals is of prime importance for correct diagnosis of health. Consequently, accurate measurement of temperature requires highly stable and efficient temperature sensors [73]. Moreover, recent progress in artificial skin, commonly, referred to as electronic skin (e-skin) fabrication essentially requires accurate temperature monitoring with conformal and spatial resolution. Thus, many organic material based flexible temperature sensor arrays are developed for precise temperature monitoring [74].

For real time monitoring of patient's vitals, such as, body temperature, heat flow, respiration rate and skin temperature, Jung *et al.* [75], in 2006, proposed organic semiconductor based flexible sensor system. These sensors have the ability to measure physiological parameters like strain and temperature. The sensors were fabricated employing pentacene TFTs and Wheatstone bridge structure. It is further proposed that integrating these sensors into textile structures will enable real time point of contact (POC) monitoring of a patient's vitals at an early stage of the disease.

In 2007, Jung *et al.* [76] proposed pentacene based TFTs temperature sensor and discussed transport mechanism in saturation and threshold region of operations. The reliability of these sensors was ensured by having a time delay of 60 to 300 s between two consecutive measurements. This time delay removed the bias stress created by trapped charges at dielectric–semiconductor interface. Furthermore, TFTs temperature dependence characteristics in the saturation region, at low temperature, is due to the transport of charges associated with thermally excited hopping mechanism. However, at relatively high temperature, mobility of carriers is yet to be determined.

In 2013, Chani *et al.* [77] explored thin films for temperature sensing by employing aluminum phthalocyanine chloride (AlPcCl) as their base material. They used 50 nm thick electrodes sitting at the gap of 50 μm. A $50-100$ nm thick organic film was used to define the channel of the device and the measurements were performed to assess sensors' sensitivity by varying the temperature $25-80$ °C. They also simulated the response of the sensors and showed 99% accuracy between modelled and experimental data. Organic thermistor and OFETs based organic temperature sensors were demonstrated by Ren *et al.* [78], in 2013. The fabricated sensors had large dynamic range with operating temperature from 20 to 70 °C. The developed sensors had high resolution which made them suitable for applications, such as, electronic skin and large-area thermal sensing array.

A new technique for low voltage temperature sensors built on flexible plastic substrate has been reported in 2014 by Cosseddu *et al.* [79]. Fabricated sensors can operate reliably for temperature range from 10 to 40 °C. The proposed architecture paved way for applications like tactile sensing and wearable electronics.

In 2015, Wu *et al.* [80] proposed a flexible temperature sensing array using OFETs for biomaterial applications. The sensors showed highly stable thermal response up to 200 °C. Proposed sensors had good potential to be used in artificial skin applications. Performance comparison between traditional biomaterial polylactide (PLA) and the newly synthesized three-arm stereo complex PLA (tascPLA) demonstrated that the thermal stability of the later material is twice compared to its counterpart. The developed devices showed good sensitivity to temperature. The OFETs fabricated with tascPLA substrate/dielectric layers proved to be transparent, flexible, thermally stable, sensitive towards high-temperature and biocompatible. These features make them suitable for applications like implantable medical devices. Furthermore, an array of the fabricated tascPLA–OFETs was developed which efficiently detected a 2D temperature field.

Ren *et al.* [81], in 2016, demonstrated an array of flexible temperature sensor and showed its application in biomedical. Poly(ethylene naphthalate) (PEN) is used as a flexible substrate and Al as dielectric material which exhibited low voltage

operation (4 V) and relatively small leakage current approximately tens of pA. The operational range varies from 20–100 °C. The conductivity and sensitivity of thermistor were tunable and it has been shown that a 16×16 OFET array provided a 2D temperature information for any shape of object in contact. The developed array has a wide range of applications such as remote sensing environments, e-skin and biomedical.

In 2016, Nakayama *et al.* [82] presented an organic temperature detector that consists of flexible sensors integrated with a read-out circuit (comparator). The output of detector was a digital signal that showed the relative magnitude correlation between the sensor temperature with respect to a threshold value. A 2-bit parallel ADC was also fabricated as a read-out circuit, and analog-to-digital conversion of the sensor signal was shown.

Ye *et al.* [83] in 2016, analyzed and investigated the temperature dependent electrical properties of F_{16}CuPc/α6T heterojunction based OFETs temperature sensors. It has been shown that the charge mobility in these temperature sensors is associated with heat driven hopping process. The fabricated devices were analyzed for thermal activation energy (EA) at different temperatures. The value of EA = 40.1 meV for temperature over 200 K was reported. For temperature range 100 to 200 K, the value of EA was 16.3 meV and the charge transport mechanism was mainly controlled by shallow traps. Finally, for temperatures above 200 K, it has been shown that there is an inverse relationship between V_T and temperature. The observed variation in V_T due to the interface dipolar charges is 0.185 V/K, which is greater than the variation observed in single layer devices, i.e $V_T \sim 0.020$ V/K. It was concluded that these devices could be employed as temperature sensors to be operated at relatively lower voltages.

In 2017, flexible thermal sensors have been developed by Song *et al.* [84]. These sensors showed $p-$type transistor characteristics for temperature range 25–100 °C. The hole mobility evaluated for these sensors increased linearly with increasing values of temperature. Another such contribution in the area of flexible sensors based on OFETs was made in 2018 by Manda *et al.* [85]. They fabricated

sensors using flexible poly(ethylene terephthalate) substrate. The fabricated devices exhibited high temperature sensitivity for temperature range 20–45 °C, low power consumption (micro watts) and ultrafast response time ($\sim$ 24 ms). The performance stability of these sensors was also demonstrated by applying extreme conditions such as under water use, exposure to solution of various pH values and salt concentrations. It has been reported that these sensors are well suited for healthcare applications.

Subbar *et al.* , in 2018, reported a novel tri-layer temperature sensor which showed exceptional ambient stability and efficiency [86]. Tri-layer devices exhibited relatively high sensitivity for temperature range −30 to 80 °C, which made them a preferred candidate for many medical applications.

In 2018, Agarwal *et al.* [87] developed organic temperature sensors based on asymmetric metal insulator semiconductor capacitor with electrically tunable sensing area. Strong temperature dependence has been reported by an area-asymmetric organic metal-insulator (AMIS) capacitor. The designed structure was asymmetric and poly-4-vinyl-phenol/pentacene was used as the device organic material which exhibited a relatively high temperature coefficient. Their fabricated sensors exhibited higher sensitivity as the temperature dependent mobility of the channel carriers was controlled by the sensor threshold voltage for a given frequency.

Today's wearable electronics is considered a cutting edge technology. Key factors of such devices include stretchability and conformability without compromising on their electrical performance. Zhu *et al.* [88], in 2019, demonstrated an organic thin film flexible and stretchable temperature sensor. This sensor had the ability to respond to strain and temperature, simultaneously, and the observed accuracy was within 1 °C with 0%–30% uniaxial strains.

Haque *et al.* [89] in 2020, reported methylammonium lead iodide ($MAPbI_3$) TFT temperature sensor without an encapsulation layer. This sensor utilizes ambipolar transport mechanism to enhance temperature range and sensitivity which made $MAPbI_3$ TFT temperature sensor a potential candidate for stable, simple and cost-effective monolithic integration.

An important characteristic of a physical sensor is that it should have stable performance after many operational cycles. Rullyani *et al.* [90], in 2020 , fabricated flexible temperature sensors with detection range $30 - 45$ °C. They employed poly(N-isopropylacrylamide) and pentacene to fabricate these sensors and reported results for more than 100 bending cycles thus, paving the way for flexible and wearable monitoring devices.

In order to avoid wide spread pollution from electronic devices, there is a dire need to shift towards green electronics. One such effort in the development of green temperature sensor was reported in 2020, by Ravariu *et al.* [91]. They fabricated organic transistors at room temperature using para-aminobenzoic acid (PABA) grafted to ferrite nanoparticles. The comparison was also made between PABA-NCS and pentacne based devices, and it was concluded that PABA-NCS device showed superior I_{ON}/I_{OFF} ratio. Thus, fabrication of PABA-NCS organic transistors presents promising characteristics for the future green electronics.

An overview of recent developments in temperature sensors is presented in [92, 93]. In these articles, authors have presented a detailed classification of temperature sensors based on their working mechanism. It has been summarized that working mechanism does not affect significantly the sensor parameters like sensitivity etc. However, material type used to fabricate a sensor plays the main role in determining the power consumption and operational characteristics of a temperature sensor. Historical development of organic semiconductor based temperature sensors is outlined in Table 2.2.

TABLE 2.2: A summarized review of evolutionary research work carried out in the development of organic temperature sensors.

Author's	Year	Developments	Ref.
Jung *et al.*	2006	Pentacene based temperature sensor.	[75]
Jung *et al.*	2007	Transport mechanism in Pentacene sensor.	[76]
Chani *et al.*	2013	AlPcCl based temperature sensor	[77]
Ren *et al.*	2013	OFET based temperature sensor.	[78]
Cosseddu *et al.*	2014	Flexible temperature sensor.	[79]

Author's	Year	Developments	Ref.
Wu *et al.*	2015	OFET based flexible temperature sensor.	[80]
Ren *et al.*	2016	Array of flexible temperature sensor.	[81]
Nakayama *et al.*	2016	Flexible sensors and read-out circuits.	[82]
Ye *et al.*	2016	OTFTs based heterojunction sensors.	[83]
Song *et al.*	2016	Sensors for temperature ranges $25 - 100$ °C.	[84]
Manda *et al.*	2018	Ultra fast physiological-temperature sensors.	[85]
Subbarao *et al.*	2018	CuPc thin film based temperature sensor.	[86]
Agarwal *et al.*	2018	Tunable organic temperature sensor.	[87]
Zhu *et al.*	2019	Stretchable temperature sensor.	[88]
Haque *et al.*	2020	Perovskite temperature sensor.	[89]
Rullyani *et al.*	2020	Stimuli responsive polymer sensor.	[90]
Ravariu *et al.*	2020	Green temperature sensor.	[91]
Zhu *et al.*	2021	Temperature sensors for e-skin applications.	[92]
Polena *et al.*	2022	Progress in OFET-based temperature sensors.	[93]

2.3 Humidity Sensors

Humidity is an important physical parameter as it affects all forms of life whether living (humans) or non-living (materials). Scientific community and researchers have been continually exploring techniques to develop and explore materials for humidity sensors which should offer good stability, durability, fast response and recovery time; high in linearity and low hysteresis. Humidity sensors usually employ carbonaceous materials which change its capacitive and resistive properties as a function of ambient humidity. Effects of humidity on electrical resistance of single walled carbon nanotube (SWCNT), suspended single walled carbon nanotube (SSWCNT) and multi walled carbon nano tube (MWCNT) are discussed in [94]. Electrical impedance spectroscopy of the SWCNT films has given an insight regarding sensor performance and conduction behaviour which was observed as a

function of frequency and humidity. Based on the doping of SWCNT (undoped or Li-doped), different humidity ranges were achieved. Various film parameters like SWCNT material properties, orientation in network, concentration, and film thickness, etc. were discussed in [94].

The humidity-sensing characteristics of aligned suspended single-walled carbon nanotube films were presented in Ref. [95]. A comparison between suspended and non-suspended architectures was carried out by recording the change in resistance of the nanotubes under humidity effects. In [96], humidity effects on the properties of MWCNT epoxy nanocomposites were studied by varying frequency from 40 Hz to 110 MHz. The authors prepared MWCNT epoxy nanocomposites with different MWCNT concentrations by direct mixing method, and the composites were deposited on the glass epoxy substrate using stencil printing technique. The overall impedance of the nanocomposites tends to increase with the increase of the humidity, and the humidity effects tend to decrease with the increase of MWCNT concentration. Theoretical and experimental data on the working principles of nanotubes have been presented in Ref. [97].

In 2020, Anichini *et al.* [98] proposed a novel humidity sensor based on reduced graphene oxide (rGO) combined with hydrophilic moieties, i.e. tetraethylene glycol chains. Compared to pristine rGO, the hybrid material exhibits improved sensing performance. The developed sensor showed high sensitivity i.e an increase of 31% resistance from 2% to 97% humidity. The sensor also showed ultrafast response time of 25 ms with good reliability and repeatability towards moisture.

In 2021, Afzal *et al.* [99] proposed a surface type humidity sensor. The sensor was fabricated by depositing methyl green (MG) thin film between Al electrodes (Al/MG/Al). The change in resistance and capacitance of the sensor was observed while varying RH of the chamber. The sensor was tested for 32% to 85% RH at 1, 10 and 100 kHz. It was concluded that RH is directly proportional to capacitance and inversely to resistance. The sensors response and recovery time was reported to be 200 and 60 seconds, respectively.

Mohammedture *et al.* [100], in 2021, optimized different variables involved in defining the performance of a humidity sensor. They concluded that geometrical optimization is equally important besides material optimization. They reached to this conclusion by simulating and modeling graphene oxide based humidity sensor using COMSOL Multiphysics software. They found that response time of sensor improves many fold by decreasing the upper electrodes width and increasing inter-electrode spacing.

A vertically aligned multiwalled carbon nanotube (VA-MWCNT) based humidity sensor was fabricated by Wang *et al.* [101], in 2021. The fabricated sensor is well suited for mass production because of its fabrication technique and low manufacturing cost. The fabricated sensor displayed good linearity for 40 to 90% RH, low hysteresis (H = 1.5% RH), fast response (3.3 s) and high stability and repeatability. All these performance parameters made the VA-MWCNT sensor a promising candidate for humidity sensing.

A flexible humidity sensor made from cellulose nanofiber/carbon black (CNF/CB) composite was proposed in 2022 by Tachibana *et al.* [102]. The use of cellulose nanofiber helped in ink preparation and printing processes. The hydrophilic and porous nature of base material also enhanced the sensitivity and response time of the sensor. The sensor responded to humidity ranging from 30% to 90% RH and recovery time of 10 and 6 seconds, respectively. The reported sensor can be used in monitoring human respiration etc. Table 2.3 summarizes the recent development in organic semiconductor based humidity sensors.

TABLE 2.3: A brief overview representing technological growth observed in organic semiconductor humidity sensors.

Author's	Year	Developments	Ref.
Arunachalam *et al.*	2018	Humidity sensor fabricated using suspended carbon nanotubes.	[95]
Sanli *et al.*	2018	Impedance variation due to humidity in MWCNT epoxy.	[96]

Author's	Year	Developments	Ref.
Zaporotskova *et al.*	2018	Carbon nanotubes based humidity sensors as modern electronics.	[97]
Anichini *et al.*	2020	Novel humidity sensor based on 2D material with improved performance.	[98]
Afzal *et al.*	2021	Surface type humidity sensor with increased sensing area.	[99]
Mohammedture *et al.*	2021	Optimization of humidity sensor parameters using COMSOL Multiphysics software.	[100]
Wang *et al.*	2021	Vertically aligned multiwall carbon nanotubes based humidity sensors.	[101]
Tachibana *et al.*	2022	Cellulose Nanofiber/Carbon Black (CNF/CB) composite based flexible humidity sensors.	[102]

2.4 Strain Sensors

Electromechanical transducers based on piezoresistive effect have been reported by research groups for their use in strain sensing applications. These sensors showed good strain sensitivity for larger stain values. However, for lower strain values, new materials are to be explored to achieve good gauge factor and sensitivity. Among new materials, recently explored CNTs showed impressive properties. The unique atomic structure of the CNTs allows to achieve high sensitivity even for a smaller size [103].

In recent past, the researchers have shown a great interest in investigating electromechanical properties of CNTs; especially, the piezoresistive properties for designing new micro-strain sensors. Various pressure sensors and accelerometers based on CNTs which exploit their piezoresistive properties were also studied and reported in [103, 104].

In 2003, Cao *et al.* [103] reported the piezoresistive sensitivity of strain sensors which was 600 to 1000 under axial strain−fabricated using small band-gap quasi-metallic nanotubes. These values are much higher compared to those sensors fabricated using metallic nanotubes. The piezoresistive effect of p-CNT film was observed and reported in 2003 by Li *et al.* [104], and it was found that the sensitivity was equal to 65 under 500 micro-strains at room temperature. Regoliosi *et al.* [105], in 2004, showed deformation (mechanical) vs conductivity relationship of free standing membranes of SWCNTs and reported piezoresistive sensitivity which was $2.3 - 2.5$ times higher when compared with Si substrate. In 2005, Grow *et al.* [106] investigated CNTs piezoresistance on deformable thin-film SiN membranes and assessed variation in electronic transport as a function of strain. They also estimated band gap of the material and observed strain-induced variation in electrical properties of the sensor. Stampfer *et al.* [107] reported sensors based on nano-electromechanical piezoresistance properties using SWNTs. Their theoretical and experimental findings showed that the SWNTs exhibit non-linear piezoresistive sensitivities up to 1500 under 1% applied strain. Xue and Cui [108], in 2007, studied TFTs based on SWCNT on a flexible (plastic) substrate and observed the variation in resistance upon bending the substrate.

In 2007, Liu *et al.* [109] fabricated strain sensors for bio-mechanical implants using MWCNT-poly (L-lactide) (PLLA) nanocomposite. They observed that the mixing of PLLA with MWCNTs improves load tranfer characteristics by providing better interfacial bonding between polymer and carbon nanotubes. Their fabricated sensors exhibited linear response with relatively higher sensitivity. Vemuru *et al.* [110], in 2009, investigated strain sensing properties of MWCNT film. The aim of their study was to evaluate the effectiveness of MWCNTs in strain sensors technology. They observed real time strain response of MWCNTs under tensile load and found a linear relationship between measured voltages and the applied load. They also investigated electro-mechanical properties of MWCNT film and found that these characteristics are fully reversible after removing the load. Additionally, they studied variation in the device characteristics as a function of temperature and reported promising results and established potential use of their devices as

a temperature sensors. In 2011, N. Hu *et al.* [111] reviewed the advancements on piezoresistive strain sensors utilizing CNT based polymer nano-composites. In this review, they established that CNT offers a promising alternative as a sensing material when compared with other smart materials currently employed by the sensor industry. They reached to this conclusion by comparing electrical and physical data of the devices fabricated using CNT and other materials. Obitayo and Liu [112], in 2012, reviewed piezoresistive strain sensors based on CNTs and showed that CNTs sensors provide a predictable and stable response. They reported that CNT based strain sensor can be employed both at nano and micro scales. They also reported that CNT changes its band structure under strain and this property made CNT a promising candidate for strain sensor technology. In 2014, Grabowski *et al.* [113] developed CNTs and epoxy based strain sensors by employing a simplified fabrication technique i.e. screen printing. They tested the fabricated sensors by varying loads and observed that the screen printing technique offers an economically viable option for the fabrication of CNT/epoxy based strain sensors. Saleem *et al.* [114], in 2015, investigated strain sensors based on twin and uniform crystals of TCNQ ion-radical salts. They studied the sensitivity of the sensors and found that the twined crystals fabricated using a chemical process offer sensitivity between $4000 - 6000$ compared to uniform crystals. Sapra *et al.* [115] reported that in contrast to conventional strain sensors, CNTs sensors have high gauge factor ($\sim$22.4) at nano and macro scales. Furthermore, In 2015, Yasin *et al.* [116] investigated polymer-fullerene bulk heterojunction based flexible strain sensor worked on the principal of OFET.

OFETs using flexible materials like rubrene single-crystal nano belts, PMMA dielectric, and PET substrate were fabricated by Wang *et al.* [117], in 2017. It was reported that the sensor under tensile and compressive strain changes its current. While the field-dependant mobility showed a linear response under the same experimentation. On the other hand, fabricated sensors exhibited repeatable response when subjected to strain conditions. Thus, they showed suitability for automation and biomedical applications.

Another effort in the development of flexible strain sensor was made by the same group, i.e Wang *et al.* , in 2018 by using rubrene single crystal as the sensing material [118]. The proposed device was a two terminal device built upon a flexible PET substrate. Its operational principle involved modulation of intermolecular distance of organic crystal under applied strain; whereas, in OFET based strain sensors, the device behaviour is explained using the concept of grain boundary spacing. The proposed sensor exhibited excellent sensitivity by showing a gauge-factor of 279. The study also carried out to show a comparison between different stain sensors, and it was demonstrated that their technology offered better performance relative to conventional counterparts. These sensors can be used to detect physical movements of a human body, such as, breathing and limbs bending.

Key component in wearable electronic devices is a fiber which should be sensitive, stretchable and flexible in nature. In 2019, You *et al.* [119] proposed a graphene-based fiber strain sensor which was fabricated by immersion of graphene sheets in poly(dimethyl siloxane) (PDMS) matrix via direct ink extrusion which can respond to different deformations such as bending, twisting, compressing, and stretching. The sensor can be used for 600 cycles of stretch and release process, and the output signal has less than 6.2% attenuation. This sensor has wide application as wearable strain sensors for real time human motion monitoring.

Wearable electronic devices such as fabric based strain sensors have attracted tremendous attention, because they are light-weight and have good air permeability. However, the technology is still striving to get maturity in order to achieve improved stability and better sensitivity for a wider operational range. One such development was reported by Jin *et al.* in 2022, [120]. They developed a fabric like strain sensor using rGO and reinforced polyaniline (PANI). This sensor exhibited gauge factor of 24, operational range 0.2%–50% with good mechanical durability and sensitivity. The sensor can comfortably be used for 1500 stretching/releasing cycles test. This technology could be a game changer and might open new avenues in control and medical fields.

Flexible electronics has presently gained much importance in medical applications, and in this regards, different types of yarn for strain sensing has been developed. In 2022, Tang *et al.* [121] also proposed such strain-sensing yarn. The yarn was composed of carbon black particles, CNTs, and graphene flakes. This yarn has medical use like smart medicated plaster that can detect motions in the rehabilitation of joint pain by simple sewing.

Strain sensors encapsulation layer has its merits and demerits. It has been discussed in literature that strain sensors without encapsulation layer had good gauge factor but it limits their operational range. Lv *et al.* explored in 2022, this aspect and proposed a strain sensor with high gauge factor and extended strain range [122]. The sensing material was rGO with ultra thin polyurethane (PU) as encapsulation layer. The operational range of the proposed sensor can reach 51%, with gauge factor lied in the range of $8.02 - 125.05$. The effect of thickness of encapsulated layer on the developed strain sensor was also investigated. Finally, the sensor was used to fabricate smart gloves that has the ability to distinguish ten different gestures. This work could have huge applications in robotics and human-machine interaction.

A detailed review about strain sensors operational mechanism and their potential applications was discussed in 2022 by Ma *et al.* in [123]. They categorized the transition mechanisms observed in these sensors as: a) resistive; b) capacitive; c) inductive and d) piezoelectric or triboelectric etc. They also reviewed and compared the performance parameters of different strain sensors based on their sensing mechanism. Table 2.4 summarizes the recent development in organic semiconductor based strain sensors as discussed in the preceding paragraphs:

TABLE 2.4: Developments in organic semiconductor based strain sensors.

Author's	Year	Developments	Ref.
Cao *et al.*	2003	Flexible strain sensor based on CNTs.	[103]
Li *et al.*	2003	Piezoresistive effects in CNTs films.	[104]
Regoliosi *et al.*	2004	Piezoresistive effects in SWCNTs.	[105]
Grow *et al.*	2005	Piezoresistance in deformable CNTs film.	[106]

Author's	Year	Developments	Ref.
Stampfer *et al.*	2007	SWCNTs vs piezoresistive properties.	[107]
Xue *et al.*	2007	CNTs sensor with conformal characteristics.	[108]
Liu *et al.*	2007	Biomedical MWCNTs strain sensors.	[109]
Vemuru *et al.*	2009	Properties of MWCNTs strain sensors.	[110]
Alamusi *et al.*	2011	CNTs sensors with polymer nano-composites.	[111]
Obitayo *et al.*	2012	Review on CNTs piezoresistive sensors.	[112]
Grabowski *et al.*	2014	Strain sensors using screen printing.	[113]
Saleem *et al.*	2015	TCNQ compound based strain sensors.	[114]
Sapra *et al.*	2015	Strain sensors with high gauge-factor.	[115]
Yasin *et al.*	2015	Flexible strain sensors using TFTs.	[116]
Wang *et al.*	2017	OFETs for ultra-sensitive strain sensing.	[117]
Wang *et al.*	2018	Rubrene single-crystal based strain sensors.	[118]
You *et al.*	2019	Flexible wearable strain sensors.	[119]
Jin *et al.*	2022	Highly sensitive biomedical strain sensors.	[120]
Tang *et al.*	2022	Strain sensing yarn for medical applications.	[121]
Lv *et al.*	2022	Ultra thin gesture recognition sensors.	[122]
Ma *et al.*	2022	Review on strain sensors working mechanisms.	[123]

2.5 Pressure and Displacement Sensors

Efforts are being made in the development of organic semiconductor based pressure and displacement sensors, as these have wider applications in flexible and wearable electronics, biomedical devices and robotics. In 2017, Ma *et al.* [124], presented a high resolution, low cost and self powered 2D sensor. They used PDMS and carbon fibers to fabricate 2D sensor. The sensor had response time of ∼68 ms with sensitivity of 0.055 nAKPa^{-1}. Due to its flexible nature, the fabricated device could be employed on a curved surface including the human skin referred to as e-skin.

Fabrication of pressure sensor that has a good sensitivity with low hysteresis is considered as a challenging task. In 2019, Choi *et al.* [125] developed a capacitive pressure sensor which was fabricated using porous ecoflex-multiwalled carbon nanotube composite (PEMC) structures. The sensor was simpler in design and cost-effective. The sensitivity of the device was measured and found as 6.42 and 1.72 kPa^{-1} for a range of $0-2$ and $2-10$ kPa, respectively. It has been reported that the developed sensor can be employed in blood pressure assessment instruments.

In 2021, Mishra *et al.* [126] presented an overview regarding the developments of pressure sensors based on capacitive sensing techniques. The overview of capacitive pressure sensors includes: operating mechanism, material suitability, fabrication technique and applications. Capacitive pressure sensors, in simple words, resembled a parallel plate capacitor having a dielectric material in between. A variation in plate distance, because of external pressure, changes the capacitance which is usually measured and translated into pressure. The sensitivity of the sensor can be improved through various techniques including its dielectric material. It has been discussed by Mishra *et al.* that CNTs or metallic nanoparticles embedded in elastomers are considered good candidates for such applications.

In 2021, Cao *et al.* [127] reviewed the developments of 3D graphene based pressure sensors. The authors discussed various methods involved in the preparation of graphene based sensing material along with their potential applications in different piezoresistive sensors. In the end, a comprehensive survey was presented describing the challenges faced and future prospects of the pressure sensors.

A novel pressure sensor was proposed by Zaho *et al.* in [128] in 2021. The sensor was based on MWCNTs and laser-induced graphene. The device was fabricated using laser direct writing technique. The developed sensor offered relatively improved sensitivity for detection limit ~ 1.2 Pa. Its durability was assessed and it was observed that its performance remained stable for more than 2000 cycles with 2 ms as response/recovery time. Due to its improved exhibited performance, the device is considered to be a good candidate for wearable electronic.

Flexible pressure sensors and arrays that can retain their sensing ability for arbitrary deformation are vital for wider applications, such as: prosthetics, robotics, healthcare, human–machine interface and e-skin. An overview covering design and fabrication of flexible pressure sensor arrays is presented in 2022 by Duan *et al.* in [129]. A critical analysis was made and some issues faced by the industry were identified. Additionally, the authors discussed latest technological status of pressure sensor arrays and their potential applications in the industry such as, healthcare and aerospace.

For e-skin applications, sensitivity and flexibility are of prime importance for any type of a pressure sensor. In 2022, Gilanizadehdizaj *et al.* in [130] reported a pressure sensor having high sensitivity and good flexibility. The device was fabricated using rGO grown on a flexible PCB. The fabricated piezoresistive pressure sensors possessed many features such as mechanical stability, high sensitivity and wider operational range 0–30 kPa. The reported sensitivity was 0.13 kPa^{-1} for a pressure value less than 10 kPa and it was 0.05 kPa^{-1} for pressure higher than 10 kPa. While considering sensitivity and detection in linear range of a sensor, it is of paramount importance to have an optimum working point for improved system performance. Wang *et al.* [131], in 2022, addressed this problem by proposing a novel structure device called dual conducting layer dome (DCLD). This DCLD structure has a Ag nanowire and a low conducting layer of carbon black nanoparticles and PDMS. The device was fabricated by complying to the following sequence: a) scratch coating; b) followed by dip-coating and c) vacuum adsorption. The sensitivity of the fabricated devices was reported as 51.7 kPa^{-1} for pressure range 0.01–250 kPa. It has been explained that for long cycles, sensors based on DCLD offered better performance compared to PDMS based sensors. Table 2.5 presents a summary of organic semiconductor based pressure and displacement sensors.

TABLE 2.5: Presents a summarized view of pressure & displacement sensors developed using organic semiconductor materials.

Author's	Year	Developments	Ref.
Ma *et al.*	2017	Self-powered artificial e-skin.	[124]
Choi *et al.*	2019	Capacitive pressure sensor.	[125]

Author's	Year	Developments	Ref.
Mishra *et al.*	2021	MWCNTs and graphene based sensors.	[126]
Cao *et al.*	2021	3D graphene based pressure sensors.	[127]
Zaho *et al.*	2021	Highly responsive flexible pressure sensors.	[128]
Duan *et al.*	2022	Latest development in pressure sensor arrays.	[129]
Gilanizadehdizaj *et al.*	2022	Flexible piezoresistive pressure sensor arrays.	[130]
Wang *et al.*	2022	Dual conductive layer pressure sensors.	[131]

2.6 Multifunctional Sensors (MFS)

Multifunctional sensors (MFS) have the ability to sense multiple parameters, e.g. illumination, strain, pressure, displacement, temperature, humidity etc. For many years, a number of MFS, which can be used in different areas of technology and environmental assessment, have been fabricated and investigated. A sensor array featuring capacitive touch was fabricated by using flexible electrodes employing simple process with low strain response [132]. In [133], MFS were fabricated for detecting solutions pH-values, solvent type and ethanol percentage in water. The integration of electrical, mechanical and electromechanical properties of MFS material such as CNTs is considered a major challenge, and this issue has been discussed in detail in [134]. The authors in [135] investigated the properties of pristine OD, CNT, and graphene powders based MFS for displacement, pressure, and temperature measurements, and their potential use in the industry.

In 2013, Martin *et al.* [136] compared MWCNTs and thermally reduced functionalized graphene sheets (FGSs) in an epoxy resin. While comparing the data, they found that mechanical performance of the FGS nanocomposites was far better than the MWCNTs. An improvement of 50% and 15% of Young's modulus and strength was noted, respectively. These observed characteristics i.e. low viscosity and improved mechanical strength made FGS a great candidate to develop MFS.

To overcome high cost, low precision and operational difficulties, Yao *et al.* in 2014, developed MFS to measure oil, water, and salt contents using conductivity and ultrasound method [137]. Liu *et al.* in 2016, developed stretchable MFS to measure strain, pressure and finger touch [138]. These sensors employed the principle of capacitive sensing. The electrodes used were silver nano-wires and the base dielectric was ecoflex material. MF tactile sensors were fabricated to collect information regarding tactile interactions between a sensor and targeted object. These sensors work on the principle of piezo- and pyro-electric (ferroelectric) properties of polymeric materials. A MF stretchable and transparent sensor technology to measure atmospheric humidity and gas concentration is reported by [139].

In 2020, Chani *et al.* [140] investigated and fabricated MWCNTs and graphene pristine powders based MFS. These MFS can measure pressure, displacement and gradient of temperature. The sensor was able to measure pressure from $0 - 1.65$ kgf/cm^2 and the effect of temperature gradient from $34 - 36$ °C was also reported. Additionally, longitudinal compressive displacement up to 100 μm was studied by exploiting the resistive properties of the sensor. It has been shown that the resistance, Seebeck coefficient, thermoelectric voltage of the CNT and graphene powder decreases with increasing pressure, while the thermoelectric current increases with increasing values of pressure. The increase in longitudinal displacement resulted in the compression of the samples that caused a decrease in resistance of the sample especially, for the samples made from CNT and graphene.

In 2021, Chani *et al.* [141] presented rubber-CNTs-OD nanocomposite based resistive and impedimetric MFS. These MFS can be used for displacement, pressure, force, humidity and temperature sensing. It has been demonstrated by the authors that resistance and impedance of the sensors decrease by changing compressive displacement, pressure, humidity and temperature.

TABLE 2.6: Shows a chronological sequence experienced by the industry while developing organic semiconductor based multifunctional sensors (MFS).

Author's	Year	Developments	Ref.
Terada *et al.*	1983	Development of MFS.	[132]

Author's	Year	Developments	Ref.
Dario *et al.*	1985	Composite MF tactile sensors.	[133]
Mahar *et al.*	2007	CNTs based MFS-A review.	[134]
Cheng *et al.*	2011	Graphene & CNTs composite electrodes MFS.	[135]
M-Gallego *et al.*	2013	Fictionalized graphene sheets for MFS.	[136]
Yao *et al.*	2014	MFS using printed stretchable conductors.	[137]
Liu *et al.*	2016	MFS for oil, salt and crude oil.	[138]
Choi *et al.*	2017	MF stretchable and transparent touch sensors.	[139]
Chani *et al.*	2020	MWCNTs/graphene pristine based MFS.	[140]
Chani *et al.*	2021	Rubber-CNTs-OD based MFS.	[141]
Chani *et al.*	2022	MFS using NiPc–CNT–oil composite.	[142]

In 2022, Chani *et al.* [142] presented another MFS recipe, which could measure pressure, displacement, humidity, temperature and mechanical vibrations. The device was resistive in nature and fabricated using of NiPc–CNT–oil composite. The resistance and impedance were investigated by changing associated physical parameters. For pressure ranging $0 - 850$ gf/cm^2 and displacement $0 - 50$ μm, the resistance and the impedance decreased, on the average, 1.08 and 1.04 times, respectively. Similarly, for humidity values from 60% to 90% RH and the temperature from 25 to 43 °C, the observed decrease in resistance and impedance (R & Z) was up to 1.04 times and 1.05 times, respectively. Moreover, to gauge vibration, a decrease in R & Z up to 1.03 times, was reported. The authors claimed that the developed sensors can be used in various medical applications. Table 2.6 summarizes the recent development in organic semiconductor based MFS.

2.7 Dissertation Motivation

Keeping in view the data of literature survey presented in the preceding sections one can conclude that sensors are playing an important role in providing ease

to human life. Additionally, the industrial automation and environmental data acquisition is heavily dependent on sensors technology. To make this technology convenient, reliable, accurate and cheaper, a special attention is to be given on: a) sensor design; b) material involved in a sensor fabrication; c) an accurate characterization of sensing material; d) sensitivity of the sensing material; e) durability; f) multifunctionality and compatibility of the design.

It is evident from the literature review that CNTs, graphene and their composite can be exploited further by organic sensors fabrication industry to achieve sensitive, linear and multifunctional characteristics. Repeatability and functional durability are other notable challenges which are currently faced by organic semiconductor based sensor industry. In the nutshell, the dissertation in-hand aims to deal with fabrication and characterization of sensors that are: a) novel in design along with ease in fabrication; b) cheaper in cost c) improved in performance such as: sensitivity, reproducibility, reliability etc., when compared to those listed in the literature. The strength of the proposed design shall be established through a comparative analysis. Defining a realistic and achievable target and keeping in view their potential applications, it has been decided that the following questions shall be answered while working on this dissertation:

2.7.1 Research Objectives

The primary objective of this research is to explore sensors based on organic and nano-materials as an economical alternative to exiting state-of-the-art sensor technology. The proposed sensors should have wider adaptability in various industries and can be utilized in medical technologies and environmental applications.

Following are the research objectives, which would possibly be addressed during the course of this research.

1. To design, fabricate and characterize humidity sensors by employing orange dye (OD) as sensing material. The design of the device should be optimized

keeping in view the fabrication ease, but not on the expense of device performance. The design should have compatibility with organic semiconductor device technology. The characterization of sensing material (OD) should be carried out to achieve maximum sensitivity and linearity by exploring both two and three terminal designs. The response of the device with respect to other environmental variables such as ambient temperature etc, would also be checked to assess the device multifunctionality, if any.

2. To investigate the properties of pristine OD/CNTs/graphene composite as a function of pressure, temperature and displacement for their potential use in MFS. After characterization, sensors would be fabricated by varying the thickness of OD, and its effects on the sensitivity of the sensors would be assessed. It is assumed that, the proposed MFS could potentially replace individual sensors usually employed in the industry to measure displacement, pressure and temperature.

3. To develop flexible humidity sensors using a composite comprising of OD/-graphene/silicon adhesive, so that it can comfortably be integrated to flexible electronics. These sensors would be optimized involving low-cost substrate (rubber) coupled with simple device design to make them cost effective, light weight, suitable for hand-held gadgets and should be conformal to human skin.

4. To develop strain sensors using CNTs or any other suitable material to define sensing composite. To keep the cost low, simple fabrication technique would be applied such as drop-casting. Furthermore, to make the sensor versatile, efforts would be made to have the sensor fabricated on flexible substrate.

2.8 Summary

In this chapter, a comprehensive literature survey of organic semiconductor technology, its associated material, including nanomaterials based sensors and their

potential applications have been discussed. It has been shown that organic semiconductor electronics has got a great potential in industrial automation, environmental assessment and biomedical applications. An increased use of organic semiconductor technology has been witnessed because of the ease associated with organic semiconductor materials and their fabrication technology. It has been noticed that nanomaterials are playing a phenomenal role in improving the characteristics of devices and circuits. Thus, it can be safely be stated that organic semiconductor devices will play a significant role in future consumer electronics.

Sensors are widely used in the industry for automation and data acquisition. It is always desired that a sensor should offer high sensitivity, better compatibility, quick response and accuracy in the acquired data. For this purpose, various types of organic sensors have been discussed in detail in this chapter including: temperature sensors, humidity sensors, pressure sensors, strain sensors, displacement sensors and sensors with multifunctionality.

In general, it is discussed that the performance of a sensor is dependent upon three parameters: a) sensor design; b) sensing material and c) fabrication technology involved. The literature review highlights that while designing a sensor its target applications shall be kept in mind; and those sensors which are meant for human body and other such needs should be made using flexible substrate to make them conformal with the body or to any other surface where they will be employed. Finally, it has been established that the sensors are critical for industrial automation and human comfort. Based on the listed literature review, it has been noted that still there is a room to improve sensor performance and to design sensors with improved multifunctionality.

Chapter 3

Organic Field Effect Transistor as Humidity and Temperature Sensor

This chapter presents Organic Field Effect Transistor (OFET) as humidity and temperature sensors. OFETs have the abilities to change their electrical properties as a function of humidity as well as temperature. Their electrical properties have been exploited to design sensors to assess humidity and temperature in order to assist and automate an industrial environment. The device structure and fabrication technique for both the sensors are the same. However, their electrical response as a function of humidity and temperature is quite different. This has been discussed in detail in this chapter. The first part of the chapter deals with OFET based humidity sensors fabrication and characterization, followed by the evaluation of the same device as a temperature sensor.

3.1 Humidity Sensors

Humidity sensors are widely used in the industry to automate its processes. Majority of the humidity sensors are based on the electrical properties of the material

involved in their fabrication. On this basis, three groups of humidity sensors have been reported in the literature: a) electrolytes; b) organic polymers and c) porous ceramics [143]. Barker *et al.* developed OFET based sensors and investigated their characteristics as a function of ambient humidity [144]. Chen and Lu presented review of materials and mechanisms for different kinds of humidity sensors [145]. They discussed sensors which were fabricated using ceramics, semiconductors and polymers to measure relative and absolute humidity for an industrial environment. Additionally, they presented data pertaining to sensitivity, response time and stability of the sensors, including Al_2O_3 based sensors. Suri *et al.* in 2002, fabricated sensors using composites of iron oxide and polypyrrole for humidity and gas sensing purposes [146]. They observed that by increasing concentration of polypyrrole, the sensitivity of the sensors increased. Gas sensing properties of the sensors were investigated for CO_2, N_2 and CH_4. Recent development in miniaturized humidity sensors is presented in Ref. [147] wherein capacitive, hydrometric, gravimetric, optical and integrated humidity sensors are discussed. Recently, a number of papers have been published on humidity sensors based on organic semiconductors and composites. A humidity sensing organic-inorganic composite for environmental monitoring has been investigated and reported in Ref. [148]. Additionally, Karimov *et al.* in 2014, presented a number of resistive humidity sensors fabricated using vanadium complex [VO_2(3-fl)] films [149]. They also developed OD and CNTs based humidity sensors using a high gravity thin film deposition technique [150]. Fabrication and investigation of cellulose acetate-copper oxide nano-composite based humidity sensors are presented in Ref. [151]. Effects of moisture contents on the performance of organic bi-layer ITO/OD thermoelectric cell have been investigated by Ahmad *et al.* [152]. Chan *et al.* developed organic photo FET using NiPc film and studied the device response as a function of ambient humidity [151]. Currently, OFET based humidity sensors attracted a lot of attention because of their good response and versatility. In this chapter, an effort has been made to develop and characterize a novel and economical OFET based sensors which can potentially be used by the industry. The fabrication and characterization details of the developed OFET based sensors are presented in the

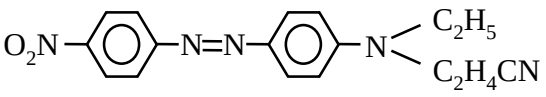

FIGURE 3.1: Molecular structure of an orange dye (OD) molecule.

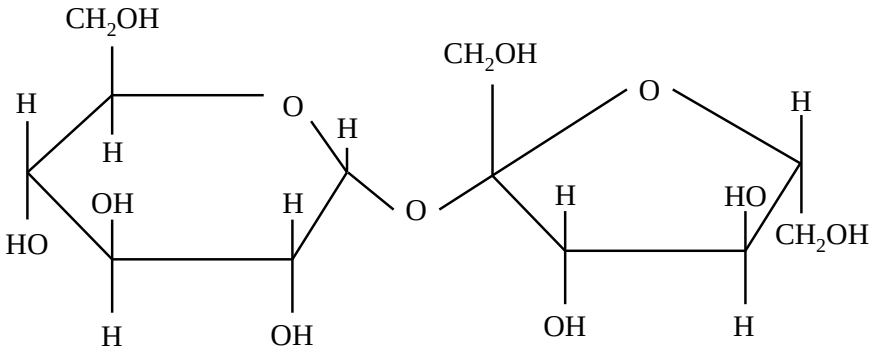

FIGURE 3.2: Molecular structure of a disaccharide molecule.

sections to follow.

3.2 OFET Fabrication

To fabricate OFET, the first and the foremost thing is to select an organic material which can act as a semiconductor. OD which has chemical structure as shown in Fig. 3.1 is a commercially available organic semiconductor whose electrical properties can comfortably be modified by mixing it with another appropriate organic material. Keeping this in view, an aqueous solution of commercially available organic semiconductor OD (8 wt.%) and sugar (8 wt.%) was prepared. As both OD and sugar (disaccharides) are fully soluble in water, one can assume that the resultant solution based on these ingredients will form a complex. The sugar whose molecular structure is shown in Fig. 3.2, was used to attain a conducting coating [153]. Additionally, it was observed that the presence of sugar provides a better adhesion of the deposited OD-sugar film compared to OD alone. To prepare aqueous solution distilled water was used. To get OFET structure, commercially available surface-type interdigitated silver electrodes coated with ceramic alumina sheet, fabricated by screen printing and chemical etching technology were used to define a FET along with its substrate [150]. The chosen substrate was 14 mm×7

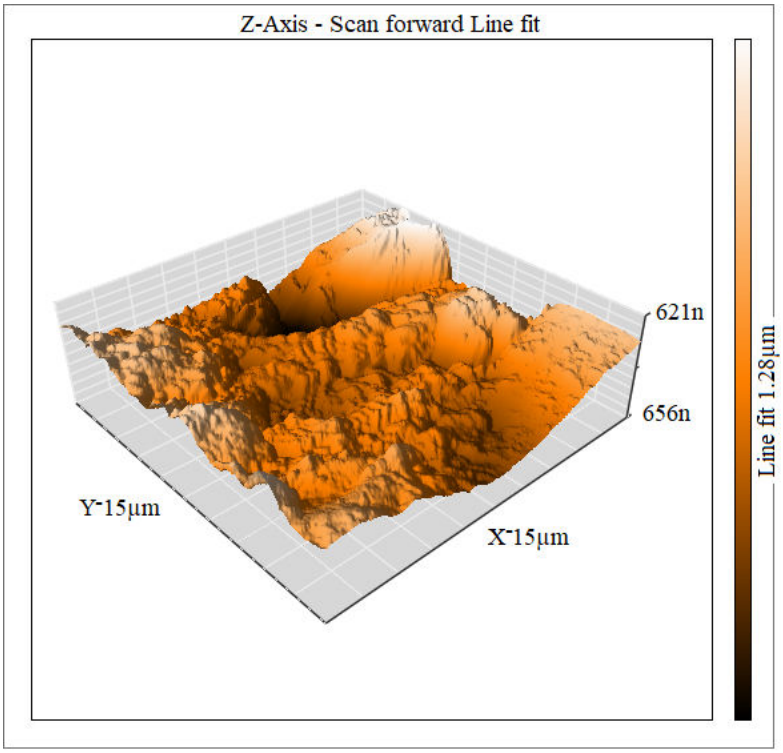

(a)

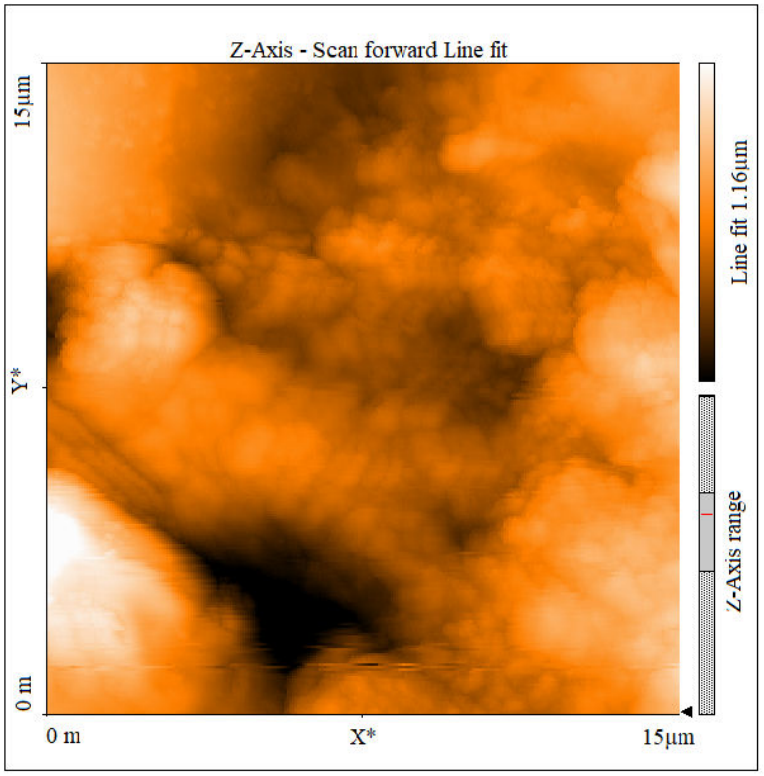

(b)

FIGURE 3.3: Atomic force microscope image of the OD-sugar film used in humidity-temperature sensors.

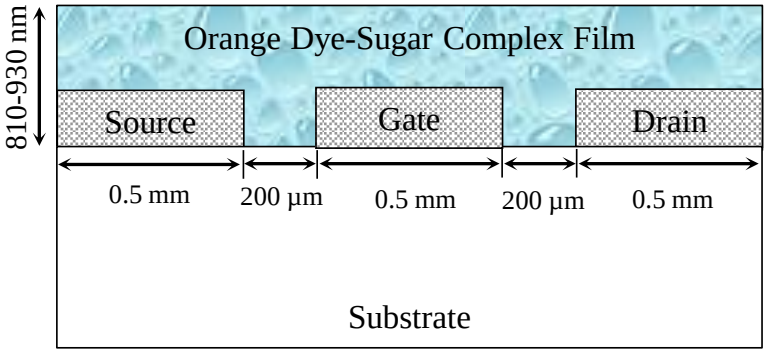

FIGURE 3.4: Crossectional view of an OD-Sugar based field effect transistor.

mm and the width of each electrode was 0.5 mm with 7 mm length and 200 μm as interelectrode spacing. The devices were fabricated using drop-casting of the solution. The thickness of the OD-sugar thin film was in the range of 810–930 nm. By using thermoelectric (Seebeck) effect, it was observed that grown OD-sugar film possessed $p-$type semiconductor characteristics. Fig. 3.3 shows atomic force microscope (AFM) image of an OD-sugar sample wherein a high level of surface roughness is observed. The device crossectional view along with its various dimensions is shown in Fig. 3.4. The figure clearly demonstrates that the device is three terminal FET having channel defined by OD-sugar complex sitting on top of the electrodes. One end of the each electrode was kept open to facilitate electrical measurements. For $I-V$ measurements, digital multimeters HIOKI DT4252 and HIOKI DT4253 were used. Experiments were conducted under usual room temperature conditions.

3.3 Humidity Measurements

Fig. 3.5 shows drain-source voltage (V_{ds}) – drain-source current (I_{ds}) relationships for the OD-sugar humidity sensor at 56%, 60% and 70% RH levels. These measurements were repeated number of times and a very nominal change was noticed, which was less than one percent of the values reported in the plot. Hence, the device offered stable characteristics for the range of data reported in Fig. 3.5. It

is seen that at a fixed V_{ds}, the magnitude of I_{ds} increases with the increasing percentage of RH. This relationship can be used to assess the dependence of sample resistance on ambient humidity level. The resistance vs RH profile is shown in Fig. 3.6, which exhibits a sharp decrease in the resistance value of the sample at $V_{ds} = 7$ V. Both resistive (S_R) and current (S_I) sensitivities of the sensor can be estimated by using the following expressions:

$$S_R = \frac{\Delta R}{R \Delta RH} \tag{3.1}$$

$$S_I = \frac{\Delta I_{ds}}{I_{ds} \Delta RH} \tag{3.2}$$

In above expressions I_{ds} has got usual meaning, R represents bulk resistance of the OD-sugar film, $\Delta R = R_{ini} - R_{fin}$ is the change in resistance because of adsorption of water molecules by the sample and $\Delta RH = RH_{ini} - RH_{fin}$, represents change in relative humidity. Using Eqns. 3.1 and 3.2, average values of S_R and S_I are found to be $-5.7\%(\text{RH})^{-1}$ and $+5.7\%(\text{RH})^{-1}$, respectively. Response and recovery times were equal to 11 s and 32 s accordingly for a humidity change from 50% to 90% RH.

3.4 Humidity Sensor–Explanation

Humidity effects on electrical properties of organic thin film transistors were investigated by Dawen *et al.* [154] and it was observed that both output current and mobility, exhibited decreasing trend with increased values of RH. It was attributed to charge trapping by polar water molecules reducing the rate of charge transport. In metal oxides (ceramics), two types of conduction has been classified: ionic and electronic conduction [155]. In the first type, the ionic current was observed which could primarily be associated with the conduction of H^+ ions due to the capillary condensation of water vapor. In the second type of materials, water molecules played the role of electron donating gas. Resultantly, the conductivity

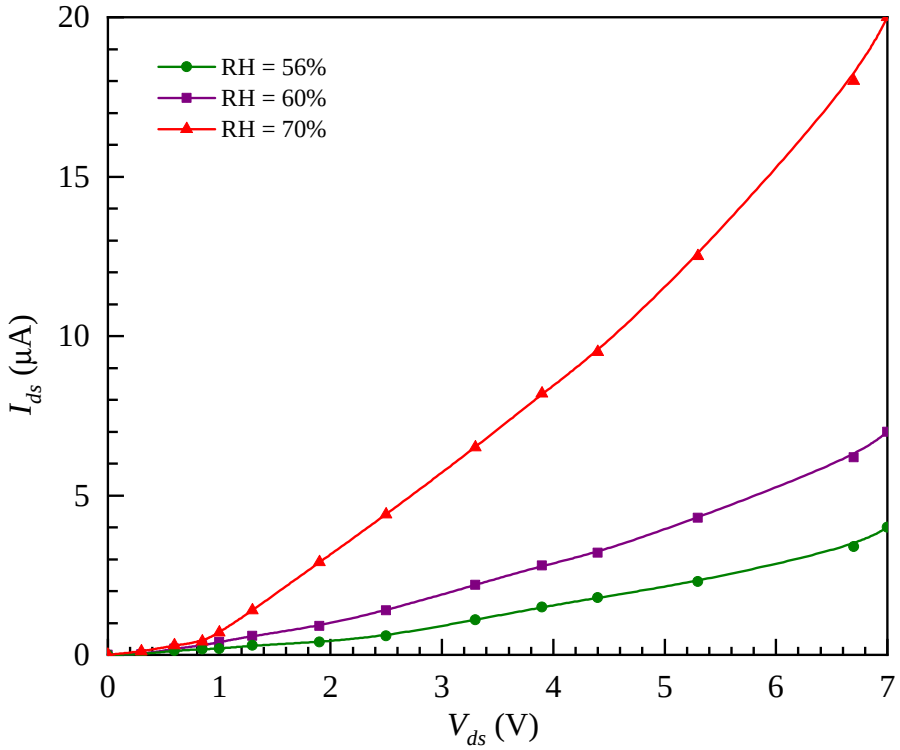

FIGURE 3.5: $I_{ds} - V_{ds}$ relationships at $V_{gs} = 0$ V for the OD-sugar humidity sensor for different humidity levels: 56%, 60% and 70%.

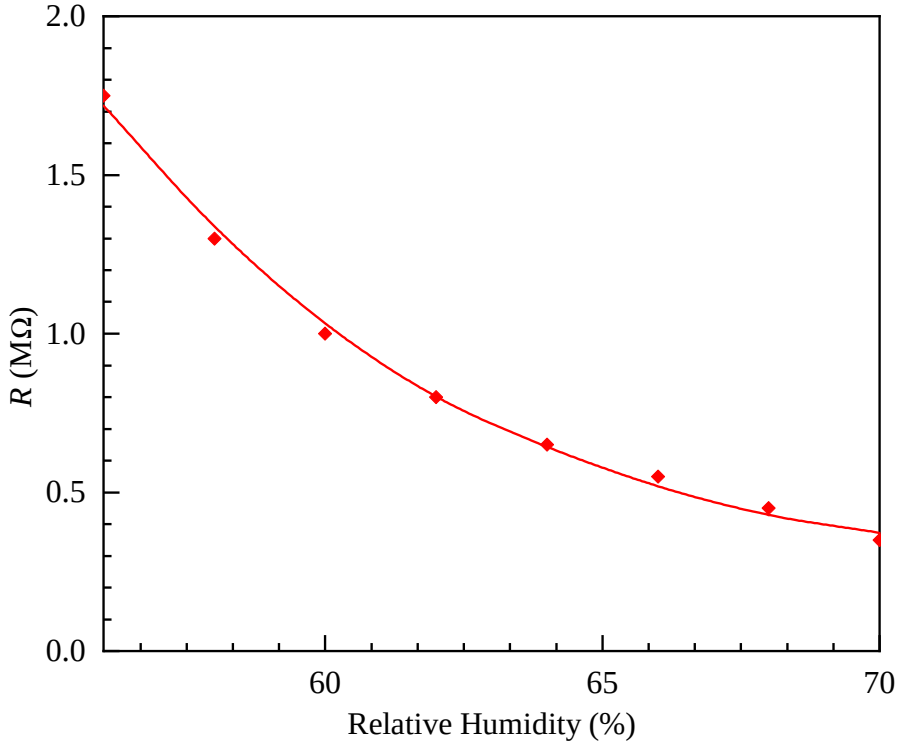

FIGURE 3.6: Dependence of resistance of the OD-sugar humidity sensor on humidity.

could either be increased or decreased depending upon the n or $p-$nature of the semiconductor.

Generally speaking, several humidity sensing mechanisms have been proposed and studied. Based on that, humidity sensing mechanism could be associated with any of the following or their combination [156]:

i. ionic conduction;

ii. proton based sensing;

iii. water molecules assisted conduction;

iv. electronic conduction;

v. solid electrolyte conduction;

vi. capacitive type conduction (impedance variation);

vii. chemical adsorption;

viii. physical adsorption or

ix. capillary condensation.

In general, when a humidity/temperature sensor is subjected to a changed environment, it will experience an alteration either in its physical and electrical properties or both. This change will be in the active material of the sensor and under usual conditions is a reversible one. If the changed environment modifies the physical properties of the active material, it is usually explained by chemical/-physical adsorption or/and capillary condensation. Such a change also modifies permittivity/permeability of the sample which results into impedance alteration of the active material of the sensor as a function of ambient humidity/temperature. Apart from that, more carriers/ions can also be generated in the active portion of the sensor which enhance the conductivity of the device, and the magnitude of alteration corresponds to the change in ambient where the sensor is installed.

In our case, OD and sugar were dissolved well in water. It can therefore, be assumed that apart from proton conductivity caused by H^+ there is donor-acceptor

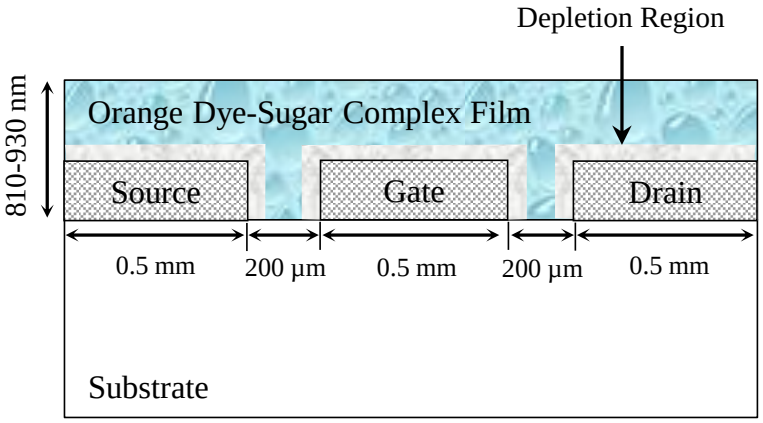

FIGURE 3.7: Metal-semiconductor Schottky junctions with depletion region shown in the Ag-(OD-Sugar)-Ag structures.

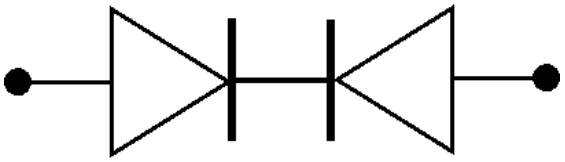

FIGURE 3.8: Equivalent circuit of two Ag-(OD-Sugar) metal-semiconductor junctions which can be represented as opposite connected semiconductor diodes.

charge transfer, responsible for electronic conduction in an organic semiconductor. This eventually increases carrier concentration and accordingly, the total conductivity of the device. On the other hand, as shown in Fig. 3.5, I_{ds}, V_{ds} characteristics are non-linear because of the presence of a Schottky junction at metal-semiconductor (Ag–OD) interface. This has been shown in Fig. 3.7. From electronic point of view, these junctions can be represented as oppositely connected semiconductor diodes as illustrated in Fig. 3.8. Presence of depletion region at Ag–OD influence the performance of the sensor positively [157].

Figure 3.9 shows $I_{ds}(V_{ds}, V_{gs})$ characteristics for the OFET having conducting channel defined by OD-sugar complex. These characteristics are similar to the one shown in Fig. 3.5. Additionally, $I_{ds} - V_{gs}$ relationship for the OFET at $V_{ds} = 7$ V is presented in Fig. 3.10. It is obvious from these figures that the operation of the OFET under investigation is similar to that of an enhancement type FET, which is in conformity to well reported traditional inorganic FETs operation [158] . It is worth mentioning that in a standard thin film OFET technology,

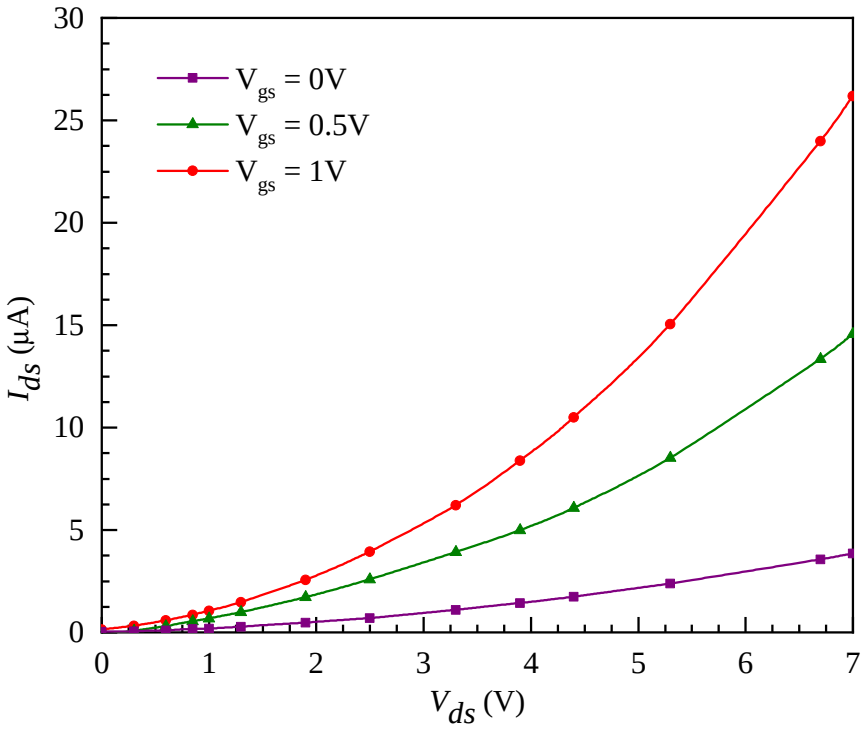

FIGURE 3.9: $I_{ds} - V_{ds}$ characteristics of an OD-Sugar based OFET at different V_{gs} voltages.

source and drain terminals are placed on the same plane and the gate terminal is placed in between, but on top of the organic layer [15]. On the other hand, in conventional single crystal inorganic FET technology, all terminals are placed on the same plane, i.e., on top of the crystal referred to as co-planner topology [15]. In our case (Fig. 3.4), all three terminals are fabricated on substrate, which is non-active, and the organic-sugar film is grown afterward on top of these electrodes to define active layer of the OFET. This structure is easier to fabricate and potentially more efficient, especially for sensor applications. In the absence of top-gate, there is more surface area for impinging molecules of gas or humidity to interact with the conducting channel of the OFET which results into improved sensor response.

As is known, I_{ds} of a FET depends on its conduction channel width, W length, L carrier mobility, μ and gate capacitance, C. The magnitude of I_{ds}, in the saturation region of operation ($I_{ds(sat)}$), under applied bias (V_{gs}, V_{ds}) can be approximated as [159]:

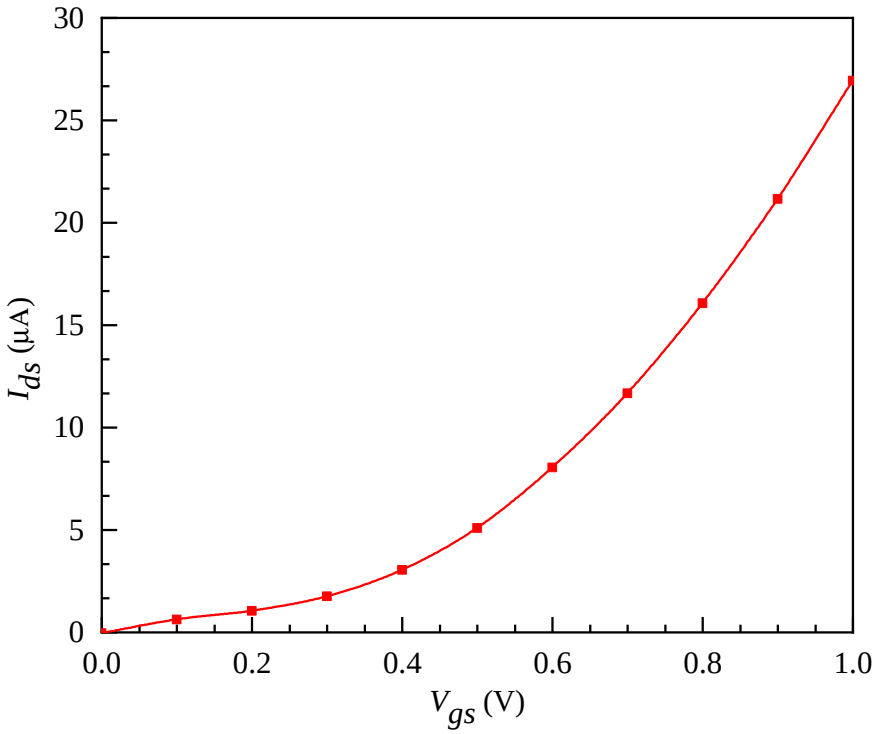

FIGURE 3.10: $I_{ds} - V_{gs}$ characteristics of an OD-sugar based OFET at $V_{ds} = 7$ V.

$$I_{ds(sat)} = \frac{\mu WC}{2L}\Big(V_{gs} - V_t\Big)^2 \tag{3.3}$$

And for linear region of operation, where FET behaves nothing but as a resistor, the value of $I_{ds(lin)}$ can be given as:

$$I_{ds(lin)} = \frac{\mu WC}{L}\Big(V_{gs} - V_t\Big)V_{ds} \tag{3.4}$$

where V_t represents threshold voltage. It is worth mentioning here that OFETs do not follow Eq. 3.4 in its true spirit. They usually exhibit non-linear or quasi-linear behavior in the linear region of operation [160] as observed in Fig. 3.9. Furthermore, the device drain and source terminals are not offering ideal ohmic characteristics, and there is usually a finite depletion, as shown in Fig. 3.7, which causes a non-linear response in the device characteristics.

According to Eqns. 3.3 & 3.4, the magnitude of I_{ds} changes by changing V_{gs} and the same has been observed in Fig. 3.9. On the other hand, although the plot of

Fig. 3.5, exhibits the same behavior, it is due to humidity and not V_{gs}. Observing Figs. 3.5 & 3.9 juxtaposition, one can clearly conclude that the humidity causes the same effect to the device as that of V_{gs}, in terms of gate depletion modification and hence the I_{ds} of the device.

Sensitivity of the OFETs can be determined by evaluating its transconductance, g_m, which, at a given V_{ds}, can be expressed as:

$$g_m = \frac{\partial I_{ds}}{\partial V_{gs}} \tag{3.5}$$

In fact, Eq. 3.5 represents a change in the channel resistance of the device. This change occurs due to the device gate depletion variation caused by either the gate bias or, in case of a sensor; this could be associated to a relative change in the ambiance because of any physical change such as: humidity, temperature, pressure, flow rate or any other variable for which the sensor is designed. As mentioned before, unlike the well-known structures of FETs, for the devices under consideration the depletion region is present around all terminals (Fig. 3.7) and not only the gate as observed in conventional FETs [15, 158]. This structure potentially allows to fabricate sensors with improved sensitivity for practical applications.

Traditional semiconductor-metal ohmic or rectifying Schottky contacts did not encompass all types of metal-semiconductor contacts. Recently, contact resistances between organic semiconductors poly (3-hexylthiophene) and metal electrodes in OFET have been investigated and reported in [161]. It was observed that the contact resistances play a dominant role in electronic charge injection properties of an OFET. Therefore, it was assumed that this effect should not be ignored when examining intrinsic properties such as μ and its dependence on temperature or bias voltages for both ohmic and nonlinear charge injection. It is considered an important step toward improved understanding and modeling of OFETs.

3.5 OFET as a Temperature Sensor

Temperature is the most often-measured environmental parameter. It is a well established fact that temperature affects physical, electronic, chemical, mechanical and biological characteristics of a sample. It is known that many processes work well within a specific temperature range. The performance of a chemical, biological or of an electronic circuit depends upon the ambient temperature [162–165]. Temperature sensors based on p or $n-$type OFETs are discussed in Ref. [82]. The characteristics of an OFET vary as a function of temperature because the conductivity and the mobility of carriers both are dependant upon the temperature of the device. This property can be exploited to design temperature sensors involving OFETs. Temperature sensors can be realized by developing a Wheatstone bridge composed of temperature sensitive element such as OFET. Flexible temperature sensors based on OFETs with polymeric channel/gate-insulating and light-blocking layers have been discussed in [84]. These flexible OFET-based thermal sensors exhibit typical $p-$type transistor characteristics for a temperature range of $\sim 25 - 100$ °C. In [86], effects of temperature on hysteresis of dipolar dielectric layer based OFETs have been studied. OFET based ultrafast, flexible, physiological–temperature sensors with hexagonal barium titanate nanocrystals in amorphous matrix as sensing material is discussed in [85]. And it has been shown that the sensors are highly stable and work reasonably well under extreme conditions. Ravariu *et al.* [91], reported fabrication of para-aminobenzoic acid (PABA) grafted to ferrite nanoparticles based OFET. The measurements of output characteristics in the saturation region of operation and transfer characteristics at negative gate voltages showed the functioning of OFET, which can be employed as a temperature sensor.

In [87], an organic temperature sensor based on asymmetric metal insulator semiconductor capacitor with electrically tunable sensing area is discussed. It has been shown that an area-asymmetric organic metal–insulator (AMIS) capacitor exhibits strong temperature dependent profile. The gate electrode in the device is made much larger than the top electrode so that a significant fraction of the capacitance

comes from the channel. Tactile and temperature sensors based on OFETs for e-skin fabrication are discussed in [92]. Printable, highly sensitive flexible temperature sensors for human body temperature monitoring are presented in [166]. In this article, a comprehensive review has been carried out pertaining to current research status of sensitive patterned flexible temperature sensors used to monitor body temperature. Fully printed PEDOT:PSS based temperature sensor with relatively high stability as humidity sensor for health care monitoring has been discussed in [167]. This sensor exhibits sensitivity of -0.77% $^{\circ}C^{-1}$ for temperature range 25–50 °C. Moreover, a wireless temperature sensing platform was obtained by integrating a sensor to a printed flexible hybrid circuit to develop a stable real-time health care monitoring system. In [77], a detailed study has been carried out for temperature sensors fabricated using aluminum phthalocyanine chloride (AlPcCl) thin films. Impedimetric humidity and temperature sensing properties of chitosan-$CuMn_2O_4$ spinel nanocomposite have been studied by Chani *et al.* and they published their data in [168].

3.6 Temperature Measurements

It is pertinent to mention that OD FET sensors for temperature measurements are the same as explained in Section 3.2. For measurements of voltage and current, digital multimeters, HIOKI DT4252 and HIOKI DT4253 were used; whereas, for temperature assessment FLUKE87 multimeter with built-in thermocouple was employed. During the experimentations, measurements were repeated and it was noted that OD FET sensors offered stable characteristics and the variations in data, for a given set of variables, were negligible. Samples heating was carried out using Torrey Pines Scientific hot plate. Opened OD FET along with encapsulated sensor, as shown in Fig. 3.11, were used to assess the change in electrical response as the function of temperature.

Fig. 3.12 shows impedance Z (100 Hz) and temperature relationship for OD-sugar based OFET operating as opened temperature sensors (without encapsulation).

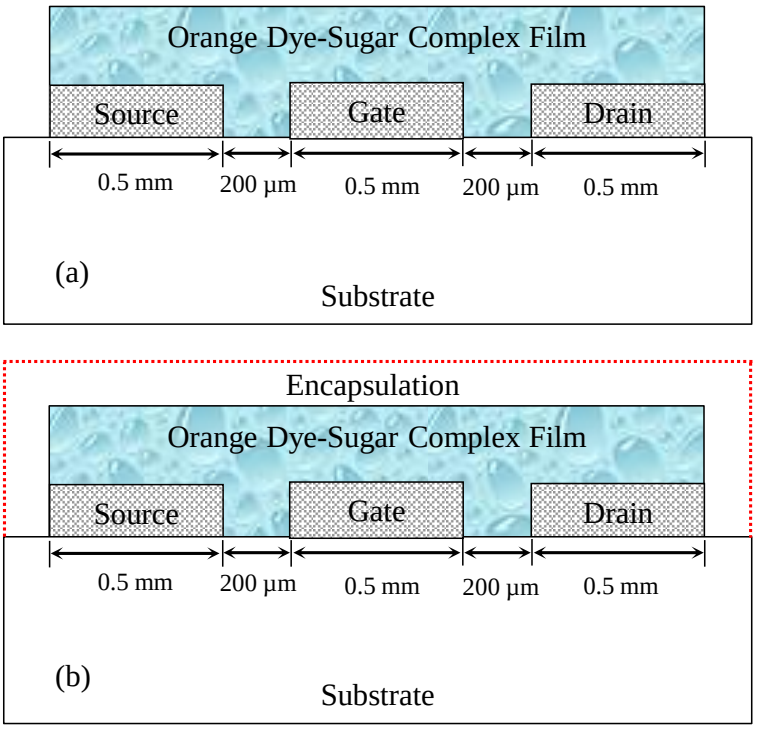

FIGURE 3.11: Crossectional view of OD FET used for temperature measurements (a) device is exposed to open environment (b) encapsulated device.

It is observed that with increasing temperature, impedance also increases. This behaviour of the temperature sensor is associated with the physical properties of the polymer involved in its definition and the effect so observed is referred to as posistor [169]. At temperature equal to 28 °C, the coefficient of temperature based impedance (α) is equal to:

$$\alpha = \frac{\Delta Z}{Z \Delta T} \times 100 \tag{3.6}$$

where ΔZ, Z and ΔT are increment of impedance, impedance and increment of temperature, respectively. For the sensor under consideration, α is calculated and found as +150% $°C^{-1}$.

Fig. 3.13 shows impedance Z (100 Hz) and temperature relationship for the OD-sugar based OFET operating as encapsulated temperature sensor. It is observed that when temperature increases, impedance of the sensor exhibits a decrease in its magnitude. This is a standard thermistor like characteristics caused by the

TABLE 3.1: Comparison of various organic semiconductor based humidity sensors and their response time.

Ref.	**Sensing Material**	**Sensing range (RH)**	**Response time (s)**	**Recovery time (s)**
[170]	Keratin	16 – 82%	36	55
[171]	Cellulose-PPy	30 – 90%	418	418
[172]	LiCl-KIT-6	11 – 95%	15	28
[173]	MCM-48 fiber	33 – 95%	15	28
[174]	HKUST-1	11 – 84%	20	20
[175]	MIL-101 (Cr)	33 – 95%	17	90
[176]	KOH/M050	20 – 90%	36	118
[177]	EuW-MOF	53 – 100%	380	398
[178]	TpPa-SO_3Na	11 – 95%	6	69
This work	OD-sugar	50 – 90%	11	32

polymer used in sensor fabrication [169]. At 28 °C, the coefficient of temperature based impedance is equal to –9.7% $°C^{-1}$.

3.7 Temperature Sensor–Explanation

The results shown in Fig. 3.12 and Fig. 3.13 are contradictory in nature such that in the first case, the impedance is increasing with increasing values of temperature. Whilst, in the second case, there is an exponential decline in the impedance by increasing ambient temperature. In the first experiment, measurements were made while keeping the sensor exposed to the environment (Fig. 3.11a). It is assumed that water molecules while heating the sample get evaporated and released from the film. As a result, water concentration in OD-sugar film reduces. Experimental data, as observed in Fig. 3.12, suggest that reduction in water molecules concentration increases the impedance of OD-sugar film. This is so, because the assistance offered by the polar water molecules to the flow of charges was no more there. This resulted in increased impedance of OD-sugar film.

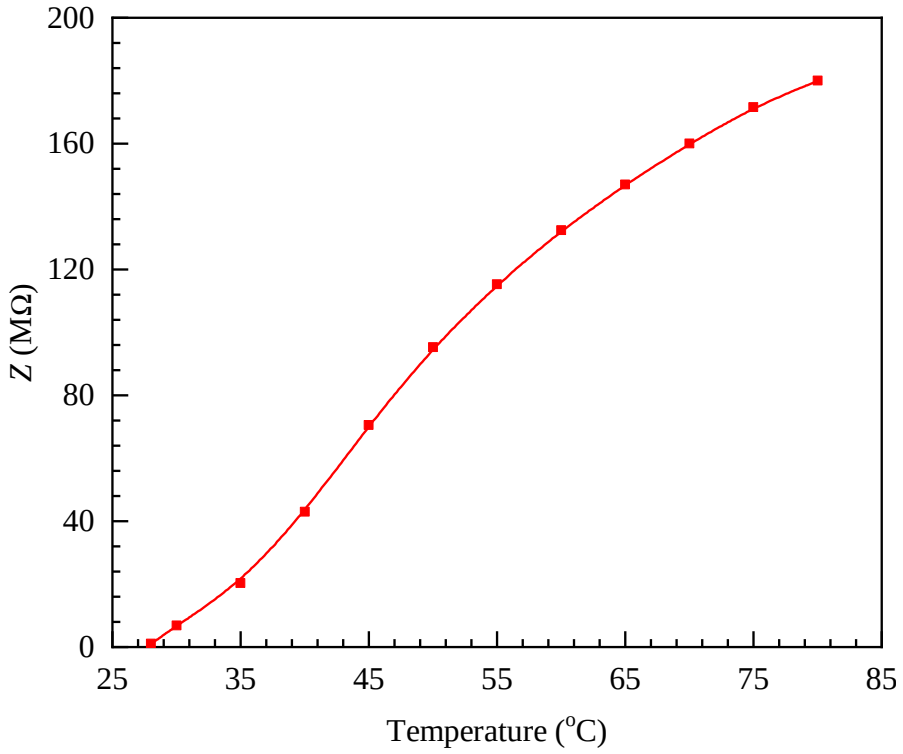

FIGURE 3.12: Impedance Z (100 Hz) and temperature relationship for the OD-sugar based OFET operating as opened temperature sensor.

In the second case, OD-sugar based OFET was subjected to increased temperature after encapsulating the device as shown in Fig. 3.11b. Since the sample was heated while it was fully covered; this did not allow the water molecules to evaporate. Further, it is assumed that humidity level in the sample either remained constant or experienced an insignificant change. On the other hand, heating of the sample, by maintaining humidity level, can increase its conductivity which results into reduction in impedance as evident from the plot of Fig. 3.13. Moreover, a reduction in impedance at elevated temperature can also be observed due to an increase in conduction process which could be associated with: a) increased in carrier concentration in organic semiconductor; b) improved carriers mobility or c) improved hopping mechanism at elevated temperature [179, 180].

A comparative analysis of various humidity sensors is presented in Table 3.1. The data of the table show that the proposed design is simpler and offers an equally good response as that of other reported sensors. Hence, it could be a good alternative for industrial applications where controllability of ambient humidity is

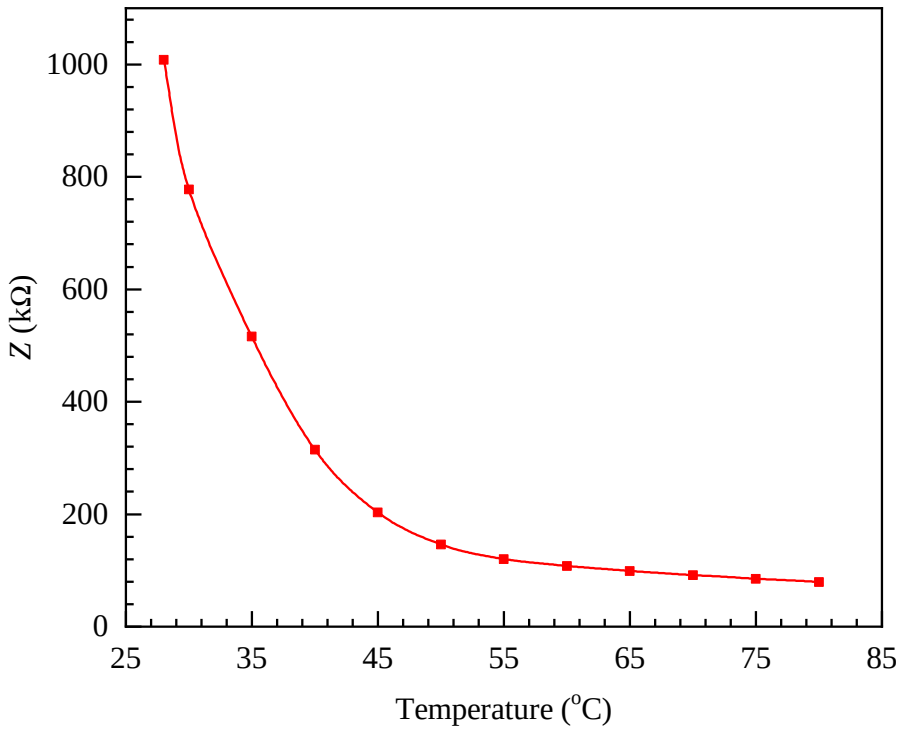

FIGURE 3.13: Impedance Z (100 Hz) and temperature relationship for the OD-sugar based OFET operating as encapsulated temperature sensor.

considered a crucial variable.

3.8 Summary

This chapter presents fabrication and characterization of OD-sugar complex based OFETs as humidity and temperature sensors. Contrary to the traditional configuration, source, drain and gate terminals of the FET were placed on a co-planar substrate and the conducting channel was attained by growing OD-sugar film using a drop costing method. Fabricated OFETs based humidity sensors were evaluated and it was observed that response and recovery times were equal to 11 s and 32 s for a change of humidity from 50% to 90% RH, respectively. It has also been demonstrated that increased concentration of water molecules in OD-sugar film causes the same effect as that of gate bias. Thus, by increasing RH values, the device functionality changes which is identical to that of enhancement type OFET.

Additionally, the properties of OFETs were also investigated as a temperature sensor. It has been observed that channel impedance of OD-sugar based FET sensor increases with increasing values of temperature provided the device is exposed to air. On the other hand, the same variable decreases by increasing temperature if the device under investigation is encapsulated. Thus, opened surface and encapsulated samples showed positive and negative temperature coefficients, respectively. It has been shown that fabricated OFETs are highly sensitive to temperature and can potentially be employed by the industry as thermistor and as a posistor.

Chapter 4

Orange Dye, Graphene and Silicon Adhesive Composite Based Flexible Humidity Sensors

4.1 Introduction

New and low cost flexible humidity sensors are actively pursued by both research groups and industries to accommodate the needs of flexible electronics for various monitoring applications. Humidity sensors are used to measure the concentration of water vapours present in any environment. As water concentration is of great significance in many sectors, control of humidity for the human comfort; as well as for a broad spectrum of industrial applications, is of crucial importance. For the last two decades, humidity sensors have been actively used in various applications, such as, fax machines, printers, automobiles, weather stations, agriculture, laboratories, and food processing units [156, 181, 182]. To meet the industry requirements, it is important that humidity sensors should have good material reliability with high sensitivity, rapid response and recovery time with minimal hysteresis [183]. Humidity sensors can be fabricated by employing various materials, including electrolytes, organic and inorganic polymers, ceramics and

composite materials. In spite of different sensing materials, most of the sensors exhibit similar sensing phenomenon, i.e., physical absorption of water molecules resulting into changed electrical response. Nonetheless, some materials also utilize the phenomenon of chemical absorption to exhibit variation in their response for some special applications [143].

On the basis of sensing principle and characterization technique, sensors are categorized into capacitive, resistive, hydrometric, optical and surface acoustic wave (SAW) sensors [184]. Researchers have been trying to develop sophisticated humidity sensors by manipulating several sensing characteristics such as capacitance, impedance, refractive index and dielectric constant. These characteristics are strictly determined by the properties such as porosity, surface area and pore size distribution of the sensing material. [185]. Furthermore, the fabrication of humidity sensors on flexible materials are set to revolutionize the industry using printed electronics, which is a rapidly emerging technique within the industry. Many studies, engaging traditional printing methods have been reported on fabrication of flexible humidity sensors, mostly for wearable smart gadgets and RFID tags using plastics, textiles and carbon fibers [184, 186–188].

A number of humidity sensing devices have been reported by research groups and industries in the past. Among those, mechanically flexible thin film humidity sensors are of most interest by the industry due to their vast and modern applications. Su *et al.* [189] fabricated flexible resistive-type humidity sensors using in situ co-polymerization of methylmethacrylate (MMA) and [3(methacrylamino)propyl] tri-methyl-ammonium-chloride (MAPTAC) co-polymer on a polyester substrate. The response of this sensor was reported to be linear for logarithmic impedance while changing relative humidity (RH) from 10% to 90 %. Its response time was 45 seconds whereas, the recovery time was reported to be 150 seconds. The long-term stability evaluation of this sensor showed a stable output for 120 days measured at 1 V, 1 kHz and at 25°C.

Reddy *et al.* [184] fabricated capacitive type humidity sensors that employed interdigitated capacitors (IDC) printed with silver nanoparticle ink on a flexible

poly ethylene terephthalate substrate. A humidity sensitive polymer poly (2-hydroxyethyl methacrylate) of thickness 1 μm and width 500 μm was realized using gravure printing technique. The capacitive response of the sensor was measured for RH range of 30%–80%. A 172% change in the capacitive response was reported at 80% RH relative to 30% RH.

Recently, nanocomposite of various nature have been widely explored by Yousefi *et al.* for their high-tech applications [190–196]. Naturally occurring organic materials, such as, cellulose has also been reported as a sensing material for thin film flexible humidity sensors. Mahadeva *et al.* [171] used a cellulose material, termed as electro-active paper along with nanoscaled polypyrrole (PPy) to fabricate humidity and temperature sensors. PPy layer was introduced on the cellulose surface via in situ polymerization technique without disrupting the cellulose structure. The combination of aforementioned materials is referred to as a cellulose–PPy nano composite which works as a sensing layer. Effects of polymerization-time on sensing behavior of cellulose–PPy nano composite were investigated and it was observed that cellulose-PPy nano composite with 16 hours of polymerization time was appropriate to fabricate humidity and temperature sensors.

Su *et al.* [197] studied the effects of TiO_2 concentration on electrical and humidity sensing properties of flexible resistive-type humidity sensors. These sensors were fabricated by an in situ photo polymerization process wherein TiO_2 nanoparticles / polypyrrole (TiO_2NPs/PPy) and TiO_2-nanoparticles/polypyrrole/poly-[3-(methacrylamino) propyl] tri-methyl ammonium chloride (TiO_2NPs/PPy/ PMAPTAC) composite thin films were deposited on a polyester substrate. PMAPTAC is used with TiO_2NPs/PPy composite thin film to increase the flexibility and sensitivity of the sensors. The flexible humidity sensors, based on TiO_2NPs/PPy/ PMAPTAC composite thin films, showed high sensitivity, low hysteresis and relatively linear response. The effects of applied frequency and ambient temperature were also reported for these sensors.

Researchers also fabricated high performance humidity sensing devices using laser

interference technique. Graphene oxide on flexible polyethylene terephthalate substrate was patterned and oxidized to form humidity sensing devices [198]. By tuning the laser power, the content of oxygen functional groups were changed within a certain range, to control the conductivity of graphene and to improve the response or recovery time of sensors. Laser interference is a large area processing technique of graphene oxide films which is mask and surfactant free. Additionally, it has a great potential to fabricate graphene-based micro devices. Capacitive humidity sensors for RFID systems were fabricated on a polymer foil using spray deposition or screen printing.[199]. The developed system, thus, showed stable and reproducible response under appropriate operating conditions.

Most recently, a number of humidity sensors based on OD have been reported in the literature [150, 200–204]. These OD based humidity sensors were fabricated using flexible plastic substrates which made them light weight, thin and easy to integrate in flexible electronics. Printed flexible humidity sensors composed of a polymer sensing material with extremely low hysteresis were presented in [205]. Asgher *et al.* [206] reported multifunctional sensors fabricated on a rubber substrate having nickel phthalocynine colourant and multi-walled carbon nanotubes as sensing material. Wu *et al.* [207] reported FET based humidity sensors wherein variation in sub-threshold swing, gate leakage current, and off-state drain current were used to assess changes in ambient humidity. Biswas *et al.* [208] in 2022, fabricated FET based flexible humidity sensors and demonstrated that such sensors have better sensitivity and quicker response, when compared with conventional sensors.

In continuation, resistive and OFET based flexible humidity sensors using a composite comprising of OD/graphene/silicon adhesive have been developed which can comfortably be integrated in flexible electronics. These sensors have been fabricated involving low-cost substrate (rubber) coupled with simple device design, making them cost effective and light weight; hence, suitable for hand-held gadgets. The performance of fabricated sensors has been assessed at various frequencies, in a humidity chamber, using impedance and capacitive measurements and results

are compared with other similar devices. It has been shown that OD/graphene/silicon adhesive based humidity sensors are stable for a wider range of temperatures and exhibited a stable frequency dependent sensitivity profile; making them a potential choice for industrial applications including conformal electronics, where a device is transferred on human skin for various sensing purposes.

4.2 Device Fabrication

In this study, two types of sensors are fabricated; a) resistive and, b) OFET humidity sensors. Cross-sectional view of resistive and OFET type humidity sensors are shown in Figs. 4.1 and 4.2, respectively. It is evident from these pictorial representations that both types of sensors are almost identical. The only difference is that the OFET has an extra layer acting as gate of the OFET, which will allow current modulation resulting into a change in electrical response as a function of ambient humidity.

OD is an organic semiconductor ($C_{17}H_{17}N_5O_2$) with a molecular weight and density equal to 323.35 g/mol and 0.9 g/cm^3, respectively [202]. OD is a harmless organic semiconductor. It has been extensively used by our group in standalone as well as in combination with other organic and nanomaterials, as it shows good response when exposed to different physical parameters. It offers stable characteristics under normal operating conditions. Owing to all these attributes, OD is a favourite organic semiconductor in sensor industry. For the proposed sensors, OD was purchased from Sigma Aldrich CAS Number: 31482-56-1. Graphene is also sensitive to humidity and it enhances the conductivity of OD when mixed in it. OD/graphene combination has greater surface area which can elevate the response of a sensor, if appropriately mixed. Graphene powder was purchased from Sun Nanotech Co. Ltd. China, having thickness range 5–20 nm and dimensions of 10 μm^2. To improve the bonding of OD/graphene with rubber substrate, it has been mixed with commercially available silicone adhesive. Commercially available

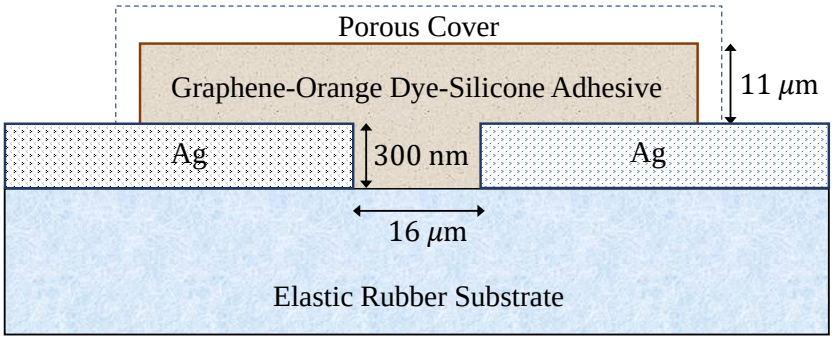

FIGURE 4.1: Schematic diagram of resistive humidity sensor fabricated on a flexible substrate.

silicone adhesive and porous rubber from 3M manufacturer were used, whereas, Ag metal used in electrodes was purchased from Sigma Aldrich with 5N purity.

For device fabrication, a porous flat rubber having dimensions 15 mm × 5 mm × 5 mm was used as a substrate material as shown in Fig. 4.3 (a). Two silver (Ag) electrodes of thickness 300 nm were deposited on rubber in vacuum thermal evaporator at a base pressure of 10^{-6} Torr. These electrodes were deposited using a shadow mask with 16 μm inter-electrode spacing. In our group, for majority of sensors fabrication, this separation showed reasonable results, hence the mask was designed accordingly. Additionally, instead of vacuum evaporation, Ag electrodes could be realized by any other technique compatible to the process. A composite of OD (20 wt.%), graphene (30 wt.%) and silicone adhesive (50 wt.%) was prepared and deposited at the top of the metal electrodes filling up the gap between them. The thickness of the composite film above Ag electrode was measured as 11 μm. An optical micrograph of the grown film is shown in Fig. 4.3 (b).

OFET based humidity sensor has a similar structure as that of the resistive type humidity sensor. However, in addition to the layers discussed earlier, an extra layer of 6 μm thickness made up of graphene (50 wt.%) and silicone adhesive (50 wt.%) was deposited on earlier grown OD/graphene/silicone adhesive layer to define the gate of OFET. Surface morphology of the deposited gate layer is shown in Fig. 4.3 (c).

To measure the response, the sensors were placed inside a humidity chamber, wherein, RH can be varied from 33% to 94%. The sensors were connected with

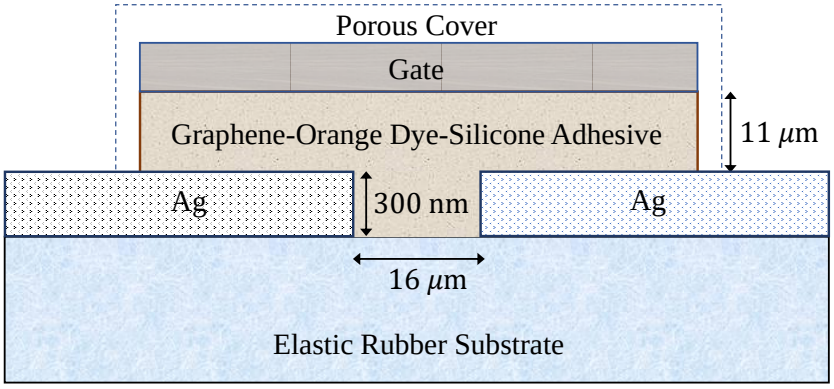

FIGURE 4.2: Schematic diagram of the OFET based humidity sensor fabricated on a flexible substrate. The figure shows two ohmic contacts and an encapsulated gate layer of the OFET.

measuring equipment through Ag electrode which made contact with OD as explained in band diagram shown in Fig. 4.4. Changes in impedance and capacitance, as a function of RH, were measured both at low (100 Hz) and high frequencies (200 kHz). Along with transient response, temperature dependence performance of these sensors were also investigated. During experimentation, the temperature and humidity were controlled by TECPEL-322 installed in humidity chamber. The sensors impedance and capacitance variation as a function of RH were measured using a digital LCR meter (MT 4090). While measuring the impedance, the voltage of the input signal was set at 1 V (RMS).

4.3 Results and discussion

Fig. 4.5 exhibits the impedance-RH relationship of resistive humidity sensor at the given frequencies. As shown, the impedance of resistive type humidity sensor exhibits a drop with increasing RH. This could be associated with increase in conduction carriers generated inside the sensor because of water molecules absorption as $C_{17}H_{17}N_5O_2 + H_2O \rightarrow (C_{17}H_{17}N_5O)(OH)+(OH)^- + h^+$ [209]. Furthermore, by examining Fig. 4.5, it can be seen that the sensor offers higher impedance as well as higher sensitivity at lower frequencies. The impedance measured at 100 Hz and 1 kHz, decreased 2140 and 1642 times, respectively, with increase in RH from 33% to 94% as shown in Table 4.1. For the same resistive type humidity sensor when

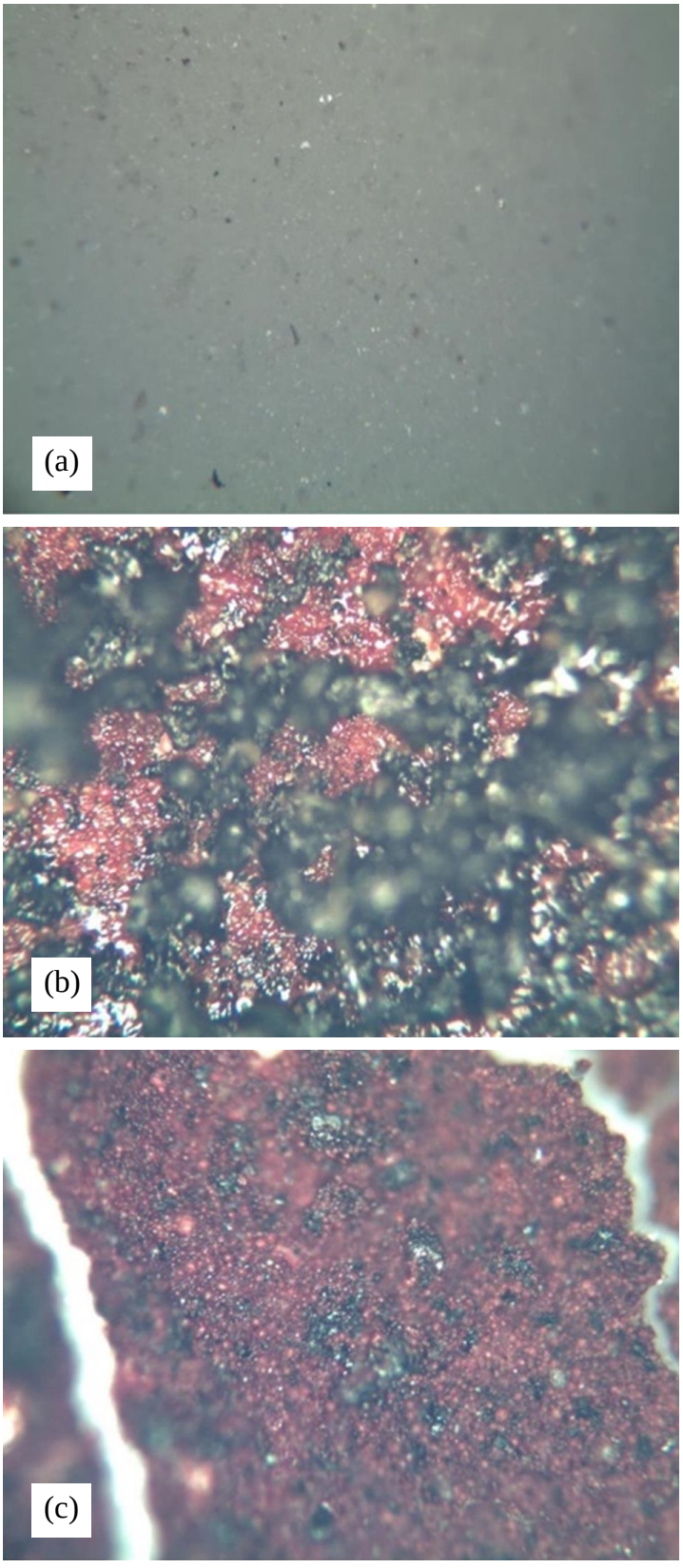

FIGURE 4.3: Optical microscope images of (a) rubber substrate surface (b), OD/graphene/silicone adhesive composite film employed as sensing material and (c) graphene (50 wt.%) and silicone adhesive (50 wt.%) composite film used as OFET sensor gate.

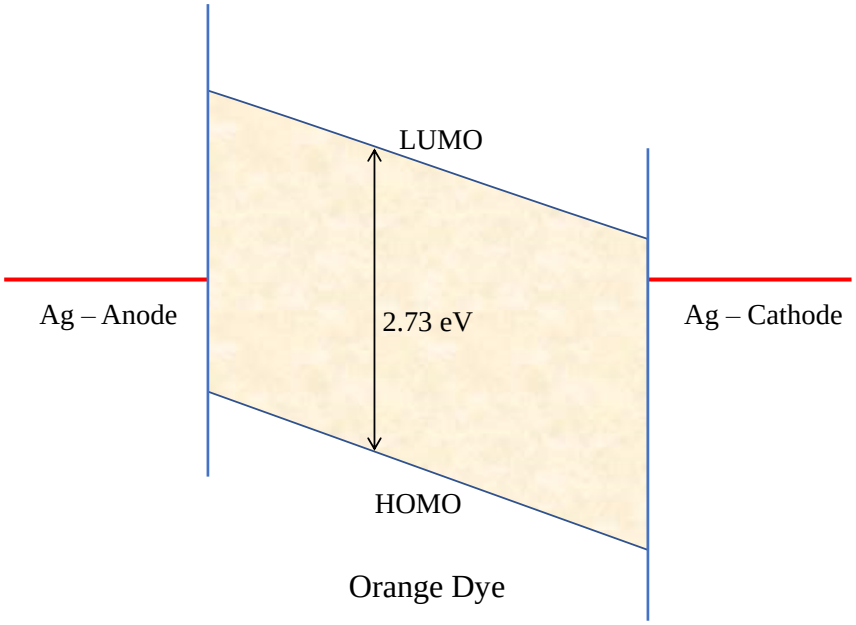

FIGURE 4.4: Band diagram explaining a junction between orange dye (OD) and Ag electrodes used in humidity sensor fabrication

TABLE 4.1: Frequency dependent impedance ratio (Z_{max}/Z_{min}) of resistive and OFET type humidity sensors.

Frequency	Resistive Type	OFET Type	Ref. [210]
100 Hz	2140.00	3716.66	14.04
1 kHz	1641.67	3375.00	24.28
10 kHz	300.00	400.00	20.80
100 kHz	122.00	125.00	–
200 kHz	56.67	80.00	–

measured at higher frequencies, i.e., 10 kHz, 100 kHz and 200 kHz, as shown in the inset of Fig. 4.5, 300, 122 and 57 times decrease in impedance, respectively, is observed (Table 4.1). Comparing the variation in impedance of the fabricated sensor with Ref [210] at three reported frequencies, it is evident that the proposed composite sensors offer better response.

The change in impedance is assumed to be due to the interaction of water molecules with composite materials, i.e., OD and graphene. With increase in RH, a layer of water molecules is formed at the surface of active film. The presence of these water

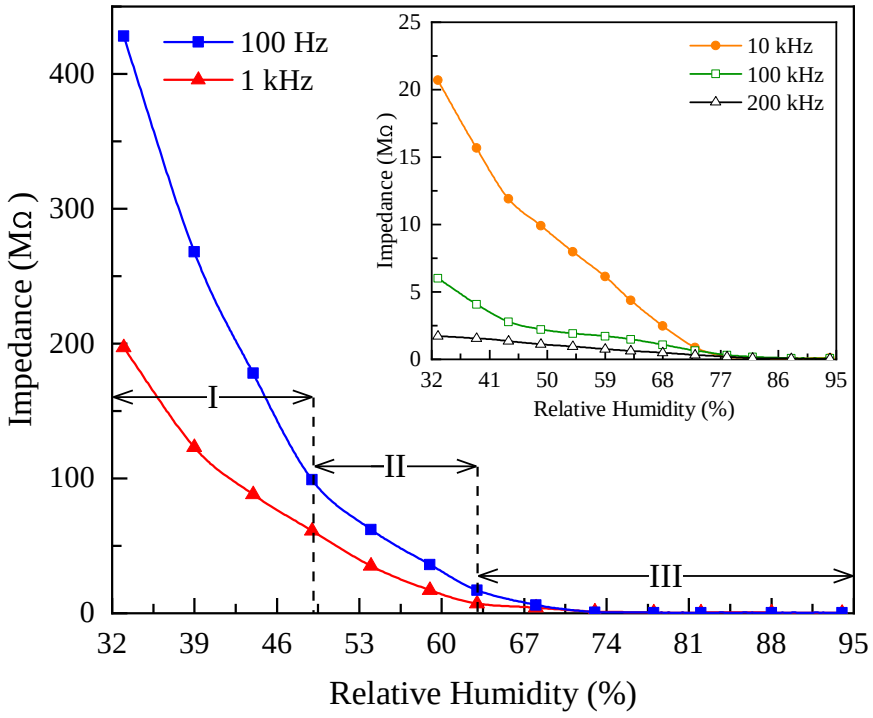

FIGURE 4.5: Impedance-relative humidity relationship of resistive type humidity sensors at 100 Hz and 1 kHz whereas, the inset shows the same response at 10 kHz, 100 kHz and 200 kHz. In Region-I and Region II, the change in impedance by changing RH is significant whilst its saturates for Region III

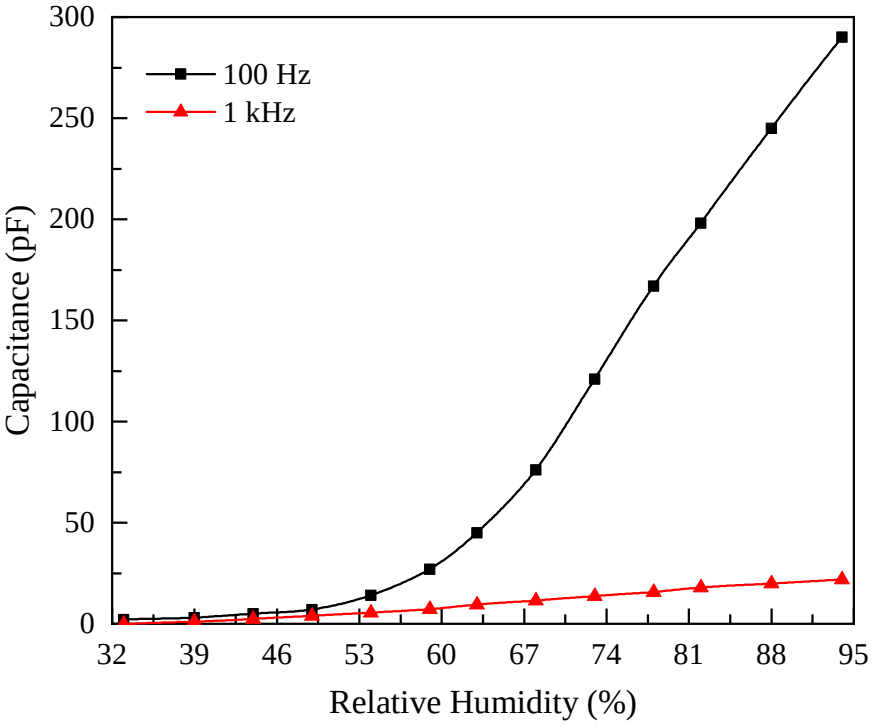

FIGURE 4.6: Capacitance variation as a function of relative humidity at 100 Hz and 1 kHz, observed in resistive type humidity sensors. The plot shows that the device response is relatively better at 100 Hz compared to 1 kHz

TABLE 4.2: Frequency dependent capacitance ratio (C_{max}/C_{min}) of resistive and OFET type humidity sensors.

Frequency	Resistive Type	OFET Type	Ref. [210]
100 Hz	145.00	314.00	44.22
1 kHz	23.00	34.00	39.00

molecules causes an electrostatic dipole moment in organic semiconductor which could potentially enhance the doping concentration and, hence, the conductivity of sensors. The variation in dipole is also apparent in Fig. 4.6, where, output capacitance of fabricated humidity sensors as a function of RH is plotted. It can be seen from the figure that changing RH values from 33 % to 94 %, causes 145 and 23 times change in capacitance when measured at 100 Hz and 1 kHz, respectively as shown in Table 4.2. Comparing the response of fabricated composite resistive type sensor with the one reported in Ref [210], it is clear that OD/graphene/silicone adhesive based sensors offer better variation in capacitance, thus such sensors could be a preferred choice for industrial applications.

In Fig.4.5, three different regions, where the sensor is offering a linear response, have been identified, namely: Region I; Region II and Region III with respect to the response observed at 100 Hz. In Region I, it is obvious from the figure that the sensor is offering highest variation in impedance whereas in Region II, it is relatively lower and in Region III it is further reduced i.e., from MΩ to kΩ. The observed high variation in impedance, in Region I, could be associated with modified conduction properties of composite layer used in sensor fabrication. The capacity of composite layer to absorb further moisture or water molecules reduces for the ambient associated with Region II, and it almost reaches to saturation level for the profile of Region III; resulting into relatively low impedance variation.

The response of OFET based humidity sensors is also measured under same ambient conditions as that of Fig. 4.5 for comparative purposes. Fig. 4.7 shows the measured impedance of OFET based humidity sensors as a function of RH at various frequencies. The main plot of the figure is measured at 100 Hz and 1 kHz, whereas inset shows the response of the sensor at 10 kHz, 100 kHz and 200

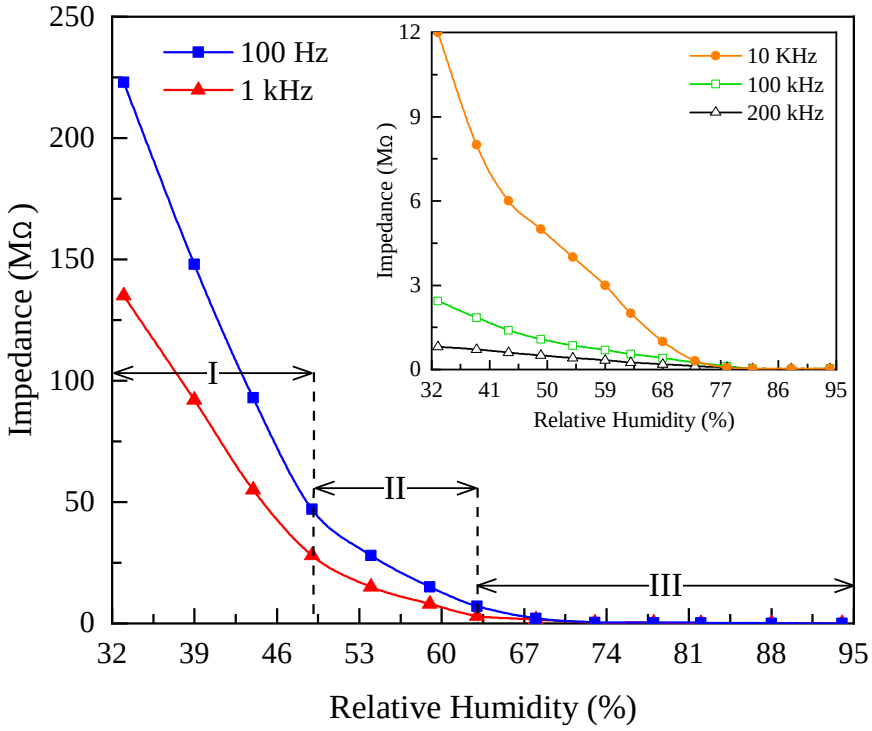

FIGURE 4.7: Impedance-relative humidity relationship of OFET type humidity sensors at 100 Hz and 1 kHz whereas, the inset shows the same response at 10 kHz, 100 kHz and 200 kHz. The plot shows that with increasing frequency the sensitivity of the sensor decreses and relatively higher sensitivity is observed in Region-I

kHz. It is obvious from the plot that the response of the fabricated sensors is a function of frequency, offering highest variation in impedance at 100 Hz; and the value of impedance reduces while increasing the frequency. For 100 Hz profile, a 3716 times reduction in impedance is observed by changing RH from 33 % to 94 %, whereas, it shows low variation at 200 kHz as evident from the data of Table 4.1. A comparative analysis of the two designs i.e., resistive and OFET, revealed that OFET sensors offer better response compared to resistive type sensors.

Fig. 4.8 shows measured output capacitance at 100 Hz and 1 kHz of OFET type humidity sensors as a function of RH as given in Table 4.2. The observed change in capacitance was 314 times at 100 Hz and 34 times at 1 kHz. Comparison of the observed data for both the resistive and OFET based sensors with Ref [210] showed that the proposed design offers better performance at 100 Hz and it is relatively poor at 1 kHz as evident in Table 4.2.

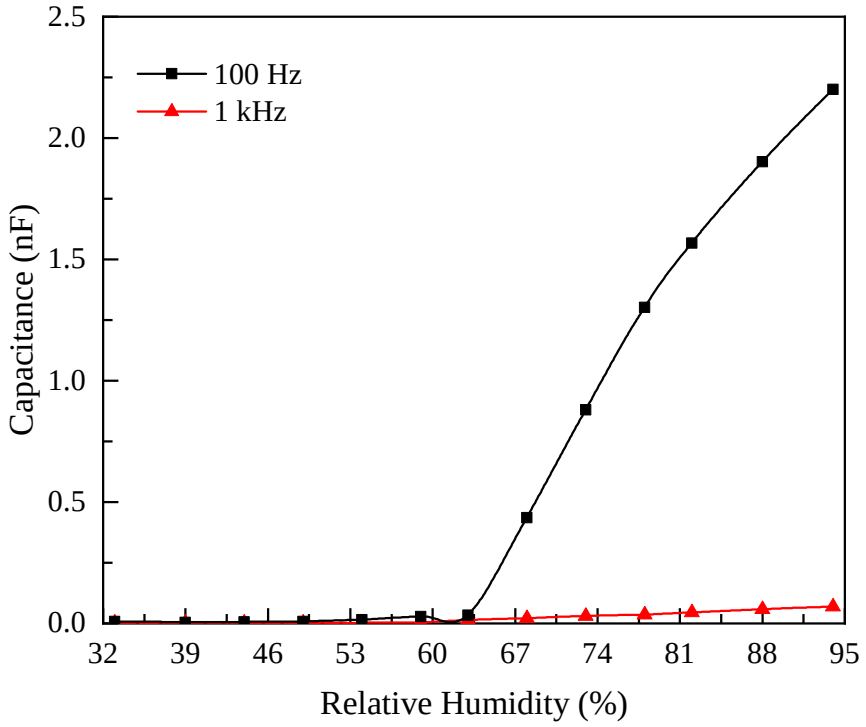

FIGURE 4.8: Capacitance variation as a function of relative humidity at 100 Hz and 1 kHz, observed in OFET type humidity sensors.

TABLE 4.3: Frequency dependent region-wise sensitivity (S_Z) evaluation of resistive type humidity sensors as explained in Fig. 4.5.

Frequency (kHz)	Region-I	Region-II	Region-III	Average
0.1	20.50 MΩ	5.85 MΩ	0.540 MΩ	8.98 MΩ
1	8.50 MΩ	3.85 MΩ	0.222 MΩ	4.19 MΩ
10	687.50 kΩ	392.86 kΩ	142.90 kΩ	407.75 kΩ
100	243.75 kΩ	50.00 kΩ	46.77 kΩ	113.51 kΩ
200	31.25 kΩ	42.86 kΩ	18.39 kΩ	30.83 kΩ

With reference to Figs. 4.5 and 4.7, the sensitivity of resistive and OFET based sensors, as a function of frequency, was evaluated for each region. The data, thus attained, is shown in Table 4.3 and Table 4.4 for $S_Z=(Z_{max} - Z_{min})/(RH_{max}-RH_{min})$, where, Z_{max} is the impedance at RH_{max} and Z_{min} defines its value at RH_{min}. Here *max* and *min* values of any variable are the two extreme values of a given region defined in Fig 4.5 and Fig 4.7.

Examining the data of Table 4.3 and Table 4.4, it is obvious that in each region, a different sensitivity is offered by the sensor. Usually, sensitivity is reported

TABLE 4.4: Frequency dependent region-wise sensitivity (S_Z) evaluation of OFET type humidity sensor as explained in Fig. 4.7.

Frequency (kHz)	Region-I	Region-II	Region-III	Average
0.1	11.00 MΩ	2.85 MΩ	0.224 MΩ	4.69 MΩ
1	6.68 MΩ	1.78 MΩ	0.955 MΩ	2.85 MΩ
10	437.50 kΩ	214.29 kΩ	63.55 kΩ	238.44 kΩ
100	93.75 kΩ	21.43 kΩ	21.94 kΩ	45.7 kΩ
200	18.75 kΩ	17.86 kΩ	7.74 kΩ	14.78 kΩ

by considering two extreme values; one at the highest RH and 2nd at the lowest RH. A sensitivity value attained by such a technique, when compared with the data of Table 4.3, reflects a significant variation which could potentially generate a calibration error. Based on this observation, it is, therefore, proposed that the sensitivity of a sensor may be reported by considering its profile for various regions of RH. Additionally, with the increase in frequency, it can be noted that the sensitivity value is decreasing for each region and also the average sensitivity value of the sensor, as shown in the last column of Table 4.3. A similar behavior is also observed in the data provided in Table 4.4 for OFET type humidity sensors. To explain the observed results, equivalent circuit diagrams of resistive and OFET type sensors under investigation are presented in Fig. 4.9. The capacitors represent the charge polarization in different layers of the sensor, whereas, the resistance shows different conducting paths within the composite. Resistive humidity sensor can be represented by a parallel combination of resistor and capacitor, whereas, in OFET, an extra layer representing gate terminal. This further adds up to the capacitance and resistance of the sensor and is represented by an additional RC combination as evident from Fig 4.9 (b).

The resistive type OD/graphene sensor impedance can be expressed as $Z_A = R_A/(1 + j\omega C_A R_A)$; such that $C_A = \varepsilon A/d$, where, A is the area defining the capacitor, $\varepsilon = \varepsilon_0 \varepsilon_m$ is permittivity defined by the active layer of the sensor, d is the separation between two electrodes and ω is angular frequency. At a given applied voltage, V and for a finished device having fixed device geometry, the impedance

TABLE 4.5: Comparative analysis of frequency dependent sensitivity (S_Z) of various sensing materials used in flexible humidity sensors.

Ref	Year	Sensing Material	100 Hz	1 kHz	10 kHz	100 kHz	200 kHz
[187]	2012	Textile/Ag	2.79 MΩ	310.86 kΩ	35.07 kΩ	3.71 kΩ	-
[211]	2012	Graphene Oxide	25.74 kΩ	2.61 kΩ	184.94 Ω	-	-
[212]	2018	Graphene/CNT	71.97 Ω	58.97 Ω	29.1 Ω	-	-
[213]	2020	Graphene Oxide	811.56 Ω	668.33 Ω	502.51 Ω	226.12 Ω	-
[214]	2021	Graphene-Flower Composite	-	-	1.55 kΩ	1.26 kΩ	-
This Work-1	2022	OD/Graphene/Silicone Adhesive (Res)	8.98 MΩ	4.19 MΩ	407.75 kΩ	113.51 kΩ	30.83 kΩ
This Work-2	2022	OD/Graphene/Silicone Adhesive (OFET)	4.69 MΩ	2.85 MΩ	238.44 kΩ	45.7 kΩ	14.78 kΩ

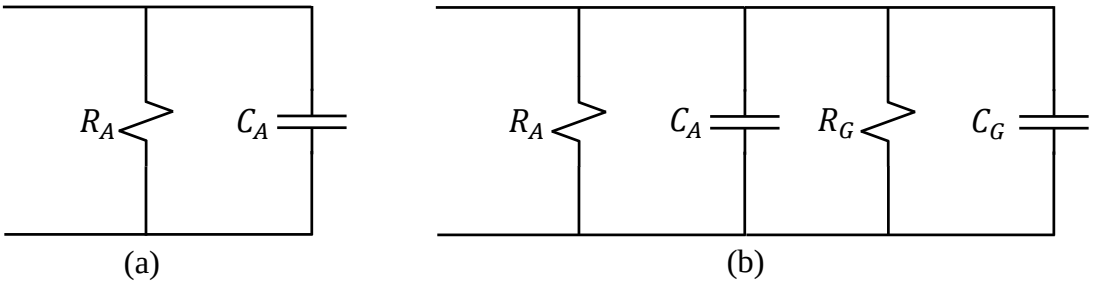

FIGURE 4.9: Equivalent circuits of a) resistive and b) OFET based sensors.

defined in Eq. 4.1 can also be written as

$$Z_A = \frac{R_A}{(1 + j\omega Q R_A/V)} \tag{4.1}$$

Water, which is a polar molecule with dielectric constant of 80 [215], causes $Q = C_A \times V$ in the composite layer to increase, which eventually reduces Z_A of the sensor as given by Eq. 4.1 and observed in Fig. 4.5. Additionally, with the increase in Q by increasing RH, C_A bond to increase to ensure validity of $Q = C_A \times V$, and the same behaviour is observed in Fig. 4.6.

It can be seen from Figs. 4.5 and 4.6 that the response of the sensor is also dependent upon the frequency and by increasing frequency, the corresponding response of the sensor is decreasing. This can be explained by considering $Z_A = (1/\omega C_A)$, which indicates that with increasing ω, the magnitude of Z_A decreases and the same is observed in Fig. 4.5. And the same explanation is valid for the plot of Fig. 4.6.

In the literature, two independent mechanisms have been reported to give fundamental understanding of electrical characteristics of sensors as a function of ambient humidity [150, 200–203, 206, 216]. First, water being a polar molecule, after interacting with a p-type polymer converts into H^+ and OH^- which increases the concentration of charges and, as a result the polymer becomes more p-type in nature. This increases the hole concentration in the polymer which eventually

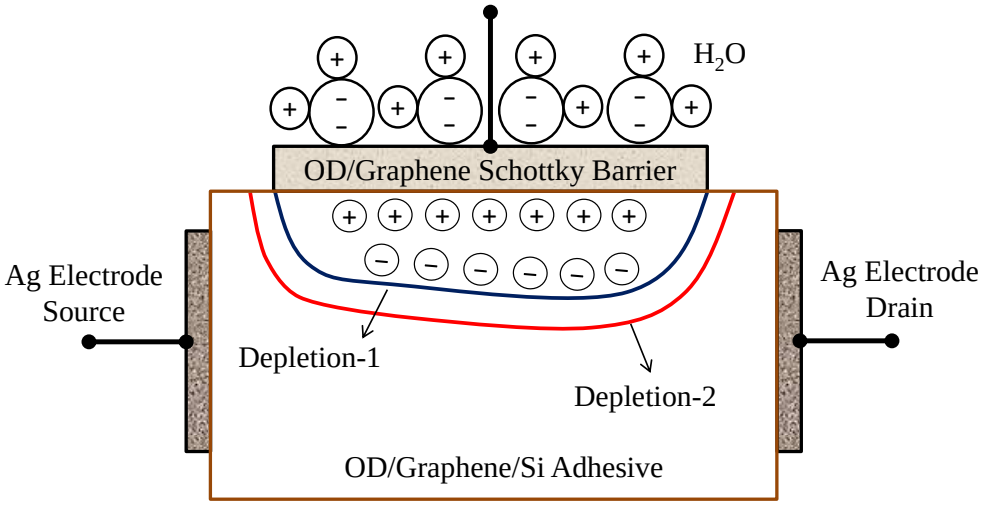

FIGURE 4.10: Effects of polar water molecules on junction depletion region: depletion-1 represents region at low humidity whereas depletion-2 at relatively high humidity.

improves the conductivity of the sample. Second, the absorbed water molecules occupy the empty space between the polymer molecules which modifies its dielectric constant and, hence, Z_A and C_A [201].

On the other hand, in OFET humidity sensor, there is an extra layer which acts as gate of the device. This additional layer at the top, adds up the resistance R_G and capacitance C_G in parallel to C_A and R_A, as shown in Fig. 4.9. This additional RC combination of OFET increases its overall capacitance and decreases resistance compared to the resistive humidity sensor. It is pertinent to mention here that C_G is primarily defined by the Schottky depletion caused by the gate of OFET. It is assumed that the surface and diffused H_2O molecules collectively modify the Schottky depletion of the device as shown in Fig. 4.10. However, the dominating factor will remain the modification from inside the channel caused by the diffused H_2O molecules. As a result, both impedance and capacitance of the sensor change as evident from Figs. 4.7 and 4.8.

A comparative analysis of flexible humidity sensors made using different materials is carried out and a summary of results is presented in Table 4.5. The data of Table 4.5 are evaluated at different frequencies but by using the reported RH_{max}

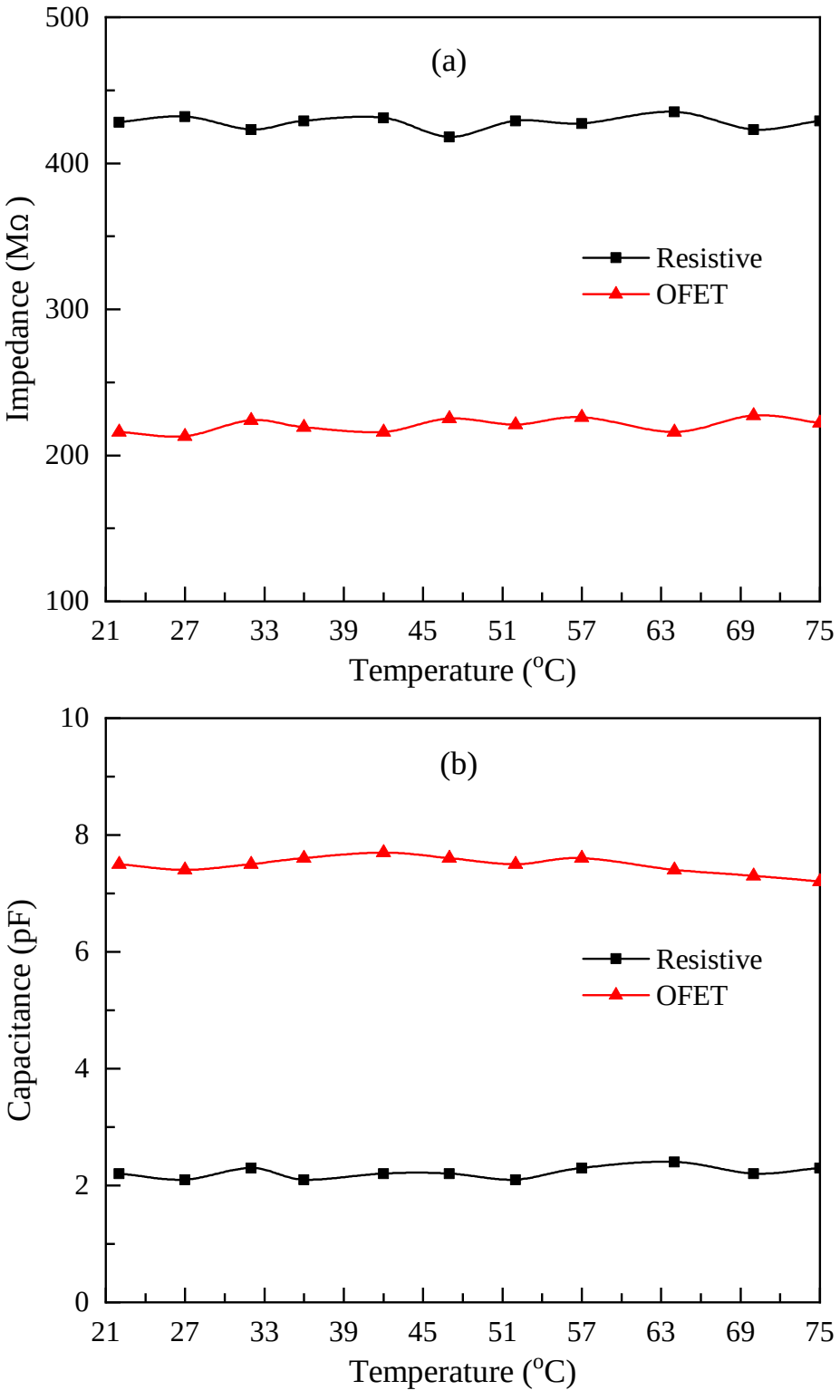

FIGURE 4.11: Temperature dependent (a) impedance and (b) capacitance profile of resistive and OFET type humidity sensors, measured at 100 Hz, RH = 33%.

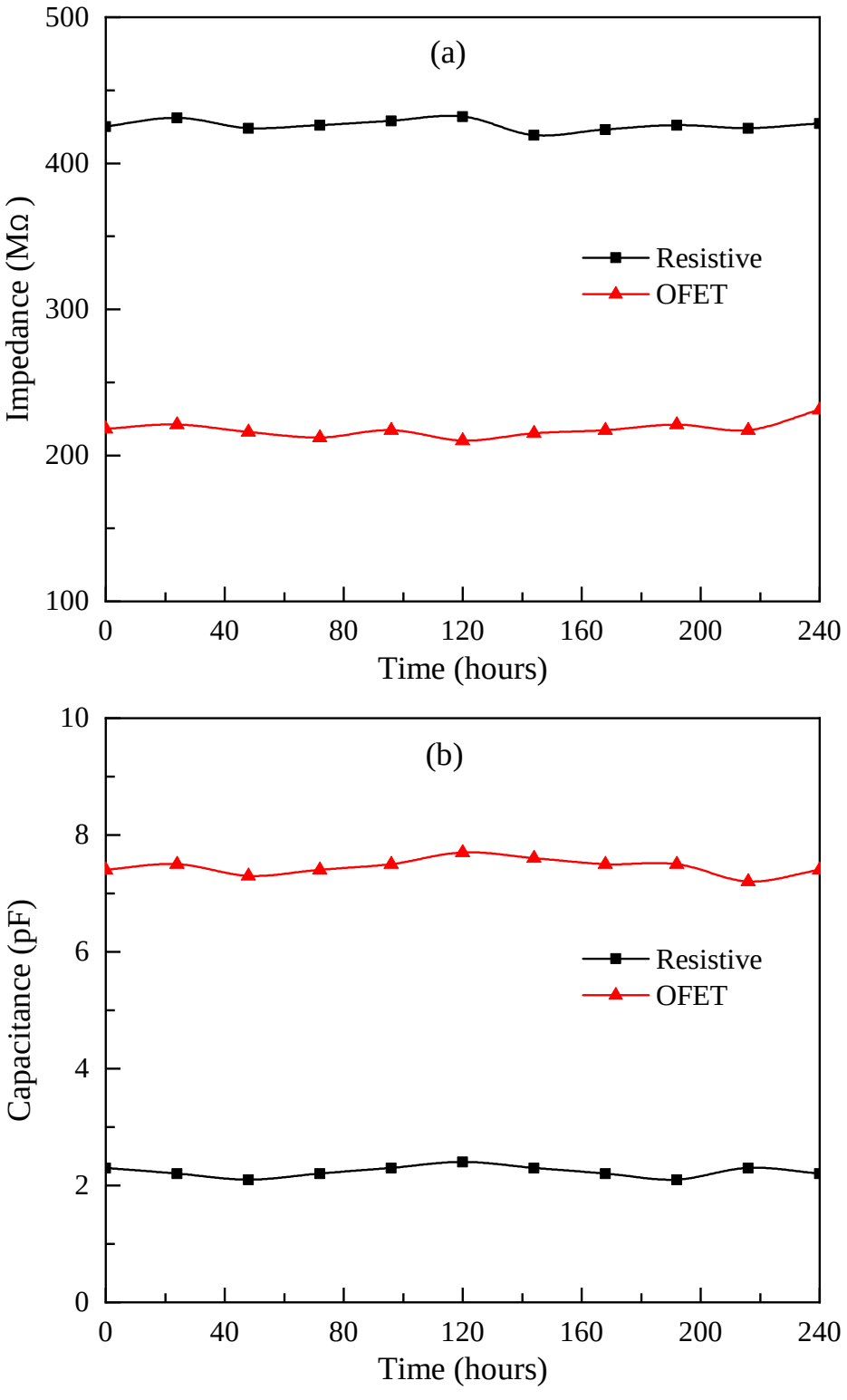

FIGURE 4.12: Time dependent (a) impedance and (b) capacitance profile of resistive and OFET type humidity sensors, measured at 100 Hz, RH = 33%.

and RH_{min} values without considering the shape of response profile of a sensor. This table shows that the performance of proposed OD/graphene/silicone adhesive

resistive type sensor as a function of frequency is relatively better than other reported flexible sensors. OFET based humidity sensor made from similar structure offer low sensitivity value for chosen frequency which is almost 50 % than that of resistive composite sensors investigated in this research. The reduction in S_Z of OFET based sensor is primarily due to the addition of a parallel combination of R_G and C_G as shown in Fig. 4.9 (b). It is observed that, OD/graphene/silicone adhesive sensors are performing relatively better than the other sensors presented in Table 4.5.

The operating temperature of humidity sensor usually affect the sensor performance and it is always extremely crucial to assess its stability for the range of temperature in which the sensor will be deployed. In order to investigate the impact of temperature on sensor impedance and capacitance, the fabricated sensors were subjected to elevated temperature ranging from 22 °C to 75 °C, and the results are shown in Fig. 4.11. It is evident from this figure that the developed resistive and OFET type humidity sensors are providing stable response, at least for the range of temperature shown in the figure.

Variation of a sensor response because of temperature is an accumulative effect of materials and their properties i.e. conductivity, dielectric permittivity and thermal expansion. This shows that the composite used in the fabrication of these sensors i.e., OD/graphene/silicone adhesive offers stable material properties for the range of temperature shown in Fig. 4.11. Thus, the performance of fabricated sensors remain independent for the given temperature range.

In order to assess long term operability and stability of the proposed humidity sensors, these sensors were also tested for various time intervals to observe changes in their impedance and capacitance and the results are presented in Fig. 4.12. Examining the data of Fig. 4.12, one can clearly claim that the proposed sensor design offers stable characteristics at least for the time interval shown in the plot. Keeping in view the characteristics of Figs. 4.11 and 4.12, it can be safely assumed that the proposed OD/graphene/silicone adhesive humidity sensors offer

stable characteristics and thus they could be considered as potential candidate for industrial applications for humidity measurements.

4.4 Summary

This work presents fabrication and characterization of flexible humidity sensors realized using a composite active layer comprising upon orange dye (30 wt.%), graphene (20 wt.%) and silicon adhesive (50 wt.%). Two type of sensors have been fabricated namely: a) resistive and, b) OFET sensors. To define the channel, in both the designs, two 300 nm thick Ag electrodes having 16 μm inter electrode spacing, were first deposited on a rubber substrate followed by the deposition of $9 - 11$ μm thick composite layer, on top of Ag electrodes. For OFET sensors, an additional layer comprising upon OD (50 wt.%) and graphene (50 wt.%) was also deposited on top of the channel layer, to achieve a floating Schottky barrier gate. Finished devices were then tested in a chamber, where, relative humidity (RH) was varied from 33% to 94%. Impedance and capacitance variations as a function of humidity and frequency were evaluated for both types of fabricated sensors. It has been shown that at 100 Hz, resistive type sensors offer 2140 times change in their impedance by changing RH from 33% to 94% which reduces to 56.67 times at 200 kHz. Whilst for OFET type sensors such a variation in RH at 100 Hz causes 3716 times change in the sensor impedance and the same reduces to 80 times at 200 kHz. On the other hand, it was observed that the capacitance of resistive type sensor at 100 Hz, changes 145 times by changing RH from 33 % to 94 % and this variation is 314 times for the OFET type sensor. Thus, impedance and capacitance variations of the proposed design demonstrated that the chosen composite is sensitive enough to be employed as an active material for humidity sensors. The design in general can be employed in any industrial process where humidity and temperature are ought to be controlled including biomedical instrumentation. To ensure the industrial applicability of the proposed design, it has been demonstrated that the finished sensors offered stable characteristics for

temperatures ranging from 20 °C to 75 °C and for a time interval of at least 240 hours.

Chapter 5

Multifunctional Temperature, Pressure and Displacement Sensors

Multifunctional sensors unlike ordinary sensors, can measure a number of parameters such as temperature, humidity, strain, displacement etc., that are important for both research and industrial applications. For the past few years, a number of sensors, which can be used in different areas of technology such as environmental assessment were fabricated and investigated by various research groups [133, 137–139, 217, 218]. A capacitive touch sensor array was fabricated by employing stretchable and transparent electrodes with a simple selective patterning process, and by selecting an appropriate dielectric and substrate materials having low strain response [217]. Multifunctional sensors to measure oil, water, and salt contents are fabricated and investigated using conductivity and ultrasound method to overcome high cost, low precision and operational difficulties [137]. Multifunctional sensors, reported in [133], are fabricated using silicone hydrogels to detect pH value of solutions, types of solvent and ethanol percentage in water. Multifunctional tactile sensors, reported in [218], are fabricated to collect a set of information concerning tactile interaction between a manipulator and an object to be recognized. These sensors are based on piezo- and pyro-electric (ferroelectric)

properties of polymeric materials; such as polymer polyvinylidene fluoride (PVF_2 or PVDF), different polypeptides and copolymers of PVF_2 and TrFE. Stretchable multifunctional sensors using capacitive sensing mechanism are fabricated using silver nanowires as electrodes and Ecoflex as dielectric to measure strain and finger touch [138]. In 2017, Choi *et al.* developed a multifunctional sensor using single sensing element of $p-$type metal-oxide ceramic semiconductor to measure humidity and concentration of gases in the atmosphere [139].

Primary techniques involved in the integration of carbon nanotubes (CNTs) into various devices along with their electrical, mechanical and electromechanical properties are discussed in [134]. CNTs based electrochemical biosensor fabrication, characterization, theoretical understanding and working principles are presented in [97]. They also reported CNT based modified sensor properties; such as structural regularities and energy parameters, by analysing the mechanisms of nanotubes interaction with functional groups, metallic nanoparticles and polymers; leading to the formation of chemically active sensors.

Conor *et al.* in 2014, reported a simple method to infuse liquid-exfoliated graphene into natural rubber to create conducting composites [219]. They presented excellent strain sensors, displaying 104-fold increase in resistance while working at strains exceeding 800%. They reported gauge factors up to 35 and the sensors could effectively track dynamic strain, working at vibration frequencies up to 160 Hz. These composites can be used for bodily motion sensors, effectively monitoring joint and muscle motion including breathing and pulse [219]. In [220] pressure sensors are fabricated and investigated using graphene in-plane and tunnelling. Their findings were that in case of in-plane pressure sensor, current is negatively correlated to pressure; whereas, in a tunneling pressure sensor, current is positively correlated to pressure.

Recently, different sensors; such as flexible impedance and capacitive tensile load sensors based on CNT composite are fabricated and characterized [221]. CNT-silicone nano composites based resistive temperature sensors are reported in [222]. In [223], flexible resistive tensile load cells based on multiwall CNT (MWCNT)/

rubber composites are investigated. Pressure sensitive organic sensor based on CNT-VO2(3fl) composite [224], temperature gradient measurement sensor using thermoelectric effect in CNTs-silicone adhesive composite [225] and temperature gradient sensor based on CNT composite [226], are fabricated and investigated for their potential use in the industry.

Taking into account CNT and graphene compositions similarity [135, 136, 227–229] and to continue exploring organic materials based electronic devices, in the present paper, authors have investigated the properties of pristine orange dye (OD), CNT and graphene based multifunctional sensors as a function of pressure, temperature and displacement. Multiple sensors have been fabricated by varying the thickness of OD and its effects on the sensitivity of the sensors were assessed. The proposed multifunctional sensor could be a potential candidate to replace individual sensors usually employed in the industry (e.g. flex bonding head) for the measurement of displacement, pressure and temperature. Because, it offers an economical solution being lighter in weight, simpler in design and low in maintenance and cost.

5.1 Experimental

Fig. 3.1 shows schematic diagram of molecular structure of commercially available pristine Orange Dye OD. Fig. 5.1 shows a simplified schematic diagram of the proposed multifunctional temperature, pressure and displacement sensor and its different constituent parts.

The length and external diameter of the cylindrical body of the multifunctional sensor were set as 22 mm and 10 mm; diameter and height of the fixed electrode was 6 mm and 5 mm and movable metallic electrode was 6 mm and 10 mm, respectively; and sensor was hermetically sealed by an airtight elastic ring as shown in Fig. 5.1. To assess temperature dependent variation in resistance and impedance, the movable electrode of the sensor was kept fixed by deploying fixtures, and for pressure and displacement measurements, the movable electrode was allowed to

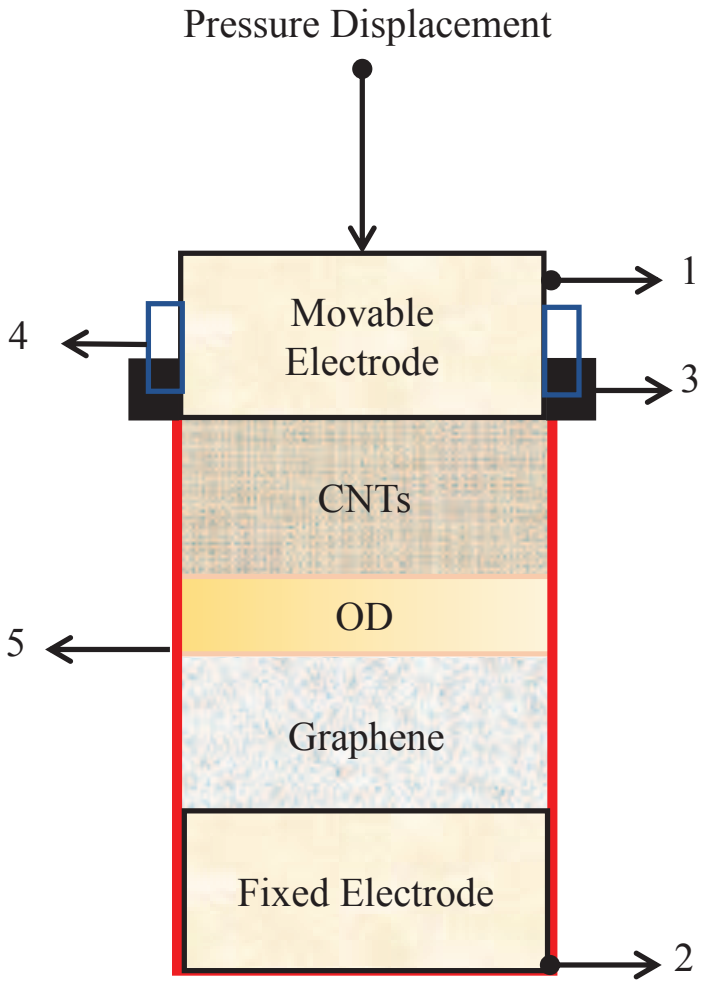

FIGURE 5.1: Schematic diagram of a CNTs-OD-Graphene multifunctional temperature, pressure and displacement sensor: terminals for measurements (1 and 2), fixtures for fixing of movable metallic electrode (3), air tight elastic ring (4), transparent plastic cylindrical body (5).

move freely within the transparent plastic cylindrical body. Thickness (d) of the OD powder was calculated using the following expression

$$d = RA\sigma \tag{5.1}$$

where R represents resistance, A crossectional area and σ conductivity of the sample.

The conductivity of OD was previously reported by us in [230] as 2.4 $\times 10^{-4}$ Ω^{-1}

TABLE 5.1: CNT-OD-Graphene Based Multifunctional Sensor Layer Thicknesses

Sample Number	**CNT Thickness (mm)**	**Orange Dye Thickness (μm)**	**Graphene Thickness (mm)**
Sensor 1	5 mm	300 μm	5 mm
Sensor 2	5 mm	380 μm	5 mm
Sensor 3	5 mm	570 μm	5 mm

cm^{-1}. Using reported conductivity value of OD and the measured resistance, the thicknesses of OD of three samples under investigation were calculated, using Eq. 5.1, and found to be 300 μm, 380 μm and 570 μm as shown in Table 5.1. The obtained thickness of the OD layer of each sample was then verified by optical microscope as colour of OD was different from CNT and graphene. This ensured that the OD powder layer separated the highly conductive CNT and graphene powders columns with a specific thickness as given in Table 5.1. It was also observed that the replacement of CNT and graphene or vice versa, or variation in the height of the CNT or graphene powder column did not have a substantial affect on the characteristics of the sensors as compared to the thickness of the OD powder layer. This primarily is due to the fact that the multifunctional sensor operates as a resistor where each layer, i.e. CNT, OD and graphene has its own characteristic resistance. The resistance of OD when compared to CNT and graphene is significantly higher therefore, any change in CNT and graphene thicknesses becomes relatively insignificant.

The effect of pressure and compressive displacement on multifunctional sensors was investigated using experimental setup and methodology presented in [231]. The multifunctional sensor was loaded with the organic materials CNTs, OD and graphene powders. The commercially available MWNTs particles used in our research work have diameter variation from 10–30 nm. Multifunctional sensors exhibited a good resistive response as a function of pressure; therefore, their properties were investigated at pre-pressed conditions, i.e. by creating initial pressure, which defined the corresponding initial resistance and impedance. This initial resistance and impedance of the sensors were then allowed to change as a function of temperature, pressure and displacement to obtain the sensor characteristics.

Temperature was measured using a digital multimeter FLUKE 87 while resistance and impedance (at 100 Hz and 100 kHz) were assessed using digital MT 4090 LCR meter.

5.2 Results and Discussion

Fig. 5.2 shows variation in resistance and impedance (at frequency 100 Hz and 100 kHz) as a function of temperature of multifunctional sensors whose fabrication details are given in Table 5.1. Examining the response given in Fig. 5.2(a) to 5.2(c), it is obvious that by increasing the thickness of OD layer, the initial resistances and temperature dependent response of the the sensors, both are increasing. Such a behavior is known for posistors; positive temperature coefficient resistors, usually based on rare earth elements as barium titanate ($BaTiO_3$). Recently, posistors are also fabricated on the basis of conducting polymer/graphene and composite as well [232].

Fig. 5.3 shows resistance and pressure relationships for the CNT-OD-Graphene powders multifunctional sensors. With an increase in pressure up to 0.1 kgf/cm^2, the resistance is decreased by 1.29 and 12.7 times (from 6730 Ω to 5210 Ω; and from 3410 Ω to 269 Ω), and is attributed to the geometrical factors i.e. under pressure, resistances between particles decrease due to increase in area of contacts between the particles. Secondly, there is increase in the conductivity of the materials due to increase in concentration of charges and mobility. The increase in the mobility may be associated with the reduction of the mean free time of the carriers which can hop with ease at elevated pressure.

Fig. 5.4(a) and Fig. 5.4(b) show resistance and compressive displacement relationships for the CNT-OD-Graphene based multifunctional sensors. The data of the figure exhibit that there is 3.18 and 7.53 times decrease in the resistance of sensor 2 and sensor 3 (from 2235 Ω to 702 Ω; and 6787 Ω to 901 Ω), respectively, for a compressional displacement of 0 μm to 110 μm between the two electrodes of the

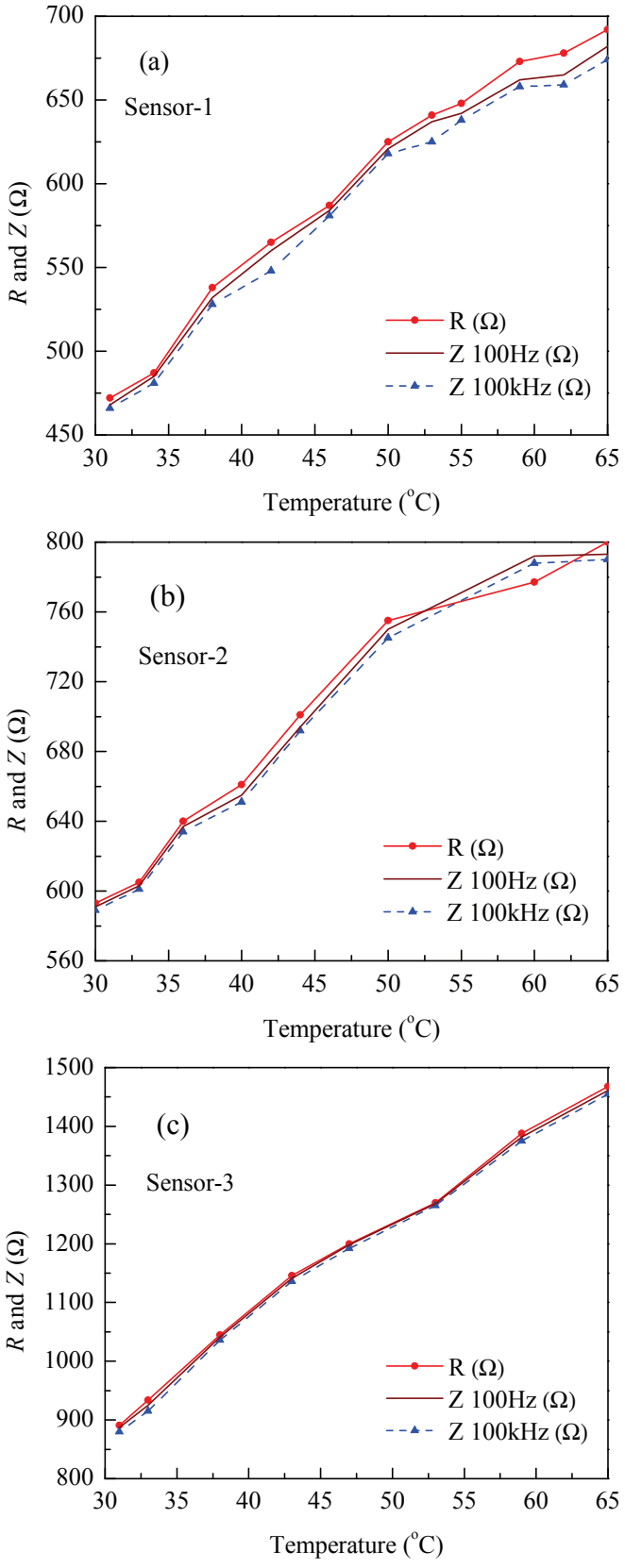

FIGURE 5.2: Resistance and impedance (at 100 Hz and at 100 kHz) variation as a function of temperature for CNT-OD-Graphene based multifunctional senors. (a) Sensor 1: OD thickness = 300 μm, (b) Sensor 2: OD thickness = 380 μm and (c) Sensor 3: OD thickness = 570 μm.

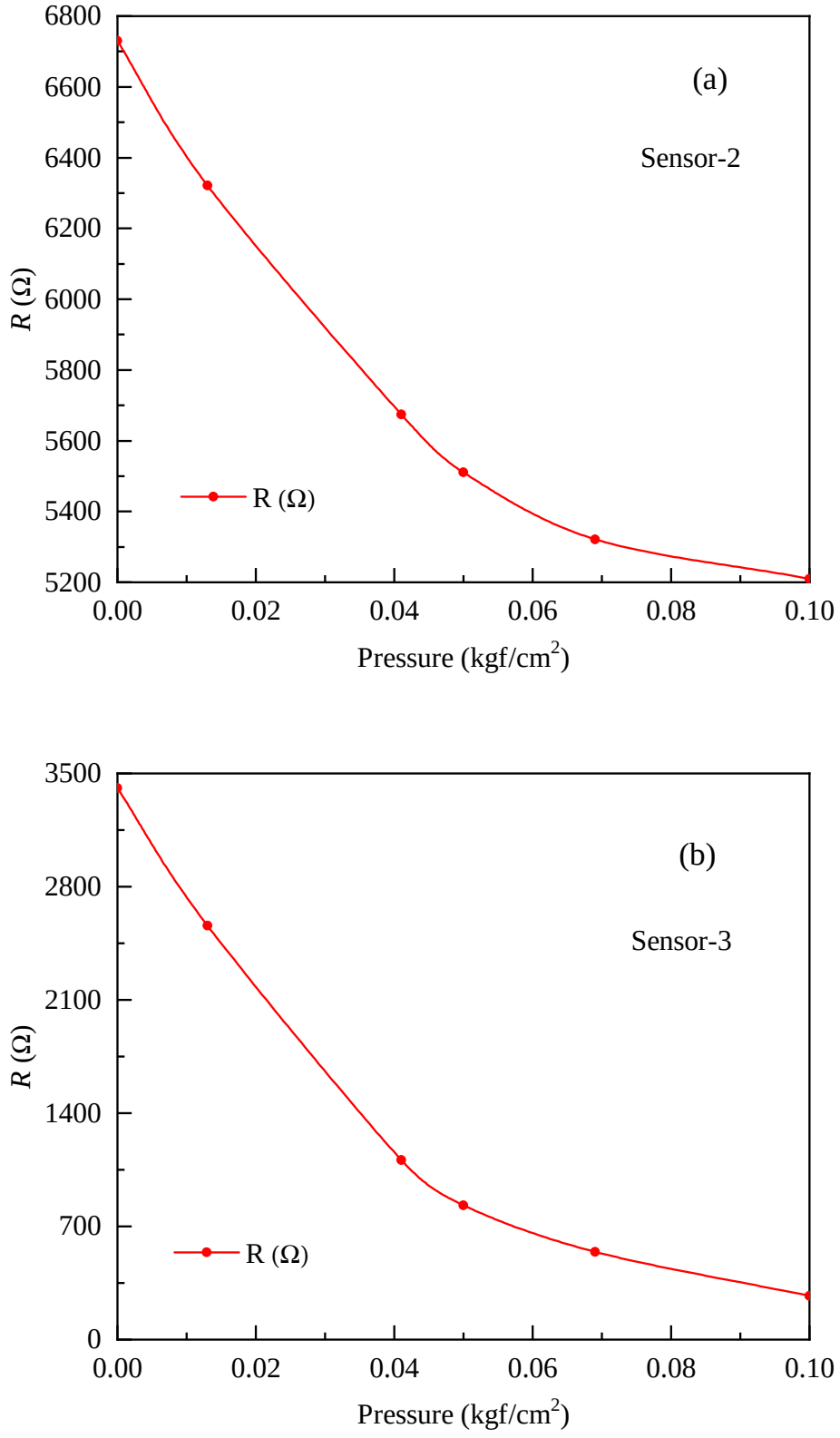

FIGURE 5.3: (a) Variation in resistance (R) as a function of pressure of a multifunctional CNT-OD-Graphene based sensors (a) OD thickness = 380 μm i.e. Sensor 2 (b) OD thickness = 570 μm i.e. Sensor 3

sensors. Three conduction mechanisms in principle can be realized in organic semiconductors, i.e. hopping, band and/or tunneling [233]. CNT and graphene used in this study showed metallic resistance-temperature behavior. Taking into account that the resistance of the OD was considerably larger than the resistances of CNT and graphene; thus, at CNT-OD and graphene-OD interfaces, the charge-transfer complexes may be formed, which may have relatively higher resistance than not only of CNT or graphene, but even of OD due to transfer of charges from OD into CNT or graphene. In this case, the interface resistance values would be large as of posistors because, the usual temperature dependent behavior of a metal is different than what is exhibited by OD as a semiconductor in its conductivity-temperature profile [230].

It is observed that due to exerted pressure or displacement, the contact and the bulk resistances of the CNT or graphene sample with OD particles may decrease. It is known that CNT and graphene have distinct structures. CNTs can be either metallic with no bandgap, or of distinct bandgap defining its nature as semiconductor material. It has also been shown that the nature of CNT bandgap can be controlled by using thin graphene sheets of specific orientation [234, 235]. The single-particle band structure and electronic band structure of graphene based on rectangular 4-atom unit cell is developed and discussed in [236]. On the other hand, CNT showed high mechanical and thermal stability and high thermal conductivity [237–241]. Metallic CNTs have been identified as possible interconnect materials of future technology, and they can possibly replace Al and Cu interconnects [242].

In order to explain electrical conductivity in graphene and CNTs, the following expression is proposed in [243, 244]:

$$\sigma = ne^2\tau/m \tag{5.2}$$

where σ, n, e, τ and m are conductivity, concentration of charges, electron charge, mean free time and mass of electron, respectively.

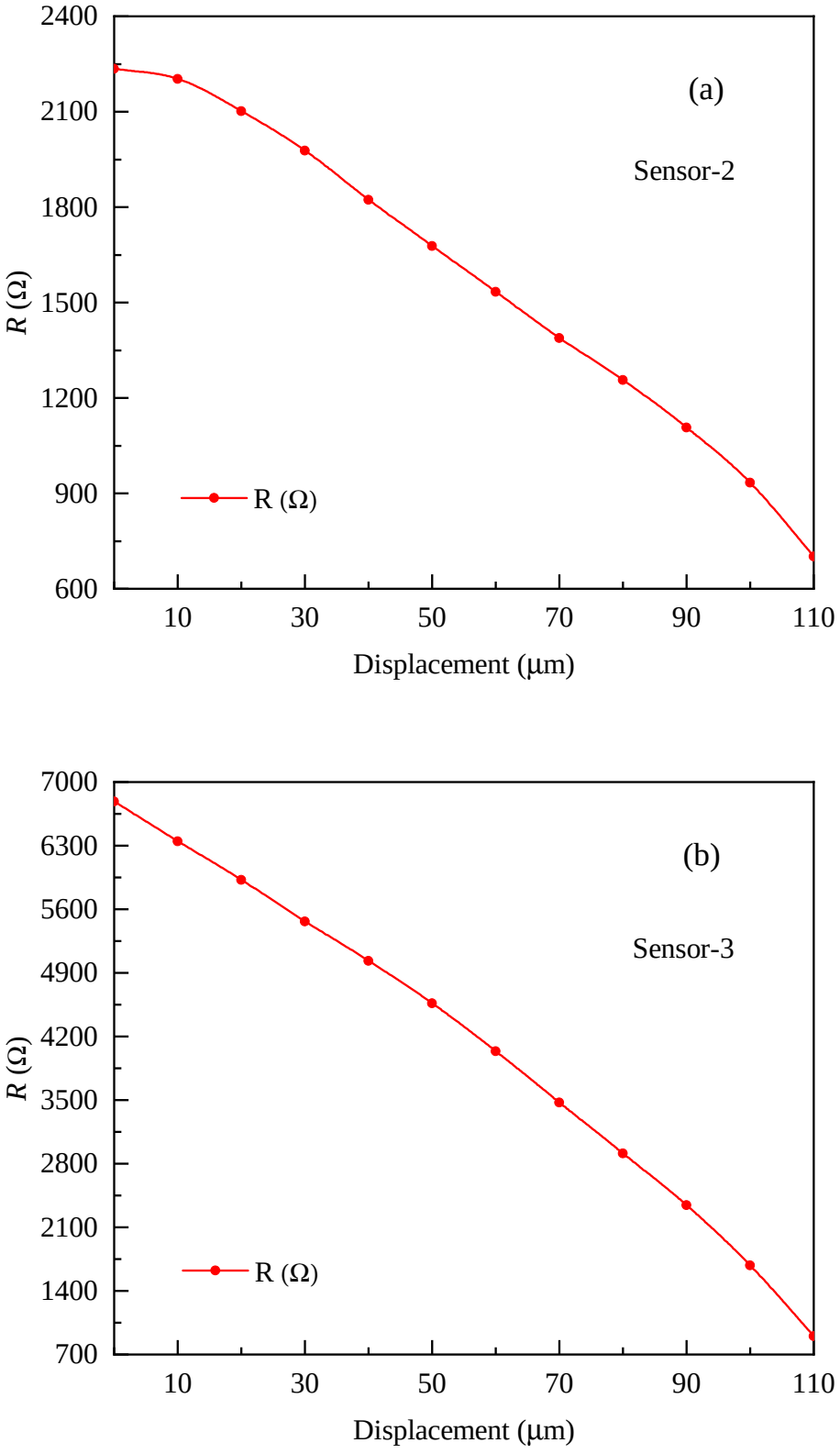

FIGURE 5.4: Resistance-displacement relationships of CNT-OD-Graphene based multi-functional sensors (a) having OD thickness = 380 μm: Sensor 2 and (b) OD thickness = 570 μm: Sensor 3.

By using Eq. 5.2, OD-CNT and OD-graphene interface electric properties can be explained. The increase in temperature will decrease the mean free time and increase the transfer of charges from OD into CNT or graphene, as a result, charge transfer complexes formation will take place. This will decrease the conductivity of CNT-OD and graphene-OD interfaces and accordingly the resistance of the sample will go up, and the same was observed experimentally (Fig. 5.2). Charge transfer form OD to CNT has previously been reported by our group [245]. An increase in positive temperature coefficient (PTC) of the graphene nano-sheets (GNS) and ultrahigh molecular weight polyethylene composite, with a two-dimensional conductive network, was observed when they were thermally treated at elevated temperatures [232, 243, 246–251]. This anomalous phenomenon could be originated from the reduced viscosity of polymer matrix, crystallization induced local flow and/or weak interactions among the overlapping joints of GNSs, which allow GNSs to migrate to the polymer matrix; thus, weakening the conductive paths and increasing the value of PTC. A facile approach is accordingly developed to prepare a conductive polymer composite with a tunable PTC value.

At elevated pressure, the resistance of CNT-OD-Graphene sample decreases (Fig. 5.3) and a plausible explanation of such a behavior could be that at increased pressure, there is an increase in mean free time of electrons, which in return decreases inter-particle resistance in CNT and graphene. Moreover, the inter-particle contact resistance may also be decreased under increased pressure causing an overall reduction in the resistance of the samples [140]. Furthermore, OD, which is sandwiched between CNT and graphene, is an organic semiconductor and at elevated pressure, there could be more available free charges for conduction and hence, reduction in resistance of the samples. Additionally, at elevated pressure, there could be a possibility of increased hopping; thus, improving the mobility and as result reducing resistance of the samples was observed experimentally [251]. Since the pressure and compressional displacement response profiles are similar in nature, i.e. each one is declining with the increase of its respective variable (pressure or compressional displacement), as shown in Figs. 5.3 and 5.4, therefore,

TABLE 5.2: Comparison of organic semiconductor based temperature sensors.

Ref.	**Sensing Material**	**Sensitivity ($\Delta R/R$)**	**Temperature Change (°C)**
[74]	CNT-PEDOT:PSS	0.15	$20-80$
[252]	CNT-PEDOT:PSS	0.3	$20-55$
[253]	R-GO/PU	0.7	$30-80$
This work	CNT-OD-Graphene	0.62	$30-65$

TABLE 5.3: Organic semiconductor based pressure sensors with associated sensitivities.

Ref.	**Sensing Material**	**Sensitivity (kPa^{-1})**	**Pressure Range (kPa)**
[254]	PPy film	0.4	> 1
[255]	PPy-Ag NWs	0.33	< 10
[256]	Sponge-CNTs	2.12	$2.24-11$
[257]	GPN-PDMS foam	0.09	< 103
[258]	RGO-PU sponge	0.26	< 3
[259]	NWs-PDMS	1.14	< 5
[260]	PDMS	0.23	< 6.7
[261]	rGO	0.46	$< 0.5-8$
This work	CNT-OD-Graphene	2.57	< 1

for compressional displacement, a similar explanation, as given in the case of pressure, could be offered.

In this chapter, a multifunctional sensor is developed and its characteristics as temperature, pressure and displacement are studied. The proposed design is novel in nature and it is hard to compare it on one-to-one basis with other sensors reported in the literature. However, to have a feel about the proposed design viz-a-viz the other organic sensors meant for a specific application; such as, temperature and pressure. Data in this respect have been collected and presented in Table 5.2 and 5.3 for temperature and pressure sensors, respectively. Examining the data of these tables, it can safely be claimed that the proposed design offers multitasking

facility on one hand and on the other hand, it exhibits competitive sensitivities for the designed variables.

5.3 Summary

We have presented a new resistive type multi-functional sensor fabricated using orange dye (OD) sandwiched by carbon nanotube (CNT) and graphene material. The proposed sensor, as a one device, can be employed to measure temperature, pressure and displacement. It has been observed that the output resistance and impedance of the fabricated sensor is directly proportional to temperature, inversely proportional to pressure and displacement change. The temperature coefficients of the multifunctional sensors are measured and found equal to 1.0% $^{\circ}C^{-1}$ for sensors having initial resistance ∼470 Ω and 1.9% $^{\circ}C^{-1}$ for those sensors having initial resistance ∼890 Ω. Under the applied pressure of 0 kgf/cm^2 to 0.1 kgf/cm^2, the measured resistance of the multifunctional sensors showed a decrease from 6730 Ω to 5210 Ω (1.3 times) and from 3410 Ω to 269 Ω (12.7 times) for two different thicknesses of OD layer; whereas, for the displacement of 0 to 110 μm, the decrease in resistance value is from 2235 Ω to 702 Ω (3.18 times), and 6787 Ω to 901 Ω (7.53 times). It has been shown that the sensitivity of the proposed sensor can be controlled by changing the thickness of OD layer. The proposed sensor can potentially replace multiple sensors needed to measure temperature, pressure and displacement in industrial applications; such as flex bonding head, with a single sensor involving simpler design; lighter weight, low maintenance and eventually of low cost.

Chapter 6

Carbon Nanotubes-Silicon Adhesive Composite Based Strain Sensors

6.1 Introduction

Modern design and construction of high rise civil structures are based on safety and serviceability criteria prescribed in practice codes of the relevant body. These criteria involved allowable stresses and deflections, which, in the design phase, are typically predicted using structural analysis. Prediction of external forces on a concrete structure plays a crucial role in the life span of a building. The stress measurements can be performed easily on steel cables but cannot be studied on steel beams or concrete structures. Therefore, strain is a parameter that can be used and is in direct relation with the stress through constitutive equations; and any change in the latter would result in a change in the former [262]. Strain measurements are not only limited to buildings, but also have diverse application areas including railway lines, aircraft wings, turbines, ship propellers, and ship hulls.

Electromechanical transducers based on piezo-resistive effect have been reported previously for their use in for strain sensing applications. These sensors showed good strain sensitivity for larger stain values; however, for lower strain values, new materials system are being explored to achieve good gauge factor; and hence, sensitivity. Among the recently explored new materials, CNTs show impressive properties. The unique atomic structure of the CNT allows us to achieve high sensitivity and an additional advantage of smaller size [106]. Hence, the CNT based sensors can be fabricated at a micron scale dimension with high gauge factor [106].

In the past, a good interest was shown towards the investigation of electromechanical properties of CNTs, especially, the piezo-resistive properties; for designing new micro-strain sensors [103–106, 108]. Various pressure sensors and accelerometers utilizing the piez-oresistive properties of CNTs were fabricated and investigated [103–106, 108]. The piezo-resistance of CNTs on deformable thin-film silicon nitride membrane was first investigated by Grow *et al.* [106]. It was found that the sensitivities of the semiconducting and small-gap semiconducting (SGS) tubes were up to 400 and 850, respectively; whereas, the maximum sensitivity of silicon was 200. Piezoresistive sensitivity from 600 to 1000 under axial strain was observed by Cao *et al.* [103] in the small band-gap semiconducting (quasi-metallic) nanotubes that is much larger than in metallic nanotubes materials.

Xue and Cui [108] described the fabrication of SWCNTs thin-film transistor on a plastic substrate and observed the variation in resistance upon bending the substrate. The piezo-resistive effect of P-CNT film was investigated by Li *et al.* [104], and reported a value of sensitivity equal to 65 under 500 micro-strains at room temperature. Regoliosi *et al.* investigated mechanical deformation-conductivity relationship of free-standing membrane of SWCNTs [105], and reported that the piezo-resistive sensitivity of SWCNTs is 2.3–2.5 times greater than that of Si substrate.

Stampfer *et al.* [107], investigated nano-electromechanical-piezo resistance sensors based on SWCNTs and showed both theoretically and experimentally that the

SWCNTs exhibited nonlinear piezo-resistive sensitivities of up to 1500 under an applied strain of 1%. Liu *et al.* [109], investigated the properties of MWCNTs-poly (L-lactide) nanocomposite strain sensors for biomechanical implants.

Vemuru *et al.* [110] investigated strain sensing properties of MWCNTs film and Saleem *et al.* [114] studied strain sensors based on twin and uniform crystals of TCNQ ion-radical salts. Further, Yasin *et al.* [116] investigated polymer-fullerene bulk hetero-junction based strain sensitive flexible OFET and Alamusi *et al.* [111] reviewed the advancements on the piezo-resistive strain sensors, utilizing CNTs based polymer nanocomposites.

Obitayo and Liu [263] described CNTs based piezo-resistive strain sensors and showed that CNTs sensors offered a stable and predictable response as a function of temperature. Grabowski *et al.* [113] developed strain sensors based on CNTs/Epoxy using a simplified fabrication technique involving screen printing. Sapra [115] showed that in comparison with traditional strain sensors the CNT sensors have high gauge factor (22.4) at nano and macro scales.

Karimov *et al.* in 2011 [264] designed, fabricated and investigated CNTs based strain sensors fabricated using pressurized press technique to convert CNTs powder into tablets attached to an elastic polymer beam. These sensors were characterized under DC bias and the observed strain sensitivity was 50–80, which showed a decreasing trend under compression and an increasing trend under tension. This chapter presents design, fabrication and measurement of strain sensors fabricated using a composite of commercially produced CNTs and silicone adhesive. The fabricated sensors were then tested for their potential used in the relevant industry such as civil structure etc.

6.2 Material and Fabrication

MWCNTs powder used for the strain sensor was purchased from a commercial supplier, Sun Nanotech Co. Ltd., China. Non-functionalized MWCNTs were

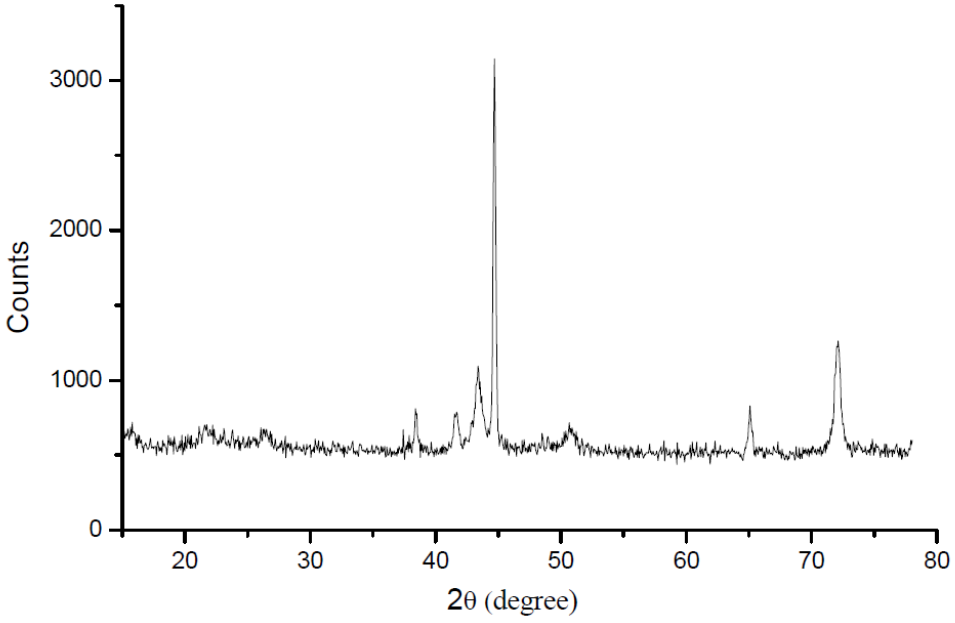

FIGURE 6.1: XRD of CNT-silicone adhesive composite film.

utilized without further purification steps. Silicone adhesive was mixed with CNTs powder to make a composite. The diameter of MWNTs varied from 10 nm to 30 nm. CNTs and silicone composite was drop casted on to Al metal electrodes contacts patterned on a triangle shape elastic polymer (poly- methyl matacrylate), beam. Al metal was 15 μm thick, and the inter-electrodes distance (length) and width of the lateral electrodes was equal to 1.5 mm and 4 mm, respectively.

The thickness of the drop casted CNT-silicone composite films was measured and found to be 15–20 μm. Three different compositions of CNTs in the composites, 80 wt.%, 45 wt.% and 20 wt.% were studied. It was found that CNTs (80 wt.%)-silicone adhesive (20 wt.%) composite was not uniformly mixed; whereas, CNTs (20 wt.%)-silicone adhesive (80 wt.%) had relatively high impedances of $20-24$ kΩ at frequency of 100 Hz. Samples contained CNTs (45 wt.%)-silicone adhesive (55 wt.%) offered 2–3 kΩ impedance at 100 Hz. Additionally, films deposited using composite of CNTs (45 wt.%)-silicone adhesive (55 wt.%) were uniform, which can potentially be employed in a strain sensor for reliable results.

Fig. 6.1 shows the XRD measurement of the film consisting of 45 wt.% of CNTs (45 wt.%) in silicone adhesive. The XRD diffraction pattern has major peaks of

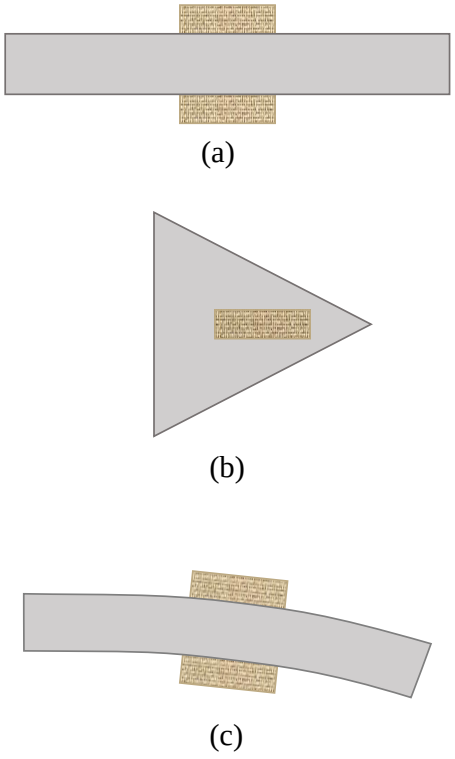

FIGURE 6.2: Simplified schematic diagrams of strain sensor attached to an elastic beam; (a) side view, (b) top view, and (c) side view of the sensor attached to the beam under loading.

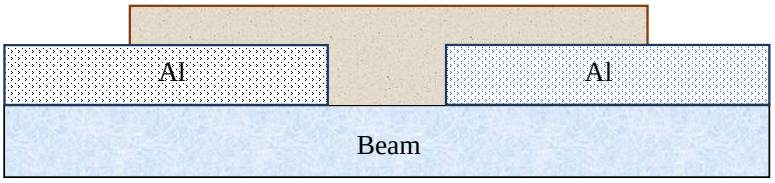

FIGURE 6.3: Cross-sectional view of a strain sensor installed on a plastic beam.

silicon compounds however, there is a minor peak at $2\theta = 26$ which belongs to CNT's.

6.3 Measurements and Characterization

Fig. 6.2 shows the schematic diagram of the strain sensor attached to a polymer beam. The strain mechanism associated with the beam bending under the action of loading has been discussed and reported in [249]. The authors explained that the longitudinal strain (ε) can be determined using Eq. 6.1:

$$\varepsilon = \frac{6LP}{b_0 h^2 E_l} \tag{6.1}$$

where $L = 150$ mm is the length, $b_0 = 30$ mm is the width at foot of the beam, h represents thickness of the beam equal to 1.5 mm. The variable E_l represents modulus of elasticity and $P = 0.68$ N represents maximum load. Fig. 6.3 shows a cross-sectional view of impedance strain sensor installed on an elastic beam. The average modulus of elasticity of the beam made from PMMA is 3000 MPa.

The experimental error of (χ) was found equal to ±5%. The impedance of the samples was measured at 100 Hz and 1 kHz with the accuracy of ±2%. As the CNT-silicone composite has good adhesion to the polymer therefore, it is considered that the samples have good adhesion to the surface of the beam. It is also assumed that metal electrode contacts have no impact on measured data [109, 110]. The X-ray diffraction measurements of the samples were conducted using Philips PW1830 X-ray diffraction system in Bragg-Brentano (θ–2θ) scan mode using Cu-Kα radiation source at room temperature. Before each scan a standard sample of silicon single crystal was measured to calibrate the system. To measure the impedance response of the strain sensor, a frequency of 100 Hz and 1 kHz was selected. An LCR meter MT-4090 was used to measure the impedance of the fabricated strain sensors.

6.4 Results and Discussion

The fabricated strain sensors impedance response was measured with and without load. It was found that the sensors fabricated using composite consisting of 80 wt.%-CNT showed inconsistent results due to non-uniformly mix of CNTs in the silicon adhesive; whereas, sensors fabricated using 20 wt.%-CNT has relatively high impedance values, in the range of 20 kΩ to 24 kΩ at frequency of 100 Hz. On the other hand, the strain sensors fabricated using CNT (45 wt.%) offered 2 kΩ to 3 kΩ impedance at 100 Hz and observed results were stable and repeatable.

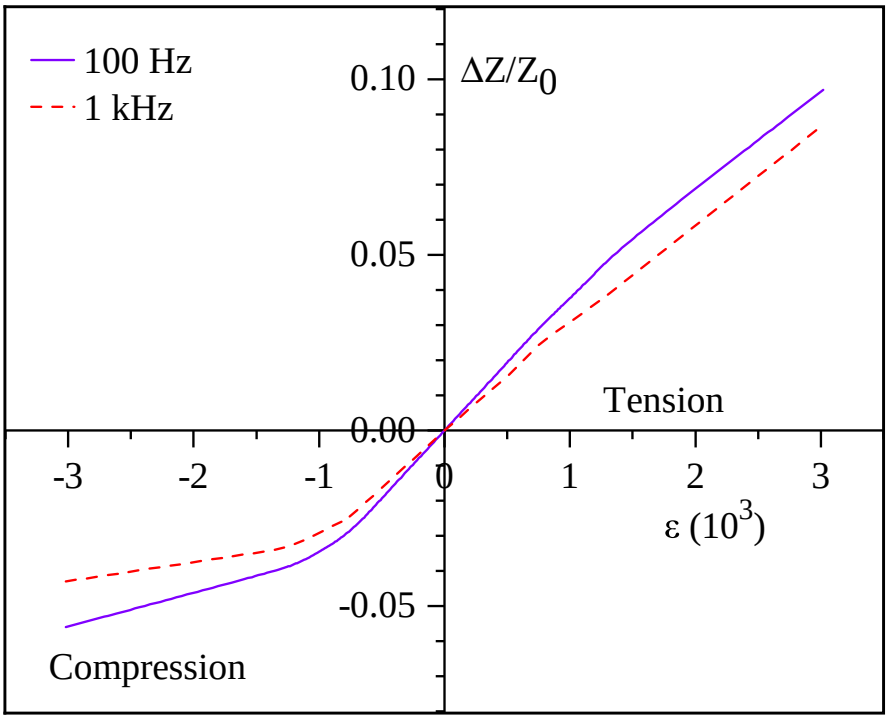

FIGURE 6.4: The impedance-strain relationships for CNT-silicone adhesive composite under tension and compression at frequencies of 100 Hz and 1 kHz.

Figs. 6.4 shows the impedance-strain relationships under tension and compression at frequencies of 100 Hz and 1 kHz. Here $\Delta Z = Z – Z_0$, where Z is impedance under load and Z_0 is initial impedance with no load condition. The strain $\varepsilon = \delta l/l_0$, where $\delta l = l - l_0$, such that l_0 defines initial length of the sensor element in the direction of applied load, and l gives length of the sensing element under load.

Examining the data of Fig. 6.4, one can clearly see that at both the frequencies under consideration, the impedance-strain relationship showed almost a linear response for the device when subjected to tension. However, at 100 Hz, the response is slightly improved compared to 1 kHz. On the other hand, when the sample is placed under compression test, it did not exhibit a linear response, as evident from 3rd quadrant of Fig. 6.4. The strain sensitivity, S of the fabricated sensor is given by Eq. 6.2 [265]:

$$S = \frac{\delta Z/Z_0}{\varepsilon} \tag{6.2}$$

The strain sensitivity was calculated using an average of five samples when a tension of 32.1 (at 100 Hz) and 28.8 (at 1 kHz) was applied, and also under a compression of 18.5 (at 100 Hz) and 14.2 (at 1 kHz). The initial impedance was measured and found 2.520 kΩ (at 100 Hz) and 2.204 kΩ (at 1 kHz). The measured results showed that, in general, the impedances of the samples increased under tension and decreased under compression.

Fig. 6.5 shows the equivalent circuit of the impedance strain sensor. The equivalent circuit is developed as a parallel connection of resistance and capacitance [265]; whereas, the impedance (Z), resistance (R) and capacitance (C) are related as shown in Eq. 6.3 [249].

$$Z = \frac{R}{1 + j\omega RC} \tag{6.3}$$

The magnitude of Z of the sample is represented as equal to the sum of the two contact and one bulk impedances connected in series.

This relationship and equivalent circuit of Fig. 6.6 shows that at tension, the impedance may increase due to increase of the resistance (R) and decrease of the capacitance (C). At compression, the impedance may decrease due to decrease of the resistance and increase of the capacitance. Moreover, by increasing frequency, impedance decreases due to the presence of capacitance.

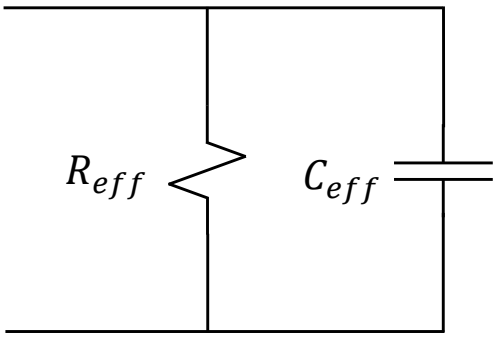

FIGURE 6.5: Equivalent circuit of the impedance as a parallel combination of resistance and capacitance.

Fig. 6.6 shows simplified structure of the fabricated samples. For simplicity, only three CNT nanoparticles surrounded by silicone adhesive are presented. Fig. 6.6

represents three different scenario possibly faced by a strain cell: (a) initial state, (b) under tension and (c) under compression. From Fig. 6.6, one can explain the change of the sample's impedance (Z) due to change of the resistance and capacitance. The resistance and capacitance changes are due to the change in geometrical parameters like inter-electrode distance (L) and cross-sectional area (A), and also due to change in the intrinsic parameters as resistivity (ρ) as given by following Eq. 6.4:

$$R = \frac{\rho L}{A} \tag{6.4}$$

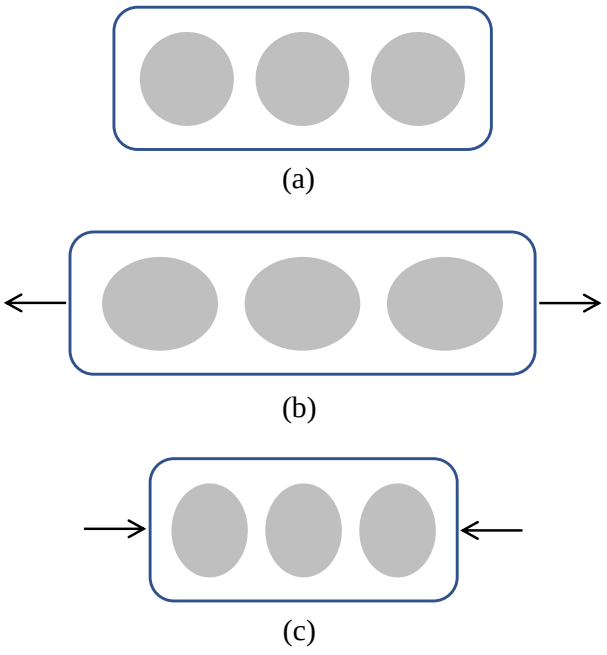

FIGURE 6.6: Simplified structure of the investigated CNT-silicone composite samples (only three CNT nanoparticles are shown): (a) natural position, (b) under tension and (c) under compression

Mechanism of conductivity for the CNT-silicone composite samples is explained as thermally assisted hopping transitions between spatially separated sites, molecules or particles explained by Percolation Theory [265–269]. The average conductivity (σ) of the CNT-silicone adhesive according to Percolation Theory, can be calculated using the following equation:

$$\sigma = \frac{1}{LZ} \tag{6.5}$$

where L is a length which depends on the concentration of the sites, Z is resistance (or impedance) of the path with the lowest average resistance between CNT particles in the silicone adhesive. Under tension L and Z may increase; whereas, under compression, it decreases accordingly due to micro-displacement of the molecules and particles. This results into decrease/increase in the conductivity of the sample as expressed in Fig. 6.6.

Recently, temperature dependent resistance of CNT and p-Si powders composites samples were reported [270]. It was found that the composite resistance decreases with increase in temperature. The temperature sensitivity was –0.53% $^{\circ}C^{-1}$ to –0.74% $^{\circ}C^{-1}$, depending on composition, ratio of components and type of adhesive materials used. For practical utilization of these strain sensors, a temperature compensation circuit is needed. One of the common circuits, the Wheatstone bridge can be used for temperature compensation of resistance strain sensors [265]. As shown in Fig. 6.7, four different types of connection can be realized. Case-1: R_1 is an active resistance strain sensor, while R_2, R_3 and R_4 are known resistors. This circuit is used when temperature compensation is not required. In case-2 and case-3, R_1 is active resistance strain sensor, and R_2 or R_3 is a dummy, while R_3 or R_2 and R_4 are ordinary resistors. The active and dummy sensors should be pasted by the same adhesive material on the beams and be placed in the same thermal environment. However, the active sensor should be under the strain and dummy sensor in the stress-free region. In case-4, the circuit contains only active strain sensors: R_1 and R_4 should be under tension, while R_2 and R_3 under compression. This circuit has a double sensitivity with respect to circuits 1, 2 and 3, and provides the temperature compensation as well [265]. Detail analysis of these four cases is given by Dally *et al.* [265].

A comparative analysis of MWCNT based strain sensors is given in Table 6.1. The data of the table show that the proposed technique is simple in fabrication but it offers relatively higher strain gauge factors at both the frequencies, i.e. 100 Hz

TABLE 6.1: Multiwall carbon nanotubes (MWCNTs) based strain sensors and their associated reported data.

Ref.	**Sensing Material & Fabrication Method**	**Conductivity (S/m)**	**Gauge Factor (Amount of CNT)**
[271]	MWCNT+Epoxy	1×10^{-4}	0.75 (0.1 wt.%)
	in-situ polymerization		
	Mould Casting		
[272]	MWCNT+Epoxy	2×10^{-4}	4.5 (0.1 wt.%)
	in-situ polymerization	1.32×10^{-2}	3.5 (0.3 wt.%)
	Mould Casting		
[273]	MWCNT+Epoxy	10.4	6.2 (5 wt.%)
	in-situ polymerization	65.8	4.8 (7 wt.%)
	Mould Casting	95.2	3.2 (10 wt.%)
[274]	MWCNT+Epoxy	0.02	22.4 (1 wt.%)
	in-situ polymerization	1	12 (2 wt.%)
	Mould Casting	10	6 (5 wt.%)
[275]	MWCNT+Epoxy	3.3×10^{-2}	22.4 (1 wt.%)
	in-situ polymerization	1.13	11.6 (2 wt.%)
	Mould Casting	10.4	6.2 (5 wt.%)
This	MWCNT	4×10^{-4}	32.1 (45 wt.%) (100 Hz)
work	+Silicon Adhesive	4×10^{-4}	28.8 (45 wt.%) (1 kHz)
	Drop Casting		Under Tension
This	MWCNT	4×10^{-4}	18.5 (45 wt.%) (100 Hz)
work	+Silicon Adhesive	4×10^{-4}	14.2 (45 wt.%) (1 kHz)
	Drop Casting		Under Compression

and 1 kHz. Thus, the proposed design could be a preferred one keeping in view its observed sensitivity coupled with ease in fabrication.

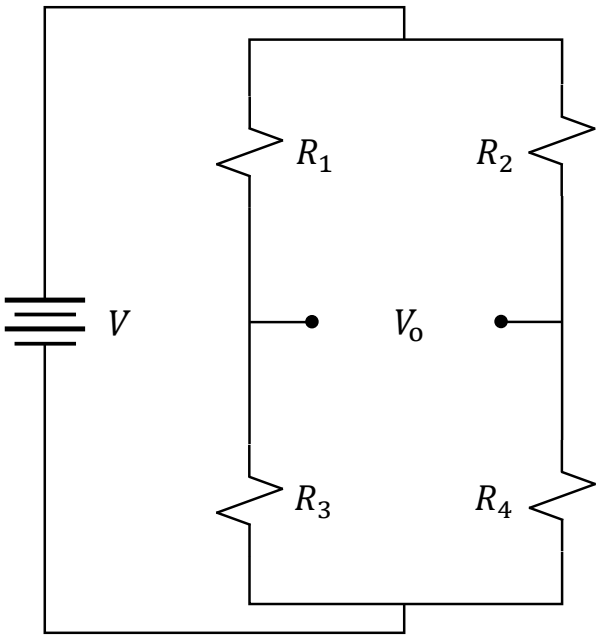

FIGURE 6.7: Schematic diagram of the strain sensors' arrangement in the Wheatstone bridge: Case-1: R_1 is the active resistance strain sensor, while R_2, R_3 and R_4 are ordinary resistors. Case-2: R_1 is the active resistance strain sensor, and R_3 is a dummy resistance strain sensor, while R_2 and R_4 are ordinary resistors. Case-3: R_1 is the active resistance strain sensor, and R_2 is a dummy resistance strain sensor, while R_3 and R_4 are ordinary resistors. Case-4: R_1 and R_4 are active resistance strain sensors under tension, while R_2 and R_3 are active resistance strain sensors under compression. The V_0 is output voltage.

6.5 Summary

The CNTs and silicone adhesive composite based strain sensors were fabricated and characterized at a frequency of 100 Hz and 1 KHz. These sensors showed strain sensitivity of 32.1 (at 100 Hz) and 28.8 (at 1 kHz) under tension whilst under compression the strain sensitivity of 18.5 and 14.2 at 100 Hz and 1 kHz were observed, respectively. Our proposed sensor is simple and can be fabricated using commercially available materials (CNT and silicon adhesive). These sensors are stable in air, they are light weight and smaller in size, making them suitable for wearable electronics and biomedical applications.

Chapter 7

Conclusion and Future Work

7.1 Conclusion

In the 20^{th} century, the world has seen phenomenal growth in industrial automation and control. This happened because of the growth observed in various scientific and technological fields simultaneously. The availability of extraordinary computational power, coupled with artificial intelligence, allowed the human being to have data gathering robots landing on far-flanged planets to explore the wonder of nature, while on the other end, it provided huge assistance on the ground in all walks of life, including automobile, construction, communication, and healthcare. All these were possible because of the accurate data gathering and its subsequent processing for decision making.

In every technology, data acquisition plays an important role, and gathering of the data is dependant upon various types of sensors. These sensors are placed at a suitable location of a system for gathering information, which is then transmitted to a central unit; where, this information is processed and further decisions are to be made. The type and nature of a sensor, which is to be employed, depends upon the automation requirements of the system. If acquisition of data is from a surface, then usually a surface conformable sensor would be required. Thus, the nature and design of a sample will always be biased toward the system where it would be

installed. In order to meet the current challenges of the industry, it is imperative that the sensor technology should improve at the same pace as happening in other fields of the industry. Owing to these requirements, researchers working in sensors development are always trying to fill the gap by establishing sensors that should offer better performance in comparison to earlier developed ones.

In general, a sensor is a device that transforms physical information into an electrical signal. In order to communicate with other parts of the circuitry, it must have ohmic electrodes to receive and transmit the data. Apart from ohmic electrodes, a sensor must have a sensing material through which it should assess a physical change for which it has been designed and translate it into an electrical response. This could be a variation in the capacitance (impedance), or/and a variation in the resistance of a material (thermistor), or/and a change in the conducting crossectional area of the device (OFETs); or any other property which at the end of day could be translated into a standard electrical information.

The sensing mechanism of a sensor could be either physical, such as a variation in two plates of a capacitor (diaphragm); or it could be a sensing material that changes its properties with a change in the ambient where the sensor has been deployed. Such a material could either be in-organic or organic semiconductors. This dissertation concentrated on the fabrication and characterization of organic semiconductors based sensors of the following types:

(a) Humidity sensors

(b) Temperature sensors

(c) Pressure sensors

(d) Strain sensors

It is worth mentioning that this dissertation also presented senors that can, simultaneously, assess multiple variables and, hence, could be called as multifunctional sensors (MFS). Moreover, in some cases, it could be the need for an application that the sensors should be made on a flexible substrate, therefore, while optimizing the recipe, the option of flexible substrate (rubber) was also taken into

consideration. In general, during the entire course of the developmental process, a due consideration was given to the fact that the sensors should be economical, compatible with the industry, and should possess durable and repeatable characteristics.

It is an established fact that organic semiconductor processing is relatively less technology-demanding compared to its in-organic counterparts. The characteristics of an organic semiconductor can comfortably be altered by involving simple techniques; such as, mixing an organic semiconductor powder (OD) with another appropriate substance (CNTs). Additionally, these characteristics are also dependent upon the chosen thin film growth technology−drop costing, spin coating or vacuum evaporation etc. Considering these facts, while working on the development of sensors, it was decided that the sensing material for this research would be organic or compound semiconductors and the sample fabrication technology would be adopted based on the requirements of design.

In the first part of the research, Organic Field Effect Transistors (OFETs) based sensors were developed which can measure both ambient humidity as well as temperature. These sensors were designed, fabricated, and tested for their potential use by the relevant industry. The channel of the OFET was defined by a complex material comprising of OD (8 wt.%) and sugar (8 wt.%). To define an OFET structure, surface-type interdigitated silver electrodes coated with ceramic alumina sheet, fabricated by screen printing and chemical etching technology were used. On a co-planar structure, source, drain and gate terminals were first fabricated; followed by, OD-sugar based conducting channel was realized using a drop costing method. Finished devices were then tested in a humidity chamber. In OD-sugar film, apart from proton conductivity caused by H^+, a donor-acceptor charge transfer process was assumed. These charges were assumed to be available for electronic conduction, which eventually increases the carrier concentration and conductivity of the device. It has been observed that increased concentration of water molecules in OD-sugar film causes the same effect as that of gate bias. As a result, the channel conductivity changes. Accordingly, this translates the variation

in ambient humidity into an electrical signal. The overall characteristics of the device were identical to that of the enhancement type OFET. It was observed that response and recovery times were equal to 11 s and 32 s when relative humidity (RH) changes from 50% to 90%, respectively.

Additionally, the properties of OFETs were also investigated as a temperature sensor. It has been demonstrated that the channel impedance of OD-sugar based OFET sensor increases with increasing values of temperature provided the device is exposed to air. On the other hand, the same variable decreases by increasing temperature, if the device under investigation is encapsulated. Thus, opened surface and encapsulated samples showed positive and negative temperature coefficients, respectively. It has been shown that fabricated OFETs are highly sensitive to temperature and can potentially be employed by the industry as thermistor and as a posistor.

In the second part of the research, a novel, low-cost composite humidity sensor technology was developed to accommodate the needs of flexible electronics for various monitoring applications. Flexible humidity sensors were realized using a composite active layer comprising upon orange dye (30 wt.%), graphene (20 wt.%) and silicon adhesive (50 wt.%). Two types of sensors were fabricated namely: a) resistive and b) OFET sensors. In both the designs, two 300 nm thick Ag electrodes having 16 μm inter-electrode spacing were first deposited on a rubber substrate followed by the deposition of 9–11 μm thick composite layer, on top of Ag electrodes, to define the channel. For OFET sensors an additional layer comprising upon OD (50 wt.%) and graphene (50 wt.%) were also deposited on top of the channel layer, to achieve a floating Schottky barrier gate.

Finished devices were then tested in a chamber where RH was varied from 33% to 94%. Impedance and capacitance variations as a function of humidity and frequency were evaluated for both types of fabricated sensors. It has been shown that at 100 Hz, resistive type sensors offer 2140 times change in their impedance by changing RH from 33% to 94% which reduces to 56.67 times at 200 kHz. Whilst for OFET type sensors such a variation in RH at 100 Hz causes 3716 times change

in the sensor impedance and the same reduces to 80 times at 200 kHz. On the other hand, it was observed that the capacitance of resistive type sensor at 100 Hz, changes 145 times by changing RH from 33 % to 94 % and this variation is 314 times for the OFET type sensor. Thus, impedance and capacitance variations of the proposed design demonstrated that the chosen composite is sensitive enough to be employed as an active material for humidity sensors. The design in general can be employed in any industrial process where humidity and temperature ought to be controlled including biomedical instrumentation. To ensure the industrial applicability of the proposed design, it has been demonstrated that the finished sensors offered stable characteristics for temperatures range 20 °C to 75 °C and for a time interval of at least 240 hours.

In the third part of the research, multifunctional sensors (MFS) which can measure temperature, pressure and displacement were designed, fabricated and characterized. They were called as resistive type MFS, fabricated using OD sandwiched by CNTs and graphene materials. The developed sensor, as a single device, can be installed to assess temperature, pressure and displacement. During characterization, it was shown that the output resistance and impedance of the fabricated sensors were directly proportional to temperature, inversely proportional to pressure and displacement change. The temperature coefficients of the MFS were measured and found equal to 1.0% $°C^{-1}$ for sensors having initial resistance ∼470 Ω and 1.9% $°C^{-1}$ for those sensors having initial resistance ∼890 Ω. Under the applied pressure of 0 kgf/cm^2 to 0.1 kgf/cm^2, the measured resistance of MFS exhibited a decrease from 6730 Ω to 5210 Ω (1.3 times) and from 3410 Ω to 269 Ω (12.7 times) for two different thicknesses of OD layer; whereas, for the displacement of 0 to 110 μm, the decrease in resistance value was from 2235 Ω to 702 Ω (3.18 times), and 6787 Ω to 901 Ω (7.53 times). It was observed that the sensitivity of the proposed sensor could be controlled by changing the thickness of OD layer. The developed sensor could potentially replace multiple sensors needed to measure temperature, pressure, and displacement in industrial applications; such as a flex bonding head, with a single sensor involving a simpler design; lighter weight, low maintenance, and eventually of low cost.

The fourth part of the research presented design, fabrication and characterization of strain sensors fabricated using a composite of MWCNTs (45 wt.%) and silicon adhesive (55 wt.%). The chosen composition, after a series of experiments was found to be the best suited composition, which provided a uniform film with reliable results. A $15 - 20$ μm thick MWCNTs and silicone composite film was drop casted on Al electrodes patterned on a triangle shaped elastic polymer (polymethyl matacrylate) beam. The Al electrodes were 15 μm thick, 4 mm wide with 1.5 mm as inter-electrode spacing.

The finished devices, after the fabrication, were characterized at a frequency of 100 Hz and 1 KHz. These sensors exhibited strain sensitivity of 32.1 (at 100 Hz) and 28.8 (at 1 kHz) under tension whilst under compression the observed strain sensitivity was 18.5 and 14.2 at 100 Hz and 1 kHz, respectively. It is pertinent to mention here that the reported sensor was easy to fabricate because of its simpler design but was compatible in performance with other strain sensors. The observed results exhibited that the sensor performance was repeatable and stable in air. Furthermore, the developed sensor was light weight and smaller in size and therefore, it could potentially be used in wearable electronics and biomedical equipment.

7.2 Future Work

During this study, different physical sensors with novel architecture were fabricated using commercially available organic and nanomaterials. The fabricated sensors demonstrated reliable and improved performance when compared to existing technology. Hence, the accomplished work has made a tangible contribution in sensor technology. However, many potential avenues could not be investigated because of the scope of work and time constraints. In order to improve further, the performance, reliability and functionality of sensors targeting different applications; especially, in industrial automation and healthcare, the following suggestions are being made:

1. The range of the temperature sensors should be enhanced for their wider applicability by exploring different organic materials and their composites other than OD. While searching for other potential materials, one should explore those which offer relatively higher mobility, since this would presumably improve the performance of the associated sensor many fold.

2. It is always an added advantage if the sensor has the ability to assess more than one variable and that too with the same level of accuracy. Such a feature is considered, on one hand, an economical; whilst on the other hand, it gives phenomenal ease to a system designer working on its automation. It would, therefore, be highly beneficial research, if the sensing material to be developed, should have multifunctional sensing capabilities..

3. It is a fundamental requirement that the sensor should have the ability to communicate with the external world, and it can do so by having good ohmic contacts. A linear organic-ohmic contact remained a challenge for the researcher working in the field, especially at low bias. Theoretical definition based on work function principles of two systems (metal & organic semiconductor) does not work fully and hence, there is a need to find out a solution where one can achieve repeatable and low contact resistance ohmic contact with a compatible metal normally employed by the industry for ohmic contacts of the devices; such as Al, Au, Ag, etc.

4. To improve the performance of a design, it is proposed that different deposition combination, for instance, organic on organic, organic on metal or organic on insulator could be explored. Such an approach is known as multijunction approach, wherein, each junction could be optimized in such a way that it should response to a given set of physical conditions better than the other junction. This presumably would improve the overall range of the sensor for the designed variables.

5. Flexible humidity sensors were fabricated on a single type of flexible material (substrate) as an initial step. However, flexible electronics have shown tremendous potential in various sectors. It is therefore, proposed that other

types of flexible substrates (fibers, polythene etc.), compatible to the sensors technology could be explored. It is pertinent to mention here that the choice of a flexible substrate would be biased toward the use of a given sensor.

6. Switching time is also an important FET based sensor performance parameters and can be improved by designing/using polymers having polymer chain length similar to that of the gate length of the OFET, to take the advantage of high intra-molecular mobility.

7. The overall electrical performance of a sensor can be enhanced by optimizing its fabrication process, involving different deposition techniques. Since a deposition method plays an important role in defining morphology and electrical characteristics of an organic thin film therefore, optimization/selection of a deposition technique would have a crucial role in defining the quality of a sensor. Comparison of different AFM results (for surface texture and roughness) of different depositions would also be helpful to improve the sensitivity, stability and performance of a sensor.

8. Charge injection and transport mechanism of an organic sensor is still not fully investigated, because of the variety of materials involved in sensor fabrication. A comprehensive mathematical framework covering both the aspect: a) simulation and b) modeling of organic sensors involving its physical parameters, including material characteristics, would be a beneficial tool for a design engineer. Once such a framework is available, this will safe enormous industrial resources, because a device characteristics could be realized in advance, before its fabrication by using its physical variables. On the other hand, an accurate mathematical model will provide an inside about the functioning of a sensor and its improvement by changing the associated design parameters.

9. Sensor packaging is also one the important area which determines the life-cycle of a sensor. Hence, suitable material selection for sensor packaging and its conformability with the device structure and function will ensure improvement in sensor life-cycle, reliability and repeatability of the sensing

devices. Sensor packaging aspect has not been touched in this dissertation. The same could be investigated in order to have a reliable outcome from a designed sensor.

Bibliography

[1] C. Reese, M. Roberts, M.-M. Ling, and Z. Bao, "Organic thin film transistors," *Materials Today*, vol. 7, no. 9, pp. 20–27, 2004.

[2] C. D. Dimitrakopoulos and P. R. Malenfant, "Organic thin film transistors for large area electronics," *Advanced Materials*, vol. 14, no. 2, pp. 99–117, 2002.

[3] G. Horowitz, "Organic field-effect transistors," *Advanced materials*, vol. 10, no. 5, pp. 365–377, 1998.

[4] E. L. Williams, K. Haavisto, J. Li, and G. E. Jabbour, "Excimer-based white phosphorescent organic light-emitting diodes with nearly 100% internal quantum efficiency," *Advanced Materials*, vol. 19, no. 2, pp. 197–202, 2007.

[5] M. Sayyad, Z. Ahmad, K. S. Karimov, M. Yaseen, and M. Ali, "Photo-organic field effect transistor based on a metalloporphyrin," *Journal of Physics D: Applied Physics*, vol. 42, no. 10, p. 105112, 2009.

[6] C. Reese and Z. Bao, "Organic single-crystal field-effect transistors," *Materials Today*, vol. 10, no. 3, pp. 20–27, 2007.

[7] M. Aziz, "Electrical properties of π-conjugated Fe-TPP molecular solar cell device," *Solid-State Electronics*, vol. 52, no. 8, pp. 1145–1148, 2008.

[8] H. Katz, "Organic molecular solids as thin film transistorsemiconductors," *Journal of Materials Chemistry*, vol. 7, no. 3, pp. 369–376, 1997.

[9] M. H. Andreasson, J. Mårtensson, and T. G. Andersson, "Porphyrin doping of Alq3 for electroluminescence," *Current Applied Physics*, vol. 8, no. 2, pp. 163–166, 2008.

[10] J. M. Shaw and P. F. Seidler, "Organic electronics: Introduction," *IBM Journal of Research and Development*, vol. 45, no. 1, pp. 3–9, 2001.

[11] G. Horowitz, "Organic semiconductors for new electronic devices," *Advanced Materials*, vol. 2, no. 6-7, pp. 287–292, 1990.

[12] B. Wang, G. M. Biesold, M. Zhang, and Z. Lin, "Amorphous inorganic semiconductors for the development of solar cell, photoelectrocatalytic and photocatalytic applications," *Chemical Society Reviews*, vol. 50, no. 12, pp. 6914–6949, 2021.

[13] H. Chen, Y. Ding, G. Zhu, Y. Liu, Q. Fang, X. Bai, Y. Zhao, X. Li, X. Huang, T.-Y. Zhang *et al.*, "A new route to fabricate flexible, breathable composites with advanced thermal management capability for wearable electronics," *npj Flexible Electronics*, vol. 7, no. 1, p. 24, 2023.

[14] Y. Yan, Y. Zhao, and Y. Liu, "Recent progress in organic field-effect transistor-based integrated circuits," *Journal of Polymer Science*, vol. 60, no. 3, pp. 311–327, 2022.

[15] W. Brütting, "Introduction to the physics of organic semiconductors," *Physics of Organic Semiconductors*, pp. 1–14, 2005.

[16] N. Karl and J. Marktanner, "Electron and hole mobilities in high purity anthracene single crystals," *Molecular Crystals and Liquid Crystals Science and Technology. Section A. Molecular Crystals and Liquid Crystals*, vol. 355, no. 1, pp. 149–173, 2001.

[17] N. Karl, "Charge-carrier mobility in organic crystals," in *Organic Electronic Materials*. Springer, 2001, pp. 283–326.

[18] P. M. Borsenberger and D. S. Weiss, *Organic photoreceptors for imaging systems*. Dekker New York, 1993, vol. 39.

[19] W. Brütting, S. Berleb, and A. G. Mückl, "Device physics of organic light-emitting diodes based on molecular materials," *Organic Electronics*, vol. 2, no. 1, pp. 1–36, 2001.

[20] J. C. Scott, "Metal–organic interface and charge injection in organic electronic devices," *Journal of Vacuum Science & Technology A: Vacuum, Surfaces, and Films*, vol. 21, no. 3, pp. 521–531, 2003.

[21] U. Wolf, V. I. Arkhipov, and H. Bässler, "Current injection from a metal to a disordered hopping system. I. Monte Carlo simulation," *Physical Review B*, vol. 59, no. 11, p. 7507, 1999.

[22] P. W. Blom and M. Vissenberg, "Charge transport in poly (p-phenylene vinylene) light-emitting diodes," *Materials Science and Engineering Reports*, vol. 27, no. 3-4, pp. 53–94, 2000.

[23] Z. V. Vardeny, A. J. Heeger, and A. Dodabalapur, "Fundamental research needs in organic electronic materials," *Synthetic Metals*, vol. 148, no. 1, pp. 1–3, 2005.

[24] Z. Xie and L. Hung, "High-contrast organic light-emitting diodes," *Applied Physics Letters*, vol. 84, no. 7, pp. 1207–1209, 2004.

[25] Y. Shen, D. B. Jacobs, G. G. Malliaras, G. Koley, M. G. Spencer, and A. Ioannidis, "Modification of indium tin oxide for improved hole injection in organic light emitting diodes," *Advanced Materials*, vol. 13, no. 16, pp. 1234–1238, 2001.

[26] A. K. Kapoor, S. Jain, J. Poortmans, V. Kumar, and R. Mertens, "Temperature dependence of carrier transport in conducting polymers: Similarity to amorphous inorganic semiconductors," *Journal of Applied Physics*, vol. 92, no. 7, pp. 3835–3838, 2002.

[27] S. Rakhmanova and E. Conwell, "Electric-field dependence of mobility in conjugated polymer films," *Applied Physics Letters*, vol. 76, no. 25, pp. 3822–3824, 2000.

[28] P. Mark and W. Helfrich, "Space-charge-limited currents in organic crystals," *Journal of Applied Physics*, vol. 33, no. 1, pp. 205–215, 1962.

[29] V. Kumar, S. Jain, A. Kapoor, J. Poortmans, and R. Mertens, "Trap density in conducting organic semiconductors determined from temperature dependence of $J - V$ characteristics," *Journal of Applied Physics*, vol. 94, no. 2, pp. 1283–1285, 2003.

[30] R. Schmechel and H. Von Seggern, "Electronic traps in organic transport layers," *Physica Status Solidi (A)*, vol. 201, no. 6, pp. 1215–1235, 2004.

[31] A. Hepp, N. Von Malm, R. Schmechel, and H. Von Seggern, "Effects of process parameters on trap distributions in organic semiconductors," *Synthetic Metals*, vol. 138, no. 1-2, pp. 201–207, 2003.

[32] F. Gutman and L. Lyons, "Organic semiconductors, Part A," 1981.

[33] F. Gutman, H. Keyzer, L. Lyons, and R. Smoano, "Organic semiconductors, Part B," *Kriger Robert E. Publishing Company*, vol. 35, 1983.

[34] C. Bartic, B. Palan, A. Campitelli, and G. Borghs, "Monitoring pH with organic-based field-effect transistors," *Sensors and Actuators B: Chemical*, vol. 83, no. 1-3, pp. 115–122, 2002.

[35] K. Kato, N. Watanabe, S. Katagiri, K. Shinbo, F. Kaneko, J. Locklin, A. Baba, and R. C. Advincula, "Electrical properties and gas response in alternate layer-by-layer films of copper phthalocyanine dyes," *Japanese Journal of Applied Physics*, vol. 43, no. 4S, p. 2311, 2004.

[36] M. C. Hamilton, S. Martin, and J. Kanicki, "Thin-film organic polymer phototransistors," *IEEE Transactions on Electron Devices*, vol. 51, no. 6, pp. 877–885, 2004.

[37] C. Bartic, A. Campitelli, K. Baert, J. Suls, and S. Borghs, "Organic-based transducer for low-cost charge detection in aqueous media," in *International Electron Devices Meeting 2000. Technical Digest. IEDM (Cat. No. 00CH37138)*. IEEE, 2000, pp. 411–414.

[38] Y. Li and M. Yang, "Humidity sensitive properties of substituted polyacetylenes," *Synthetic Metals*, vol. 129, no. 3, pp. 285–290, 2002.

[39] M. Grundmann, H. Alloul, H. U. Fuchs, W. Demtröder, R. M. Dreizler, C. S. Lüdde, K. Thyagarajan, and A. Ghatak, "Graduate texts in physics," 2010.

[40] G. Yu, G. Srdanov, J. Wang, H. Wang, Y. Cao, and A. J. Heeger, "Large area, full-color, digital image sensors made with semiconducting polymers," *Synthetic Metals*, vol. 111, pp. 133–137, 2000.

[41] P. Beckerle and H. Ströbele, "Charged particle detection in organic semiconductors," *Nuclear Instruments and Methods in Physics Research Section A: Accelerators, Spectrometers, Detectors and Associated Equipment*, vol. 449, no. 1-2, pp. 302–310, 2000.

[42] A. Koma, "Molecular beam epitaxial growth of organic thin films," *Progress in Crystal Growth and Characterization of Materials*, vol. 30, no. 2-3, pp. 129–152, 1995.

[43] X. Lu, W. Zhang, C. Wang, T.-C. Wen, and Y. Wei, "One-dimensional conducting polymer nanocomposites: Synthesis, properties and applications," *Progress in Polymer Science*, vol. 36, no. 5, pp. 671–712, 2011.

[44] A. SZENT-GYÖRGYI, "Internal photo-electric effect and band spectra in proteins," *Nature*, vol. 157, no. 4000, p. 875, 1946.

[45] A. Eley-DÖRGYI, "Phthalocyanines as semiconductors," *Nature*, vol. 162, no. 4125, p. 819, 1948.

[46] H. Akamatu and H. Inokuchi, "On the electrical conductivity of violanthrone, iso-violanthrone, and pyranthrone," *The Journal of Chemical Physics*, vol. 18, no. 6, pp. 810–811, 1950.

[47] A. Bernanose, "Electroluminescence of organic compounds," *British Journal of Applied Physics*, vol. 6, no. S4, p. S54, 1955.

[48] C. Chiang, C. Fincher Jr, Y. Park, A. Heeger, H. Shirakawa, E. Louis, S. Gau, and A. G. MacDiarmid, "Electrical conductivity in doped polyacetylene," *Physical Review Letters*, vol. 40, no. 22, p. 1472, 1978.

[49] F. Ebisawa, T. Kurokawa, and S. Nara, "Electrical properties of polyacetylene/polysiloxane interface," *Journal of Applied Physics*, vol. 54, no. 6, pp. 3255–3259, 1983.

[50] G. Chamberlain, "Organic solar cells: A review," *Solar Cells*, vol. 8, no. 1, pp. 47–83, 1983.

[51] H. Koezuka, A. Tsumura, and T. Ando, "Field-effect transistor with polythiophene thin film," *Synthetic Metals*, vol. 18, no. 1-3, pp. 699–704, 1987.

[52] T. Frängsmyr, *Les Prix Nobel*, 2000.

[53] T. Takayama, Y. Ohno, Y. Goto, A. Machida, M. Fujita, J. Maruyama, K. Kato, J. Koyama, and S. Yamazaki, "A CPU on a plastic film substrate," in *2004 Symposium on VLSI Technology.* IEEE, 2004, pp. 230–231.

[54] N. Karaki, T. Nanmoto, H. Ebihara, S. Utsunomiya, S. Inoue, and T. Shimoda, "A flexible 8b asynchronous microprocessor based on low-temperature poly-silicon TFT technology," in *2005 IEEE International Solid-State Circuits Conference.* IEEE, 2005, pp. 272–598.

[55] H. Dembo, Y. Kurokawa, T. Ikeda, S. Iwata, K. Ohshima, J. Ishii, T. Tsurume, E. Sugiyama, D. Yamada, A. Isobe *et al.*, "RFCPUs on glass and plastic substrates fabricated by TFT transfer technology," in *2005 IEEE International Electron Devices Meeting.* IEEE, 2005, pp. 125–127.

[56] E. Jacques, F. Le Bihan, S. Crand, and T. M. Brahim, "Differential amplifier using polysilicon TFTs processed at low temperature to be integrated with TFT hall sensor," in *2006-32nd Annual Conference on IEEE Industrial Electronics.* IEEE, 2006, pp. 3193–3198.

[57] K. Myny, S. Smout, M. Rockelé, A. Bhoolokam, T. H. Ke, S. Steudel, B. Cobb, A. Gulati, F. G. Rodriguez, K. Obata *et al.*, "A thin-film microprocessor with inkjet print-programmable memory," *Scientific Reports*, vol. 4, p. 7398, 2014.

[58] J. Noh, M. Jung, Y. Jung, C. Yeom, M. Pyo, and G. Cho, "Key issues with printed flexible thin film transistors and their application in disposable RF sensors," *Proceedings of the IEEE*, vol. 103, no. 4, pp. 554–566, 2015.

[59] K. Fukuda, T. Minamiki, T. Minami, M. Watanabe, T. Fukuda, D. Kumaki, and S. Tokito, "Printed organic transistors with uniform electrical performance and their application to amplifiers in biosensors," *Advanced Electronic Materials*, vol. 1, no. 7, p. 1400052, 2015.

[60] A. Dey, A. Singh, D. Das, and P. K. Iyer, "Organic semiconductors: A new future of nanodevices and applications," in *Thin Film Structures in Energy Applications*. Springer, 2015, pp. 97–128.

[61] Y. S. Rim, S.-H. Bae, H. Chen, N. De Marco, and Y. Yang, "Recent progress in materials and devices toward printable and flexible sensors," *Advanced Materials*, vol. 28, no. 22, pp. 4415–4440, 2016.

[62] T. Moy, L. Huang, W. Rieutort-Louis, C. Wu, P. Cuff, S. Wagner, J. C. Sturm, and N. Verma, "An EEG acquisition and biomarker-extraction system using low-noise-amplifier and compressive-sensing circuits based on flexible, thin-film electronics," *IEEE Journal of Solid-State Circuits*, vol. 52, no. 1, pp. 309–321, 2016.

[63] Q. Cao, J. Tersoff, D. B. Farmer, Y. Zhu, and S.-J. Han, "Carbon nanotube transistors scaled to a 40-nanometer footprint," *Science*, vol. 356, no. 6345, pp. 1369–1372, 2017.

[64] Y. van De Burgt, A. Melianas, S. T. Keene, G. Malliaras, and A. Salleo, "Organic electronics for neuromorphic computing," *Nature Electronics*, vol. 1, no. 7, p. 386, 2018.

[65] Y. H. Lee, O. Y. Kweon, H. Kim, J. H. Yoo, S. G. Han, and J. H. Oh, "Recent advances in organic sensors for health self-monitoring systems," *Journal of Materials Chemistry C*, vol. 6, no. 32, pp. 8569–8612, 2018.

[66] D. Yang and D. Ma, "Development of organic semiconductor photodetectors: From mechanism to applications," *Advanced Optical Materials*, vol. 7, no. 1, p. 1800522, 2019.

[67] "https://www.sciencedaily.com/releases/2019/03/190321130307.htm."

[68] J. Wang, S. Lee, T. Yokota, Y. Jimbo, Y. Wang, M. O. G. Nayeem, M. Nishinaka, and T. Someya, "Nanomesh organic electrochemical transistor for comfortable on-skin electrodes with local amplifying function," *ACS Applied Electronic Materials*, vol. 2, no. 11, pp. 3601–3609, 2020.

[69] Y. Huang, W. Tang, L. Feng, S. Chen, J. Zhao, Z. Liu, L. Han, B. Ouyang, and X. Guo, "Printable low power organic transistor technology for customizable hybrid integration towards internet of everything," *IEEE Journal of the Electron Devices Society*, vol. 8, pp. 1219–1226, 2020.

[70] S. J. Park, J. Lee, S. E. Seo, K. H. Kim, C. S. Park, S. H. Lee, H. S. Ban, B. D. Lee, H. S. Song, J. Kim *et al.*, "High-performance conducting polymer nanotube-based liquid-ion gated field-effect transistor aptasensor for dopamine exocytosis," *Scientific Reports*, vol. 10, no. 1, pp. 1–12, 2020.

[71] P. She, Y. Qin, X. Wang, and Q. Zhang, "Recent progress in external-stimulus-responsive 2d covalent organic frameworks," *Advanced Materials*, vol. 34, no. 22, p. 2101175, 2022.

[72] K. Kim, H. Yoo, and E. K. Lee, "New opportunities for organic semiconducting polymers in biomedical applications," *Polymers*, vol. 14, no. 14, p. 2960, 2022.

[73] Y. Khan, A. E. Ostfeld, C. M. Lochner, A. Pierre, and A. C. Arias, "Monitoring of vital signs with flexible and wearable medical devices," *Advanced materials*, vol. 28, no. 22, pp. 4373–4395, 2016.

[74] S. Harada, K. Kanao, Y. Yamamoto, T. Arie, S. Akita, and K. Takei, "Fully printed flexible fingerprint-like three-axis tactile and slip force and temperature sensors for artificial skin," *ACS nano*, vol. 8, no. 12, pp. 12 851–12 857, 2014.

[75] S. Jung, T. Ji, and V. K. Varadan, "Point-of-care temperature and respiration monitoring sensors for smart fabric applications," *Smart materials and structures*, vol. 15, no. 6, p. 1872, 2006.

[76] ——, "Temperature sensor using thermal transport properties in the subthreshold regime of an organic thin film transistor," *Applied physics letters*, vol. 90, no. 6, p. 062105, 2007.

[77] M. T. S. Chani, A. M. Asiri, K. S. Karimov, A. K. Niaz, S. B. Khan, and K. A. Alamry, "Aluminium phthalocyanine chloride thin films for temperature sensing," *Chinese Physics B*, vol. 22, no. 11, p. 118101, 2013.

[78] X. Ren, P. K. Chan, J. Lu, B. Huang, and D. C. Leung, "High dynamic range organic temperature sensor," *Advanced Materials*, vol. 25, no. 9, pp. 1291–1295, 2013.

[79] P. Cosseddu, F. Viola, S. Lai, L. Raffo, and A. Bonfiglio, "A temperature transducer based on a low-voltage organic thin-film transistor detecting pyroelectric effect," *IEEE Electron Device Letters*, vol. 35, no. 12, pp. 1296–1298, 2014.

[80] X. Wu, Y. Ma, G. Zhang, Y. Chu, J. Du, Y. Zhang, Z. Li, Y. Duan, Z. Fan, and J. Huang, "Thermally stable, biocompatible, and flexible organic field-effect transistors and their application in temperature sensing arrays for artificial skin," *Advanced Functional Materials*, vol. 25, no. 14, pp. 2138–2146, 2015.

[81] X. Ren, K. Pei, B. Peng, Z. Zhang, Z. Wang, X. Wang, and P. K. Chan, "A low-operating-power and flexible active-matrix organic-transistor temperature-sensor array," *Advanced materials*, vol. 28, no. 24, pp. 4832–4838, 2016.

[82] K. Nakayama, B.-S. Cha, Y. Kanaoka, N. Isahaya, M. Omori, M. Uno, and J. Takeya, "Organic temperature sensors and organic analog-to-digital converters based on p-type and n-type organic transistors," *Organic Electronics*, vol. 36, pp. 148–152, 2016.

[83] R. Ye, K. Ohta, and M. Baba, "Temperature dependence of electrical properties of organic thin film transistors based on pn heterojuction and their applications in temperature sensors," *Journal of Computer and Communications*, vol. 4, no. 5, pp. 10–15, 2016.

[84] M. Song, J. Seo, H. Kim, and Y. Kim, "Flexible thermal sensors based on organic field-effect transistors with polymeric channel/gate-insulating and light-blocking layers," *ACS omega*, vol. 2, no. 7, pp. 4065–4070, 2017.

[85] S. Mandal, M. Banerjee, S. Roy, A. Mandal, A. Ghosh, B. Satpati, and D. K. Goswami, "Organic field-effect transistor-based ultrafast, flexible, physiological-temperature sensors with hexagonal barium titanate nanocrystals in amorphous matrix as sensing material," *ACS applied materials & interfaces*, vol. 11, no. 4, pp. 4193–4202, 2018.

[86] N. V. Subbarao, S. Mandal, M. Gedda, P. K. Iyer, and D. K. Goswami, "Effect of temperature on hysteresis of dipolar dielectric layer based organic field-effect transistors: A temperature sensing mechanism," *Sensors and Actuators A: Physical*, vol. 269, pp. 491–499, 2018.

[87] R. Agarwal and B. Mazhari, "An organic temperature sensor based on asymmetric metal insulator semiconductor capacitor with electrically tunable sensing area," *IEEE sensors letters*, vol. 2, no. 1, pp. 1–4, 2018.

[88] C. Zhu, H.-C. Wu, G. Nyikayaramba, Z. Bao, and B. Murmann, "Intrinsically stretchable temperature sensor based on organic thin-film transistors," *IEEE Electron Device Letters*, vol. 40, no. 10, pp. 1630–1633, 2019.

[89] F. Haque, S. Lim, S. Lee, Y. Park, and M. Mativenga, "Highly sensitive and ambient air-processed hybrid perovskite tft temperature sensor," *IEEE Electron Device Letters*, vol. 41, no. 7, pp. 1086–1089, 2020.

[90] C. Rullyani, M. Singh, S.-H. Li, C.-F. Sung, H.-C. Lin, and C.-W. Chu, "Stimuli-responsive polymer as gate dielectric for organic transistor sensors," *Organic Electronics*, vol. 85, p. 105818, 2020.

[91] C. Ravariu, D. E. Mihaiescu, A. Morosan, D. Istrati, B. Purcareanu, R. Cristescu, R. Trusca, and B. S. Vasile, "Solution for green organic thin film transistors: Fe3o4 nano-core with paba external shell as p-type film," *Journal of Materials Science: Materials in Electronics*, vol. 31, no. 4, pp. 3063–3073, 2020.

[92] M. Zhu, M. U. Ali, C. Zou, W. Xie, S. Li, and H. Meng, "Tactile and temperature sensors based on organic transistors: Towards e-skin fabrication," *Frontiers of Physics*, vol. 16, no. 1, pp. 1–13, 2021.

[93] J. Polena, D. Afzal, J. H. L. Ngai, and Y. Li, "Temperature sensors based on organic field-effect transistors," *Chemosensors*, vol. 10, no. 1, 2022. [Online]. Available: https://www.mdpi.com/2227-9040/10/1/12

[94] C. Müller, A. Al-Hamry, O. Kanoun, M. Rahaman, D. Zahn, E. Matsubara, and J. Rosolen, "Humidity sensing behavior of endohedral Li-doped and undoped SWCNT/SDBS composite films," *Sensors*, vol. 19, no. 1, p. 171, 2019.

[95] S. Arunachalam, A. Gupta, R. Izquierdo, and F. Nabki, "Suspended carbon nanotubes for humidity sensing," *Sensors*, vol. 18, no. 5, p. 1655, 2018.

[96] A. Sanli, V. Jayaraman, A. Benchirouf, C. Müller, and O. Kanoun, "Study of the humidity effect on the electrical impedance of mwcnts/epoxy nanocomposites," in *9th International Workshop on Impedance Spectroscopy, Chemnitz, Germany*, 2016, pp. 26–28.

[97] I. V. Zaporotskova, N. P. Boroznina, Y. N. Parkhomenko, and L. V. Kozhitov, "Carbon nanotubes: Sensor properties-A review," *Modern Electronic Materials*, vol. 2, no. 4, pp. 95–105, 2016.

[98] C. Anichini, A. Aliprandi, S. M. Gali, F. Liscio, V. Morandi, A. Minoia, D. Beljonne, A. Ciesielski, and P. Samorì, "Ultrafast and highly sensitive chemically functionalized graphene oxide-based humidity sensors: harnessing device performances via the supramolecular approach," *ACS Applied Materials & Interfaces*, vol. 12, no. 39, pp. 44 017–44 025, 2020.

[99] U. Afzal, N. Ahmad, Q. Zafar, and M. Aslam, "Fabrication of a surface type humidity sensor based on methyl green thin film, with the analysis of capacitance and resistance through neutrosophic statistics," *RSC advances*, vol. 11, no. 61, pp. 38 674–38 682, 2021.

[100] M. Mohammedture, S. Al Hashmi, J.-Y. Lu, M. Gutierrez, A. M. Esawi, and M. Al Teneiji, "Numerical study of a capacitive graphene oxide humidity sensor with etched configuration," *ACS omega*, vol. 6, no. 44, pp. 29 781–29 787, 2021.

[101] X. Wang, Y. Deng, X. Chen, Z. Ma, Y. Wang, W. Xu, and H. Yu, "A vertically aligned multiwall carbon nanotube-based humidity sensor with fast response, low hysteresis, and high repeatability," *IEEE Sensors Letters*, vol. 5, no. 11, pp. 1–4, 2021.

[102] S. Tachibana, Y.-F. Wang, T. Sekine, Y. Takeda, J. Hong, A. Yoshida, M. Abe, R. Miura, Y. Watanabe, D. Kumaki *et al.*, "A printed flexible humidity sensor with high sensitivity and fast response using a cellulose nanofiber/carbon black composite," *ACS Applied Materials & Interfaces*, vol. 14, no. 4, pp. 5721–5728, 2022.

[103] J. Cao, Q. Wang, and H. Dai, "Electromechanical properties of metallic, quasimetallic, and semiconducting carbon nanotubes under stretching," *Physical Review Letters*, vol. 90, no. 15, p. 157601, 2003.

[104] Y. Li, W. Wang, K. Liao, C. Hu, Z. Huang, and Q. Feng, "Piezoresistive effect in carbon nanotube films," *Chinese Science Bulletin*, vol. 48, no. 2, pp. 125–127, 2003.

[105] P. Regoliosi, A. Reale, A. Di Carlo, S. Orlanducci, M. L. Terranova, and P. Lugli, "Piezoresistive behaviour of single wall carbon nanotubes," in *4th IEEE Conference on Nanotechnology.* IEEE, 2004, pp. 149–151.

[106] R. J. Grow, Q. Wang, J. Cao, D. Wang, and H. Dai, "Piezoresistance of carbon nanotubes on deformable thin-film membranes," *Applied Physics Letters*, vol. 86, no. 9, p. 093104, 2005.

[107] C. Stampfer, T. Helbling, A. Jungen, and C. Hierold, "Piezoresistance of single-walled carbon nanotubes," in *International Solid-State Sensors, Actuators and Microsystems Conference.* IEEE, 2007, pp. 1565–1568.

[108] W. Xue and T. Cui, "Electrical and electromechanical characteristics of nanoassembled carbon nanotube thin film resistors on flexible substrates," in *2007 International Solid-State Sensors, Actuators and Microsystems Conference.* IEEE, 2007, pp. 1047–1050.

[109] Y. Liu, S. Chakrabartty, D. S. Gkinosatis, A. K. Mohanty, and N. Lajnef, "Multi-walled carbon nanotubes/poly (L-lactide) nanocomposite strain sensor for biomechanical implants," in *2007 IEEE Biomedical Circuits and Systems Conference.* IEEE, 2007, pp. 119–122.

[110] S. Vemuru, R. Wahi, S. Nagarajaiah, and P. Ajayan, "Strain sensing using a multiwalled carbon nanotube film," *The Journal of Strain Analysis for Engineering Design*, vol. 44, no. 7, pp. 555–562, 2009.

[111] N. Hu, H. Fukunaga, S. Atobe, Y. Liu, J. Li *et al.*, "Piezoresistive strain sensors made from carbon nanotubes based polymer nanocomposites," *Sensors*, vol. 11, no. 11, pp. 10 691–10 723, 2011.

[112] W. Obitayo and T. Liu, "A review: Carbon nanotube-based piezoresistive strain sensors," *Journal of Sensors*, vol. 2012, 2012.

[113] K. Grabowski, P. Zbyrad, and T. Uhl, "Development of the strain sensors based on cnt/epoxy using screen printing," in *Key Engineering Materials*, vol. 588. Trans Tech Publ, 2014, pp. 84–90.

[114] M. Saleem, K. S. KARIMOV, A. Rashid *et al.*, "Strain sensors based on twin and uniform crystals of tcnq ion-radical salts," *Journal of Optoelectronics and Advanced Materials*, vol. 17, no. May-June 2015, pp. 720–726, 2015.

[115] G. Sapra, "Carbon nanotube bucky paper based strain sensor," *Journal of Basic and Applied Engineering Research*, vol. 2, pp. 289–292, 01 2015.

[116] M. Yasin, T. Tauqeer, H. U. Rahman, K. S. Karimov, S. E. San, and A. V. Tunc, "Polymer–fullerene bulk heterojunction-based strain-sensitive flexible organic field-effect transistor," *Arabian Journal for Science and Engineering*, vol. 40, no. 1, pp. 257–262, 2015.

[117] H. Wang, L. Deng, Q. Tang, Y. Tong, and Y. Liu, "Flexible organic single-crystal field-effect transistor for ultra-sensitivity strain sensing," *IEEE Electron Device Letters*, vol. 38, no. 11, pp. 1598–1601, 2017.

[118] H. Wang, Y. Tong, X. Zhao, Q. Tang, and Y. Liu, "Flexible, high-sensitive, and wearable strain sensor based on organic crystal for human motion detection," *Organic Electronics*, vol. 61, pp. 304–311, 2018.

[119] X. You, J. Yang, M. Wang, J. Hu, Y. Ding, X. Zhang, and S. Dong, "Graphene-based fiber sensors with high stretchability and sensitivity by direct ink extrusion," *2D Materials*, vol. 7, no. 1, p. 015025, 2019.

[120] F. Jin, D. Lv, W. Shen, W. Song, and R. Tan, "High performance flexible and wearable strain sensor based on rgo and pani modified lycra cotton e-textile," *Sensors and Actuators A: Physical*, vol. 337, p. 113412, 2022.

[121] J. Tang, Y. Wu, S. Ma, T. Yan, and Z. Pan, "Sensing mechanism of a flexible strain sensor developed directly using electrospun composite nanofiber yarn with ternary carbon nanomaterials," *Iscience*, vol. 25, no. 10, p. 105162, 2022.

[122] P. Lv, X. Li, Z. Zhang, B. Nie, Y.-L. Wu, H. Tian, T.-L. Ren, and G. Z. Wang, "Ultrathin encapsulated rgo strain sensor for gesture recognition," *Microelectronic Engineering*, vol. 259, p. 111779, 2022.

[123] S. Ma, J. Tang, T. Yan, and Z. Pan, "Performance of flexible strain sensors with different transition mechanisms: A review," *IEEE Sensors Journal*, 2022.

[124] M. Ma, Z. Zhang, Q. Liao, F. Yi, L. Han, G. Zhang, S. Liu, X. Liao, and Y. Zhang, "Self-powered artificial electronic skin for high-resolution pressure sensing," *Nano Energy*, vol. 32, pp. 389–396, 2017.

[125] J. Choi, D. Kwon, K. Kim, J. Park, D. D. Orbe, J. Gu, J. Ahn, I. Cho, Y. Jeong, Y. Oh *et al.*, "Synergetic effect of porous elastomer and percolation of carbon nanotube filler toward high performance capacitive pressure sensors," *ACS Applied Materials & Interfaces*, vol. 12, no. 1, pp. 1698–1706, 2019.

[126] R. B. Mishra, N. El-Atab, A. M. Hussain, and M. M. Hussain, "Recent progress on flexible capacitive pressure sensors: From design and materials to applications," *Advanced materials technologies*, vol. 6, no. 4, p. 2001023, 2021.

[127] M. Cao, J. Su, S. Fan, H. Qiu, D. Su, and L. Li, "Wearable piezoresistive pressure sensors based on 3d graphene," *Chemical Engineering Journal*, vol. 406, p. 126777, 2021.

[128] J. Zhao, J. Luo, Z. Zhou, C. Zheng, J. Gui, J. Gao, and R. Xu, "Novel multi-walled carbon nanotubes-embedded laser-induced graphene in crosslinked architecture for highly responsive asymmetric pressure sensor," *Sensors and Actuators A: Physical*, vol. 323, p. 112658, 2021.

[129] Y. Duan, S. He, J. Wu, B. Su, and Y. Wang, "Recent progress in flexible pressure sensor arrays," *Nanomaterials*, vol. 12, no. 14, p. 2495, 2022.

[130] G. Gilanizadehdizaj, K. C. Aw, J. Stringer, and D. Bhattacharyya, "Facile fabrication of flexible piezo-resistive pressure sensor array using reduced graphene oxide foam and silicone elastomer," *Sensors and Actuators A: Physical*, vol. 340, p. 113549, 2022.

[131] J. Wang, Y. Zhong, S. Dai, H. Zhu, L. Wu, F. Gu, G. Cheng, and J. Ding, "Ag nanowire/cpdms dual conductive layer dome-based flexible pressure sensor with high sensitivity and a wide linear range," *ACS Applied Nano Materials*, vol. 5, no. 9, pp. 13 227–13 235, 2022.

[132] J. Terada and T. Nitta, "Multi-functional sensing or measuring system," Dec. 6 1983, uS Patent 4,419,021.

[133] P. Dario and D. E. De Rossi, "Composite, multifunctional tactile sensor," Dec. 3 1985, uS Patent 4,555,953.

[134] B. Mahar, C. Laslau, R. Yip, and Y. Sun, "Development of carbon nanotube-based sensors—A review," *IEEE Sensors Journal*, vol. 7, no. 2, pp. 266–284, 2007.

[135] Q. Cheng, J. Tang, J. Ma, H. Zhang, N. Shinya, and L.-C. Qin, "Graphene and carbon nanotube composite electrodes for supercapacitors with ultra-high energy density," *Physical Chemistry Chemical Physics*, vol. 13, no. 39, pp. 17 615–17 624, 2011.

[136] M. Martin-Gallego, M. Bernal, M. Hernandez, R. Verdejo, and M. A. López-Manchado, "Comparison of filler percolation and mechanical properties in graphene and carbon nanotubes filled epoxy nanocomposites," *European Polymer Journal*, vol. 49, no. 6, pp. 1347–1353, 2013.

[137] S. Yao and Y. Zhu, "Wearable multifunctional sensors using printed stretchable conductors made of silver nanowires," *Nanoscale*, vol. 6, no. 4, pp. 2345–2352, 2014.

[138] D. Liu, Q. Wang, X. Liu, R. Niu, Y. Zhang, and J. Sun, "A multifunctional sensor in ternary solution using canonical correlations for variable links assessment," *Sensors*, vol. 16, no. 10, p. 1661, 2016.

[139] T. Y. Choi, B.-U. Hwang, B.-Y. Kim, T. Q. Trung, Y. H. Nam, D.-N. Kim, K. Eom, and N.-E. Lee, "Stretchable, transparent, and stretch-unresponsive

capacitive touch sensor array with selectively patterned silver nanowires/reduced graphene oxide electrodes," *ACS Applied Materials & Interfaces*, vol. 9, no. 21, pp. 18 022–18 030, 2017.

[140] M. T. S. Chani, K. S. Karimov, and A. M. Asiri, "Carbon nanotubes and graphene powder based multifunctional pressure, displacement and gradient of temperature sensors," *Semiconductors*, vol. 54, no. 1, pp. 85–90, 2020.

[141] M. T. S. Chani, K. S. Karimov, H. M. Marwani, H. Muhammad, M. M. Zeeshan, and A. M. Asiri, "Impedimetric multifunctional sensor based on rubber-cnts-orange dye nanocomposite fabricated by rubbing-in technology," *Int. J. Electrochem. Sci*, vol. 16, no. 7, 2021.

[142] M. T. S. Chani, K. S. Karimov, A. M. Asiri, M. M. Rahman, and T. Kamal, "Effect of vibrations, displacement, pressure, temperature and humidity on the resistance and impedance of the shockproof resistors based on rubber and jelly (nipc–cnt–oil) composites," *Gels*, vol. 8, no. 4, p. 226, 2022.

[143] N. Yamazoe and Y. Shimizu, "Humidity sensors: principles and applications," *Sensors and Actuators*, vol. 10, no. 3-4, pp. 379–398, 1986.

[144] P. Barker, A. Monkman, M. Petty, and R. Pride, "A polyaniline/sllicon hybrid field effect transistor humidity sensor," *Synthetic Metals*, vol. 85, no. 1-3, pp. 1365–1366, 1997.

[145] Z. Chen and C. Lu, "Humidity sensors: A review of materials and mechanisms," *Sensor Letters*, vol. 3, no. 4, pp. 274–295, 2005.

[146] K. Suri, S. Annapoorni, A. Sarkar, and R. Tandon, "Gas and humidity sensors based on iron oxide–polypyrrole nanocomposites," *Sensors and Actuators B: Chemical*, vol. 81, no. 2-3, pp. 277–282, 2002.

[147] Z. Rittersma, "Recent achievements in miniaturised humidity sensors—a review of transduction techniques," *Sensors and Actuators A: Physical*, vol. 96, no. 2-3, pp. 196–210, 2002.

[148] Z. Ahmad, Q. Zafar, K. Sulaiman, R. Akram, and K. S. Karimov, "A humidity sensing organic-inorganic composite for environmental monitoring," *Sensors*, vol. 13, no. 3, pp. 3615–3624, 2013.

[149] K. S. Karimov, M. Saleem, R. Mahroof-Tahir, R. Akram, M. S. Chanee, and A. Niaz, "Resistive humidity sensor based on vanadium complex films," *Journal of Semiconductors*, vol. 35, no. 9, p. 094001, 2014.

[150] K. S. Karimov, N. Fatima, K. Sulaiman, M. M. Tahir, Z. Ahmad, and A. Mateen, "Sensitivity enhancement of od-and od-cnt-based humidity sensors by high gravity thin film deposition technique," *Journal of Semiconductors*, vol. 36, no. 3, p. 034005, 2015.

[151] M. T. S. Chani, K. S. Karimov, S. B. Khan, and A. M. Asiri, "Fabrication and investigation of cellulose acetate-copper oxide nano-composite based humidity sensors," *Sensors and Actuators A: Physical*, vol. 246, pp. 58–65, 2016.

[152] Z. Ahmad, K. S. Karimov, F. Touati, S. Moiz, R. Ali, R. Shakoor, and N. Al-Thani, "Impact of moisture contents on the performance of organic bi-layer ito/od thermo-electric cells," *Journal of Materials Science: Materials in Electronics*, vol. 27, no. 9, pp. 9720–9724, 2016.

[153] F. Jonas, "Conductive coatings," Jun U.S. Patent 'US005766515A. ' 5,766,515. Jun. 16, 1998 1998.

[154] D. Li, E.-J. Borkent, R. Nortrup, H. Moon, H. Katz, and Z. Bao, "Humidity effect on electrical performance of organic thin-film transistors," *Applied Physics Letters*, vol. 86, no. 4, p. 042105, 2005.

[155] T. Seiyama, N. Yamazoe, and H. Arai, "Ceramic humidity sensors," *Sensors and Actuators*, vol. 4, pp. 85–96, 1983.

[156] H. Farahani, R. Wagiran, and M. N. Hamidon, "Humidity sensors principle, mechanism, and fabrication technologies: a comprehensive review," *Sensors*, vol. 14, no. 5, pp. 7881–7939, 2014.

[157] K. S. Karimov, M. Ahmed, M. Saleem, S. Shafique, M. Akmal *et al.*, "Orange dye based field effect transistor as humidity sensor," *Optoelectronics and Advanced Materials-Rapid Communications*, vol. 14, pp. 416–420, 2020.

[158] D. A. Neamen, "Semiconductor physics and devices, richard d. irwin," *Inc., New York*, 1992.

[159] M. M. Ahmed, "An improved method to estimate intrinsic small signal parameters of a gaas mesfet from measured dc characteristics," *IEEE Transactions on Electron Devices*, vol. 50, no. 11, pp. 2196–2201, 2003.

[160] S. Fatima, U. Rafique, U. Ahmed, and M. Ahmed, "A global parameters extraction technique to model organic field effect transistors output characteristics," *Solid-State Electronics*, vol. 152, pp. 81–92, 2019.

[161] B. H. Hamadani and D. Natelson, "Extracting contact effects in organic fets," *Proceedings of the IEEE*, vol. 93, no. 7, pp. 1306–1311, 2005.

[162] Y. Kurazumi, T. Tsuchikawa, J. Ishii, K. Fukagawa, Y. Yamato, and N. Matsubara, "Radiative and convective heat transfer coefficients of the human body in natural convection," *Building and Environment*, vol. 43, no. 12, pp. 2142–2153, 2008.

[163] İ. Gülseren and J. N. Coupland, "Ultrasonic properties of partially frozen sucrose solutions," *Journal of food engineering*, vol. 89, no. 3, pp. 330–335, 2008.

[164] S. Miyata, B.-R. Höhn, K. Michaelis, and O. Kreil, "Experimental investigation of temperature rise in elliptical ehl contacts," *Tribology International*, vol. 41, no. 11, pp. 1074–1082, 2008.

[165] P. Sazama, H. Jirglová, and J. Dědeček, "Ag-zsm-5 zeolite as high-temperature water-vapor sensor material," *Materials Letters*, vol. 62, no. 27, pp. 4239–4241, 2008.

[166] Y. Su, C. Ma, J. Chen, H. Wu, W. Luo, Y. Peng, Z. Luo, L. Li, Y. Tan, O. M. Omisore *et al.*, "Printable, highly sensitive flexible temperature sensors for

human body temperature monitoring: a review," *Nanoscale research letters*, vol. 15, no. 1, pp. 1–34, 2020.

[167] Y.-F. Wang, T. Sekine, Y. Takeda, K. Yokosawa, H. Matsui, D. Kumaki, T. Shiba, T. Nishikawa, and S. Tokito, "Fully printed pedot: Pss-based temperature sensor with high humidity stability for wireless healthcare monitoring," *Scientific reports*, vol. 10, no. 1, pp. 1–8, 2020.

[168] M. T. S. Chani, K. S. Karimov, S. B. Khan, N. Fatima, and A. M. Asiri, "Impedimetric humidity and temperature sensing properties of chitosan-cumn2o4 spinel nanocomposite," *Ceramics International*, vol. 45, no. 8, pp. 10 565–10 571, 2019.

[169] S. IT, "Thermistors," 1973.

[170] H. Hamouche, S. Makhlouf, A. Chaouchi, and M. Laghrouche, "Humidity sensor based on keratin bio polymer film," *Sensors and Actuators A: Physical*, vol. 282, pp. 132–141, 2018.

[171] S. K. Mahadeva, S. Yun, and J. Kim, "Flexible humidity and temperature sensor based on cellulose–polypyrrole nanocomposite," *Sensors and Actuators A: Physical*, vol. 165, no. 2, pp. 194–199, 2011.

[172] H. Zhao, S. Liu, R. Wang, and T. Zhang, "Humidity-sensing properties of licl-loaded 3d cubic mesoporous silica kit-6 composites," *Materials Letters*, vol. 147, pp. 54–57, 2015.

[173] Y. Xia, H. Zhao, S. Liu, and T. Zhang, "The humidity-sensitive property of mcm-48 self-assembly fiber prepared via electrospinning," *RSC Advances*, vol. 4, no. 6, pp. 2807–2812, 2014.

[174] J. Liu, F. Sun, F. Zhang, Z. Wang, R. Zhang, C. Wang, and S. Qiu, "In situ growth of continuous thin metal–organic framework film for capacitive humidity sensing," *Journal of Materials Chemistry*, vol. 21, no. 11, pp. 3775–3778, 2011.

[175] J. Zhang, L. Sun, C. Chen, M. Liu, W. Dong, W. Guo, and S. Ruan, "High performance humidity sensor based on metal organic framework mil-101 (cr) nanoparticles," *Journal of Alloys and Compounds*, vol. 695, pp. 520–525, 2017.

[176] P.-G. Su and X.-H. Lee, "Electrical and humidity-sensing properties of flexible metal-organic framework m050 (mg) and koh/m050 and aunps/m050 composites films," *Sensors and Actuators B: Chemical*, vol. 269, pp. 110–117, 2018.

[177] Y. Gao, P. Jing, N. Yan, M. Hilbers, H. Zhang, G. Rothenberg, and S. Tanase, "Dual-mode humidity detection using a lanthanide-based metal–organic framework: towards multifunctional humidity sensors," *Chemical Communications*, vol. 53, no. 32, pp. 4465–4468, 2017.

[178] Y. Zhang, W. Zhang, Q. Li, C. Chen, and Z. Zhang, "Design and fabrication of a novel humidity sensor based on ionic covalent organic framework," *Sensors and Actuators B: Chemical*, vol. 324, p. 128733, 2020.

[179] X. Qiao, J. Chen, X. Li, and D. Ma, "Observation of hole hopping via dopant in moo x-doped organic semiconductors: mechanism analysis and application for high performance organic light-emitting devices," *Journal of Applied Physics*, vol. 107, no. 10, p. 104505, 2010.

[180] J.-L. Brédas, J. P. Calbert, D. da Silva Filho, and J. Cornil, "Organic semiconductors: A theoretical characterization of the basic parameters governing charge transport," *Proceedings of the National Academy of Sciences*, vol. 99, no. 9, pp. 5804–5809, 2002.

[181] J.-H. Kim, S.-M. Hong, J.-S. Lee, B.-M. Moon, and K. Kim, "High sensitivity capacitive humidity sensor with a novel polyimide design fabricated by mems technology," in *2009 4th IEEE International Conference on Nano/Micro Engineered and Molecular Systems*. IEEE, 2009, pp. 703–706.

[182] W.-D. Lin, H.-M. Chang, and R.-J. Wu, "Applied novel sensing material graphene/polypyrrole for humidity sensor," *Sensors and Actuators B: Chemical*, vol. 181, pp. 326–331, 2013.

[183] T.-H. Huang, J.-C. Chou, T.-P. Sun, and S.-K. Hsiung, "A device for skin moisture and environment humidity detection," *Sensors and Actuators B: Chemical*, vol. 134, no. 1, pp. 206–212, 2008.

[184] A. Reddy, B. Narakathu, M. Atashbar, M. Rebros, E. Rebrosova, and M. Joyce, "Fully printed flexible humidity sensor," *Procedia Engineering*, vol. 25, pp. 120–123, 2011.

[185] A. Tripathy, S. Pramanik, A. Manna, S. Bhuyan, N. F. Azrin Shah, Z. Radzi, and N. A. Abu Osman, "Design and development for capacitive humidity sensor applications of lead-free ca, mg, fe, ti-oxides-based electro-ceramics with improved sensing properties via physisorption," *Sensors*, vol. 16, no. 7, p. 1135, 2016.

[186] A. Reddy, B. Narakathu, M. Atashbar, M. Rebros, E. Rebrosova, B. Bazuin, M. Joyce, P. Fleming, and A. Pekarovicova, "Printed capacitive based humidity sensors on flexible substrates," *Sensor Letters*, vol. 9, no. 2, pp. 869–871, 2011.

[187] J. Weremczuk, G. Tarapata, and R. Jachowicz, "Humidity sensor printed on textile with use of ink-jet technology," *Procedia engineering*, vol. 47, pp. 1366–1369, 2012.

[188] S. Ali, A. Hassan, G. Hassan, J. Bae, and C. H. Lee, "All-printed humidity sensor based on graphene/methyl-red composite with high sensitivity," *Carbon*, vol. 105, pp. 23–32, 2016.

[189] P.-G. Su and C.-S. Wang, "Novel flexible resistive-type humidity sensor," *Sensors and Actuators B: Chemical*, vol. 123, no. 2, pp. 1071–1076, 2007.

[190] S. R. Yousefi, D. Ghanbari, M. Salavati-Niasari, and M. Hassanpour, "Photodegradation of organic dyes: simple chemical synthesis of ni (oh) 2 nanoparticles, ni/ni (oh) 2 and ni/nio magnetic nanocomposites," *Journal of Materials Science: Materials in Electronics*, vol. 27, no. 2, pp. 1244–1253, 2016.

[191] S. R. Yousefi, A. Sobhani, and M. Salavati-Niasari, "A new nanocomposite superionic system (cdhgi4/hgi2): synthesis, characterization and experimental investigation," *Advanced Powder Technology*, vol. 28, no. 4, pp. 1258–1262, 2017.

[192] S. R. Yousefi, M. Masjedi-Arani, M. S. Morassaei, M. Salavati-Niasari, and H. Moayedi, "Hydrothermal synthesis of dymn2o5/ba3mn2o8 nanocomposite as a potential hydrogen storage material," *International Journal of Hydrogen Energy*, vol. 44, no. 43, pp. 24 005–24 016, 2019.

[193] S. R. Yousefi, O. Amiri, and M. Salavati-Niasari, "Control sonochemical parameter to prepare pure zn0. 35fe2. 65o4 nanostructures and study their photocatalytic activity," *Ultrasonics sonochemistry*, vol. 58, p. 104619, 2019.

[194] S. R. Yousefi, A. Sobhani, H. A. Alshamsi, and M. Salavati-Niasari, "Green sonochemical synthesis of bady 2 nio 5/dy 2 o 3 and bady 2 nio 5/nio nanocomposites in the presence of core almond as a capping agent and their application as photocatalysts for the removal of organic dyes in water," *RSC advances*, vol. 11, no. 19, pp. 11 500–11 512, 2021.

[195] S. R. Yousefi, H. A. Alshamsi, O. Amiri, and M. Salavati-Niasari, "Synthesis, characterization and application of co/co3o4 nanocomposites as an effective photocatalyst for discoloration of organic dye contaminants in wastewater and antibacterial properties," *Journal of Molecular Liquids*, vol. 337, p. 116405, 2021.

[196] S. R. Yousefi, M. Ghanbari, O. Amiri, Z. Marzhoseyni, P. Mehdizadeh, M. Hajizadeh-Oghaz, and M. Salavati-Niasari, "Dy2bacuo5/ba4dycu3o9. 09 s-scheme heterojunction nanocomposite with enhanced photocatalytic and

antibacterial activities," *Journal of the American Ceramic Society*, vol. 104, no. 7, pp. 2952–2965, 2021.

[197] P.-G. Su and C.-P. Wang, "Flexible humidity sensor based on tio2 nanoparticles-polypyrrole-poly-[3-(methacrylamino) propyl] trimethyl ammonium chloride composite materials," *Sensors and Actuators B: Chemical*, vol. 129, no. 2, pp. 538–543, 2008.

[198] L. Guo, H.-B. Jiang, R.-Q. Shao, Y.-L. Zhang, S.-Y. Xie, J.-N. Wang, X.-B. Li, F. Jiang, Q.-D. Chen, T. Zhang *et al.*, "Two-beam-laser interference mediated reduction, patterning and nanostructuring of graphene oxide for the production of a flexible humidity sensing device," *Carbon*, vol. 50, no. 4, pp. 1667–1673, 2012.

[199] A. Oprea, N. Bârsan, U. Weimar, M.-L. Bauersfeld, D. Ebling, and J. Wöllenstein, "Capacitive humidity sensors on flexible rfid labels," *Sensors and Actuators B: Chemical*, vol. 132, no. 2, pp. 404–410, 2008.

[200] M. Saleem, K. S. Karimov, Z. Karieva, and A. Mateen, "Humidity sensing properties of cnt–od–vetp nanocomposite films," *Physica E: Low-dimensional Systems and Nanostructures*, vol. 43, no. 1, pp. 28–32, 2010.

[201] M. T. S. Chani, K. S. Karimov, F. Khalid, S. Abbas, and M. Bhatty, "Orange dye-polyaniline composite based impedance humidity sensors," *Chinese Physics B*, vol. 22, no. 1, p. 010701, 2013.

[202] M. T. S. Chani, K. S. Karimov, and A. M. Asiri, "Fabrication and characterization of organic-inorganic (orange dye-vanadium oxide) composite based humidity sensors," *Int. J. Electrochem. Sci*, vol. 12, pp. 1434–1444, 2017.

[203] S. A. Moiz, M. M. Ahmed, and K. S. Karimov, "Effects of temperature and humidity on electrical properties of organic semiconductor orange dye films deposited from solution," *Japanese Journal of Applied Physics*, vol. 44, no. 3R, p. 1199, 2005.

[204] D. A. Neamen, *Semiconductor physics and devices: basic principles*. McGraw-hill, 2003.

[205] Z. Zhang, M. Chen, S. Alem, Y. Tao, T.-Y. Chu, G. Xiao, C. Ramful, and R. Griffin, "Printed flexible capacitive humidity sensors for field application," *Sensors and Actuators B: Chemical*, vol. 359, p. 131620, 2022.

[206] U. Asghar, K. S. Karimov, M. A. Ibrahim, and N. Fatima, "Multifunctional organic shockproof flexible sensors based on a composite of nickel phthalocyanine colourant, carbon nanotubes and rubber created with rubbing-in technology," *Coloration Technology*, 2021.

[207] M. Wu, Z. Wu, Y. Zheng, X. Jin, X. Liu, J.-H. Lee, and M. Li, "Branched polyethylenimine-based field effect transistor for low humidity detection at room temperature," *IEEE Sensors Journal*, vol. 22, no. 1, pp. 90–98, 2021.

[208] M. Biswas, A. Dey, and S. K. Sarkar, "Polyaniline based field effect transistor for humidity sensor," *Silicon*, pp. 1–7, 2022.

[209] K. S. Karimov, M. H. Sayyad, M. Ali, M. N. Khan, S. A. Moiz, K. B. Khan, H. Farah, and Z. M. Karieva, "Electrochemical properties of zn/orange dye aqueous solution/carbon cell," *Journal of Power Sources*, vol. 155, no. 2, pp. 475–477, 2006.

[210] A. F. Abdulameer, M. H. Suhail, O. G. Abdullah, and I. M. Al-Essa, "Fabrication and characterization of nipcts organic semiconductors based surface type capacitive–resistive humidity sensors," *Journal of Materials Science: Materials in Electronics*, vol. 28, no. 18, pp. 13 472–13 477, 2017.

[211] Y. Yao, X. Chen, J. Zhu, B. Zeng, Z. Wu, and X. Li, "The effect of ambient humidity on the electrical properties of graphene oxide films," *Nanoscale research letters*, vol. 7, no. 1, pp. 1–7, 2012.

[212] A. Nawab, I. Murtaza, N. Ahmad, M. Sajjad *et al.*, "Humidity dependent impedance response of graphene/carbon nanotubes composite," *Materials Research Express*, vol. 5, no. 9, p. 095028, 2018.

[213] F. J. Romero, A. Rivadeneyra, M. Becherer, D. P. Morales, and N. Rodríguez, "Fabrication and characterization of humidity sensors based on graphene oxide–pedot: Pss composites on a flexible substrate," *Micromachines*, vol. 11, no. 2, p. 148, 2020.

[214] S. A. Khan, M. Saqib, M. M. Rehman, H. M. Mutee Ur Rehman, S. A. Rahman, Y. Yang, S. Kim, and W.-Y. Kim, "A full-range flexible and printed humidity sensor based on a solution-processed p (vdf-trfe)/graphene-flower composite," *Nanomaterials*, vol. 11, no. 8, p. 1915, 2021.

[215] S. Machmudah, H. Kanda, M. Goto *et al.*, "Hydrolysis of biopolymers in near-critical and subcritical water," in *Water Extraction of Bioactive Compounds*. Elsevier, 2017, pp. 69–107.

[216] K. S. Karimov, Z. Ahmad, N. Fatima, M. M. Ahmed, and M. Abid, "Effect of humidity on copper phthalocyanine films deposited at different gravity conditions," *Pigment & Resin Technology*, 2017.

[217] J. Terada and T. Nitta, "Multi-functional sensor," Apr. 5 1983, uS Patent 4,378,691.

[218] Z.-B. Zhao, H. Li, Q.-L. Lu, Y.-L. Li, and Y. Jiang, "Multifunctional sensors based on silicone hydrogel and their responses to solvents, pH and solution composition," *Polymer International*, vol. 66, no. 4, pp. 566–572, 2017.

[219] C. S. Boland, U. Khan, C. Backes, A. O'Neill, J. McCauley, S. Duane, R. Shanker, Y. Liu, I. Jurewicz, A. B. Dalton *et al.*, "Sensitive, high-strain, high-rate bodily motion sensors based on graphene–rubber composites," *ACS Nano*, vol. 8, no. 9, pp. 8819–8830, 2014.

[220] Y. Xu, Z. Guo, H. Chen, Y. Yuan, J. Lou, X. Lin, H. Gao, H. Chen, and B. Yu, "In-plane and tunneling pressure sensors based on graphene/hexagonal boron nitride heterostructures," *Applied Physics Letters*, vol. 99, no. 13, p. 133109, 2011.

[221] Z. Ahmad, K. S. Karimov, and F. Touati, "Flexible impedance and capacitive tensile load sensor based on CNT composite," *Chinese Physics B*, vol. 25, no. 2, p. 028801, 2016.

[222] M. T. S. Chani, A. M. Asiri, K. S. Karimov, M. Bashir, S. B. Khan, and M. M. Rahman, "Carbon nanotubes-silicon nanocomposites based resistive temperature sensors," *International Journal of Electrochemical Science*, vol. 10, pp. 3784–3791, 2015.

[223] K. S. Karimov, N. Ahmed, M. M. Bashir, F. Aziz, M. Z. Rizvi, A. Khan, M. Tahir, N. A. Zaidi, M. Hafeez, and A. S. Bhatti, "Flexible resistive tensile load cells based on MWCNT/rubber composites," *Pigment & Resin Technology*, vol. 44, no. 3, pp. 187–191, 2015.

[224] A. Khan, K. S. Karimov, Z. Ahmad, K. Sulaiman, M. Shah, and S. Moiz, "Pressure sensitive organic sensor based on CNT-VO_2(3fl) composite," *Sains Malaysiana*, vol. 43, no. 6, pp. 903–908, 2014.

[225] M. T. S. Chani, K. S. Karimov, A. M. Asiri, N. Ahmed, M. M. Bashir, S. B. Khan, M. A. Rub, and N. Azum, "Temperature gradient measurements by using thermoelectric effect in CNTs-silicone adhesive composite," *PloS One*, vol. 9, no. 4, p. e95287, 2014.

[226] K. S. Karimov, M. Abid, M. Saleem, K. M. Akhmedov, M. M. Bashir, U. Shafique, and M. M. Ali, "Temperature gradient sensor based on CNT composite," *Physica B: Condensed Matter*, vol. 446, pp. 39–42, 2014.

[227] J. Du, L. Zhao, Y. Zeng, L. Zhang, F. Li, P. Liu, and C. Liu, "Comparison of electrical properties between multi-walled carbon nanotube and graphene nanosheet/high density polyethylene composites with a segregated network structure," *Carbon*, vol. 49, no. 4, pp. 1094–1100, 2011.

[228] Z. M. Markovic, L. M. Harhaji-Trajkovic, B. M. Todorovic-Markovic, D. P. Kepić, K. M. Arsikin, S. P. Jovanović, A. C. Pantovic, M. D. Dramićanin, and V. S. Trajkovic, "In vitro comparison of the photothermal anticancer

activity of graphene nanoparticles and carbon nanotubes," *Biomaterials*, vol. 32, no. 4, pp. 1121–1129, 2011.

[229] A. B. Oskouyi, U. Sundararaj, and P. Mertiny, "Effect of temperature on electrical resistivity of carbon nanotubes and graphene nanoplatelets nanocomposites," *Journal of Nanotechnology in Engineering and Medicine*, vol. 5, no. 4, 2014.

[230] K. S. Karimov, M. Ahmed, S. Moiz, P. Babadzhanov, R. Marupov, and M. Turaeva, "Electrical properties of organic semiconductor orange nitrogen dye thin films deposited from solution at high gravity," *Eurasian Chemico-Technological Journal*, vol. 5, no. 2, pp. 109–113, 2003.

[231] K. S. Karimov and T. Qasuria, "The use of displacement sensitive organic field effect transistor for telemetry system applications," *Measurement*, vol. 45, no. 1, pp. 41–46, 2012.

[232] H. Pang, Y.-C. Zhang, T. Chen, B.-Q. Zeng, and Z.-M. Li, "Tunable positive temperature coefficient of resistivity in an electrically conducting polymer/-graphene composite," *Applied Physics Letters*, vol. 96, no. 25, p. 251907, 2010.

[233] K. S. Karimov, H. Senin, I. Qazi, and M. Sadrai, "Organic semiconductors: conduction mechanisms and some applications," in *AIP Conference Proceedings*, vol. 1017, no. 1. American Institute of Physics, 2008, pp. 25–34.

[234] M. S. Dresselhaus, G. Dresselhaus, and P. Avouris, *Carbon nanotubes: Synthesis, structure, properties, and applications*. Springer, 2014.

[235] D. Fathi, "A review of electronic band structure of graphene and carbon nanotubes using tight binding," *Journal of Nanotechnology*, vol. 2011, 2011.

[236] A. Suzuki, M. Tanabe, and S. Fujita, "Electronic band structure of graphene based on the rectangular 4-atom unit cell," *Journal of Modern Physics*, vol. 8, no. 4, pp. 607–621, 2017.

[237] C. Poole and F. J. Owens, "Introduction to nanotechnology john wiley & sons," *Inc., Hoboken, New Jersey*, 2003.

[238] A. Naeemi and J. D. Meindl, "Design and performance modeling for single-walled carbon nanotubes as local, semiglobal, and global interconnects in gigascale integrated systems," *IEEE Transactions on Electron Devices*, vol. 54, no. 1, pp. 26–37, 2006.

[239] B. Wei, R. Vajtai, and P. Ajayan, "Reliability and current carrying capacity of carbon nanotubes," *Applied physics letters*, vol. 79, no. 8, pp. 1172–1174, 2001.

[240] P. G. Collins, M. Hersam, M. Arnold, R. Martel, and P. Avouris, "Current saturation and electrical breakdown in multiwalled carbon nanotubes," *Physical review letters*, vol. 86, no. 14, p. 3128, 2001.

[241] Y.-K. Kwon and P. Kim, "Unusually high thermal conductivity in carbon nanotubes," in *High Thermal Conductivity Materials*. Springer, 2006, pp. 227–265.

[242] A. Raychowdhury and K. Roy, "Modeling of metallic carbon-nanotube interconnects for circuit simulations and a comparison with cu interconnects for scaled technologies," *IEEE Transactions on Computer-Aided Design of Integrated Circuits and Systems*, vol. 25, no. 1, pp. 58–65, 2005.

[243] S. Fujita and A. Suzuki, *Electrical conduction in graphene and nanotubes*. John Wiley & Sons, 2013.

[244] A. K. Geim and K. S. Novoselov, "The rise of graphene," in *Nanoscience and technology: a collection of reviews from nature journals*. World Scientific, 2010, pp. 11–19.

[245] K. S. Karimov, K. Sulaiman, Z. Ahmad, K. M. Akhmedov, and A. Mateen, "Novel pressure and displacement sensors based on carbon nanotubes," *Chinese Physics B*, vol. 24, no. 1, p. 018801, 2015.

[246] A. C. Neto, F. Guinea, N. M. Peres, K. S. Novoselov, and A. K. Geim, "The electronic properties of graphene," *Reviews of modern physics*, vol. 81, no. 1, p. 109, 2009.

[247] S. D. Sarma, S. Adam, E. Hwang, and E. Rossi, "Electronic transport in two-dimensional graphene," *Reviews of modern physics*, vol. 83, no. 2, p. 407, 2011.

[248] M. I. Katsnelson, *Graphene: Carbon in two dimensions*. Cambridge University Press, 2012.

[249] K. S. Karimov, "Electrophysical properties of low-dimensional organic materials at deformation," *Department of Heat Physics, Academy of Sciences, Tashkent, Uzbekistan*, 1993.

[250] E. Eidelman and A. Y. Vul, "The strong thermoelectric effect in nanocarbon generated by the ballistic phonon drag of electrons," *Journal of Physics: Condensed Matter*, vol. 19, no. 26, p. 266210, 2007.

[251] H. Bässler and A. Köhler, "Charge transport in organic semiconductors," *Unimolecular and supramolecular electronics I*, pp. 1–65, 2011.

[252] K. Kanao, S. Harada, Y. Yamamoto, W. Honda, T. Arie, S. Akita, and K. Takei, "Highly selective flexible tactile strain and temperature sensors against substrate bending for an artificial skin," *Rsc Advances*, vol. 5, no. 38, pp. 30 170–30 174, 2015.

[253] T. Q. Trung, S. Ramasundaram, B.-U. Hwang, and N.-E. Lee, "An all-elastomeric transparent and stretchable temperature sensor for body-attachable wearable electronics," *Advanced materials*, vol. 28, no. 3, pp. 502–509, 2016.

[254] L. Pan, A. Chortos, G. Yu, Y. Wang, S. Isaacson, R. Allen, Y. Shi, R. Dauskardt, and Z. Bao, "An ultra-sensitive resistive pressure sensor based on hollow-sphere microstructure induced elasticity in conducting polymer film," *Nature communications*, vol. 5, no. 1, p. 3002, 2014.

[255] W. He, G. Li, S. Zhang, Y. Wei, J. Wang, Q. Li, and X. Zhang, "Polypyrrole/silver coaxial nanowire aero-sponges for temperature-independent stress sensing and stress-triggered joule heating," *Acs Nano*, vol. 9, no. 4, pp. 4244–4251, 2015.

[256] H. Zhang, N. Liu, Y. Shi, W. Liu, Y. Yue, S. Wang, Y. Ma, L. Wen, L. Li, F. Long *et al.*, "Piezoresistive sensor with high elasticity based on 3d hybrid network of sponge@ cnts@ ag nps," *ACS applied materials & interfaces*, vol. 8, no. 34, pp. 22 374–22 381, 2016.

[257] Y. Pang, H. Tian, L. Tao, Y. Li, X. Wang, N. Deng, Y. Yang, and T.-L. Ren, "Flexible, highly sensitive, and wearable pressure and strain sensors with graphene porous network structure," *ACS applied materials & interfaces*, vol. 8, no. 40, pp. 26 458–26 462, 2016.

[258] H.-B. Yao, J. Ge, C.-F. Wang, X. Wang, W. Hu, Z.-J. Zheng, Y. Ni, and S.-H. Yu, "A flexible and highly pressure-sensitive graphene–polyurethane sponge based on fractured microstructure design," *Advanced Materials*, vol. 25, no. 46, pp. 6692–6698, 2013.

[259] S. Gong, W. Schwalb, Y. Wang, Y. Chen, Y. Tang, J. Si, B. Shirinzadeh, and W. Cheng, "A wearable and highly sensitive pressure sensor with ultrathin gold nanowires," *Nature communications*, vol. 5, no. 1, p. 3132, 2014.

[260] X. Liu, Y. Zhu, M. W. Nomani, X. Wen, T.-Y. Hsia, and G. Koley, "A highly sensitive pressure sensor using a au-patterned polydimethylsiloxane membrane for biosensing applications," *Journal of Micromechanics and Microengineering*, vol. 23, no. 2, p. 025022, 2013.

[261] C. Yang, W. Liu, N. Liu, J. Su, L. Li, L. Xiong, F. Long, Z. Zou, and Y. Gao, "Graphene aerogel broken to fragments for a piezoresistive pressure sensor with a higher sensitivity," *ACS applied materials & interfaces*, vol. 11, no. 36, pp. 33 165–33 172, 2019.

[262] B. Glisic, "Concise historic overview of strain sensors used in the monitoring of civil structures: The first one hundred years," *Sensors*, vol. 22, no. 6, p. 2397, 2022.

[263] W. Obitayo and T. Liu, "A review: Carbon nanotube-based piezoresistive strain sensors," *J. Sensors*, vol. 2012, pp. 652 438:1–652 438:15, 2012.

[264] K. S. Karimov, M. T. S. Chani, and F. A. Khalid, "Carbon nanotubes film based temperature sensors," *Physica E: Low-dimensional Systems and Nanostructures*, vol. 43, no. 9, pp. 1701–1703, 2011.

[265] "A review of: "instrumentation for engineering measurements" second edition j.w. dally, w.f. riley & k.g. mcconnell, 1993 new york, chichester, john wiley and sons isbn 0471 60004 0 £18.95," *European Journal of Engineering Education*, vol. 18, no. 4, pp. 429–430, 1993. [Online]. Available: https://doi.org/10.1080/03043799308928169

[266] C. B. V. Dyakonov and J. P. N. Sariciftci, "Organic photovoltaics."

[267] H. Böttger and V. V. Bryksin, *Hopping Conduction in Solids*. Berlin, Boston: De Gruyter, 2022. [Online]. Available: https://doi.org/10.1515/9783112618189

[268] C. J. Brabec, V. Dyakonov, J. Parisi, and N. S. Sariciftci, *Organic photovoltaics: concepts and realization*. Springer Science & Business Media, 2003, vol. 60.

[269] M. Karimov, Khasan; Abid, *Organic Semiconductor Electromechanical Sensors: Pressure, Displacement and Strain Sensors*.

[270] M. Chani, A. M. Asiri, K. Karimov, M. M. Bashir, B. Khan, and M. Rahman, "Carbon nanotubes-silicon nanocomposites based resistive temperature sensors," *International Journal of Electrochemical Science*, vol. 10, pp. 3784–3791, 01 2015.

[271] M. H. Wichmann, S. T. Buschhorn, L. Böger, R. Adelung, and K. Schulte, "Direction sensitive bending sensors based on multi-wall carbon nanotube/epoxy nanocomposites," *Nanotechnology*, vol. 19, no. 47, p. 475503, 2008.

[272] M. H. Wichmann, S. T. Buschhorn, J. Gehrmann, and K. Schulte, "Piezoresistive response of epoxy composites with carbon nanoparticles under tensile load," *Physical Review B*, vol. 80, no. 24, p. 245437, 2009.

[273] G. Yin, N. Hu, Y. Karube, Y. Liu, Y. Li, and H. Fukunaga, "A carbon nanotube/polymer strain sensor with linear and anti-symmetric piezoresistivity," *Journal of composite materials*, vol. 45, no. 12, pp. 1315–1323, 2011.

[274] N. Hu, Y. Karube, M. Arai, T. Watanabe, C. Yan, Y. Li, Y. Liu, and H. Fukunaga, "Investigation on sensitivity of a polymer/carbon nanotube composite strain sensor," *Carbon*, vol. 48, no. 3, pp. 680–687, 2010.

[275] N. Hu, T. Itoi, T. Akagi, T. Kojima, J. Xue, C. Yan, S. Atobe, H. Fukunaga, W. Yuan, H. Ning *et al.*, "Ultrasensitive strain sensors made from metal-coated carbon nanofiller/epoxy composites," *Carbon*, vol. 51, pp. 202–212, 2013.